TENMAK BOREN BOR ARAŞTIRMA ENSTİTÜSÜ
TENMAK BOREN BORON RESEARCH INSTITUTE

ISSN: 2149-9020
e-ISSN: 2667-8438

BOR DERGİSİ
JOURNAL OF BORON

CİLT/VOL 09 | SAYI/ISSUE 02 | YIL/YEAR 2024

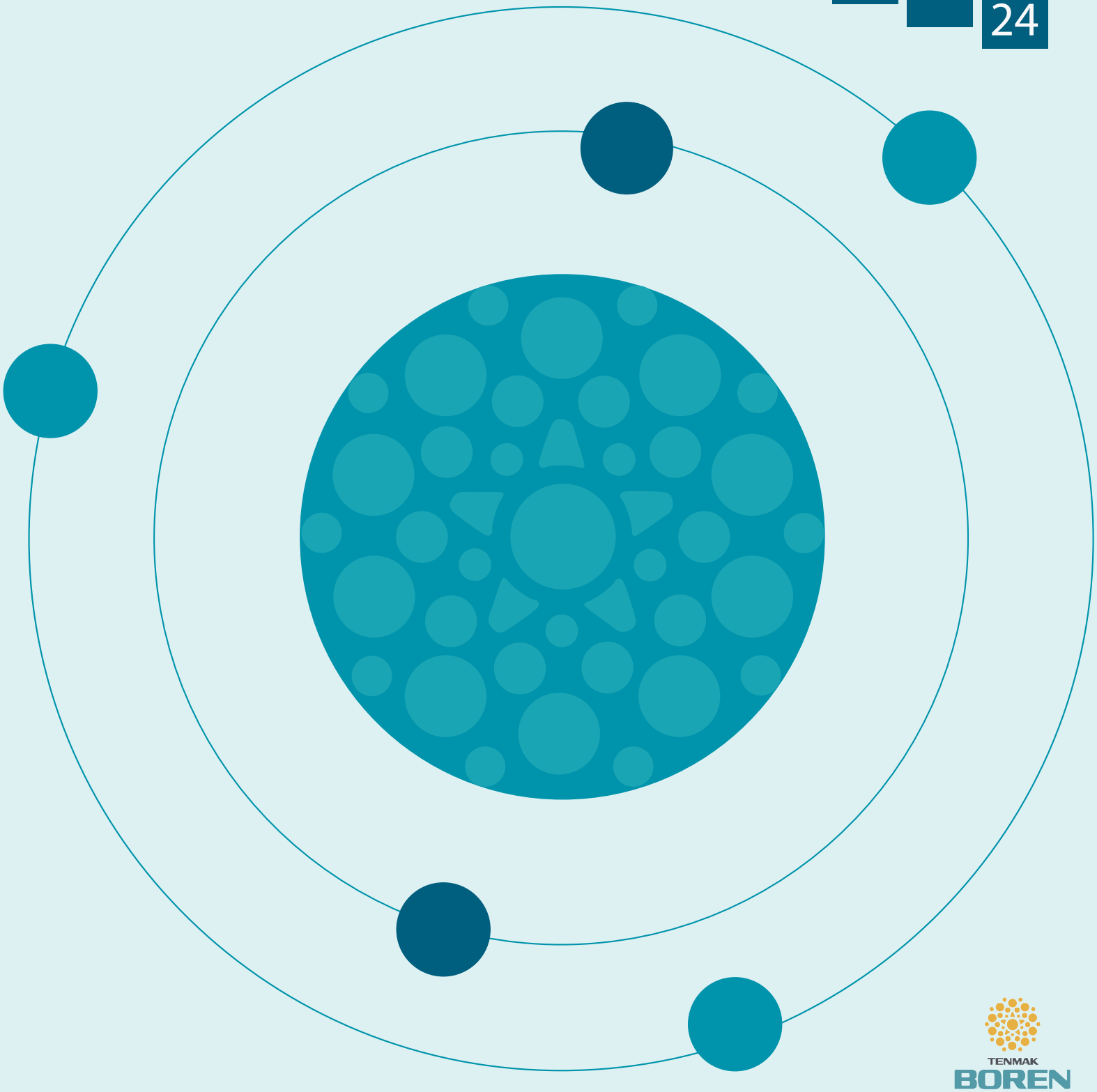

TENMAK BOREN

ISSN: 2149-9020
e-ISSN: 2667-8438

BOR DERGİSİ

JOURNAL OF BORON

CİLT VOL **09** **SAYI** ISSUE **02** **YIL** YEAR **2024**

Yayıncı/Publisher
TENMAK BOREN Bor Araştırma Enstitüsü

Yayın İdare Adresi/Adress of Publication Manager
Dumlupınar Bulvarı (Eskişehir Yolu 7. km), No:166, D Blok,
Ankara, 06530, Türkiye
Tel: (0312) 201 36 00
Fax: (0312) 219 80 55
E-posta: journalofboron@tenmak.gov.tr
Web: https://dergipark.org.tr/tr/pub/boron

Yayın Türü/Type of Publication: Yaygın süreli yayın
Yayın Aralığı/Range of Publication: 3 Aylık
Yayın Tarihi/Publication Date: 28/06/2024

ANKARA
HAZİRAN 2024 / JUNE 2024

TENMAK BOREN
BOR ARAŞTIRMA ENSTİTÜSÜ

BOR DERGİSİ

JOURNAL OF BORON

https://dergipark.org.tr/boron

İÇİNDEKİLER/CONTENTS

BOR DERGİSİ
JOURNAL OF BORON
https://dergipark.org.tr/boron

Boron-doped WO_3 thin films prepared by thermionic vacuum arc technique: The structural, surface, and optical properties

Saliha Elmas [1,*]

[1]*Kocaeli Health and Technology University, European Vocational School, Medical Imaging Techniques Program, Kocaeli, 41190, Türkiye*

ARTICLE INFO

Article history:
Received December 20, 2023
Accepted March 30, 2024
Available online June 28, 2024

Research Article

DOI: 10.30728/boron.1407455

Keywords:
Boron-doped WO_3
Dielectric constant
Optical band gap
Roughness
Surface properties

ABSTRACT

Improvement in the physical properties of WO_3 thin films is of great interest among researchers. In this work, boron as a dopant was selected to enhance the physical characteristics of the WO_3 thin films on glass and silicon wafer substrates. To achieve this aim, a plasma-based, well-known thermionic vacuum arc (TVA) technique was utilized to prepare the films with varying boron percent, followed by structural, optical, and microscopic characterization. The roughness of the films directly depends on the boron amount and nature of the substrate. The structural measurement proved the formation of WO_3 phases on both substrates. An increase in the dopant amount caused a shift in the dominant peak in the X-ray diffraction patterns. The crystallite sizes of the films varied in the range of 14-49 nm. According to the optical results, the optical band gaps (E_g) of the WO_3:B (1%) and WO_3:B (3%) films were obtained as 3.23 and 3.25 eV, respectively. The increase in the boron amount led to an increase in the packing density of the films. This behavior was not related to substrate properties. These results suggest a direct relationship between crystallite size and lower optical loss function.

1. Introduction

Due to the quality, high interest, and wide application area, the materials of oxides, nitrides, and carbides gained great attention from both scientific and industrial sides. Among those, oxides are a material group with individual and special characteristics. So far, various classes of oxide materials have been discovered, synthesized, and coated by different chemical and physical-based techniques [1-4]. In this class, tungsten trioxide (WO_3) is of great interest due to its chemical excellence, mechanical stability, physical stability, and so on [5,6]. The mentioned properties lead to extending the application area of the material. Since the discovery of the oxide material, several methods have been used for synthesizing and coating upon various substrates. Despite the advantages mentioned above, some challenges still cause the restricted use of WO_3 in all applications. To overcome this problem, some routes, such as doping, multi-layer structures, and composite with other materials, are recommended and carried out to improve the WO_3 structure [4,7]. Researchers have successfully doped WO_3 thin films with various elements such as Al [5], Mn [7], Fe [8], C [9], or oxides i.e. CuO [10], MoO_3 [11]. In this research, boron is selected as a dopant to improve the properties of the WO_3 thin film. Overall, thin films have been coated with the plasma-based thermionic vacuum arc (TVA) technique in the high vacuum regime. Then, the suitable devices measure and evaluate the boron-doped WO_3 (WO_3:B) thin films' physical properties.

Alsaad et al. [12] concentrated on the optical and optoelectronic properties of boron-doped ZnO thin films prepared by the sol-gel method. The group proposed a new mathematical equation between thickness and optical band gap for amorphous or crystalline structures. A reverse relationship between boron concentration and optical band gap was proposed. Also, a reverse correlation between Urbach and boron dopant amount was found. Eskalen et al. [13] studied radiation shielding characteristics of wurtzite-structured ZnO:B thin films prepared using a spray pyrolysis method. The researchers report deformation in the structure and worsened in the hexagonal rods respecting the surface images due to incorporating a boron dopant in the host structure. Additionally, a direct dependency between boron dopant and linear attenuation coefficient, mass attenuation coefficient, half value layer, one-tenth value layer, and mean free path results was pronounced. Wong and Lai [14] published a work investigating the temperature dependency of boron-doped ZnO thin films produced via the sputtering technique. Due to the boron activation, the results confirmed the best electrical properties at 400°C in the ZnO:B thin films. More than the boron dopant amount, according to the work, the best optical, morphological, and structural properties of the films were related to deposition temperature.

*Corresponding author: saliha.elmas@kocaelisaglik.edu.tr

This research's main target is introducing a new and quick pathway for forming WO_3:B thin films based on utilizing plasma and vacuum-based techniques. In this context, the relation between coating parameters and physical properties is described in detail.

2. Materials and Methods

2.1. Materials

The WO_3 (99.5% purity) and B powders (99.5% purity) were purchased from the Nanografi (Türkiye) company and Alfa Aesar (USA), respectively. Acetone, isopropanol, and Si substrates (N-type p-doped (111) orientation) were from ISOLAB (Germany), Detsan (Türkiye) and MTI cooperation (USA), respectively.

2.2. Methods

The WO_3 material was doped 1% and 3% in weight. The prepared pellets' diameter and thickness were 1 cm and 1 mm, respectively. The glass and Silicon (Si) wafers were used for substrates. The substrates were ultrasonically cleaned by deionized water (50°C), acetone (30°C) and isopropanol (30°C) for 5 minutes to remove the particles on the substrates, respectively. The glass and Si substrates were cleaned according to the procedure seen in Figure 1. The Si substrate is p-doped with (111) orientation.

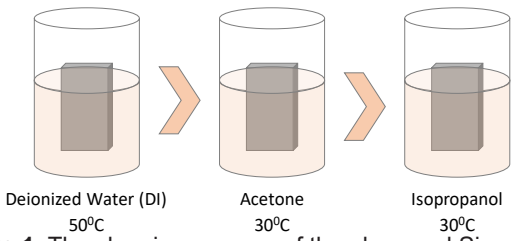

Figure 1. The cleaning process of the glass and Si substsrates.

The coating process was performed using a plasma-based technique that well-known as TVA in a high vacuum regime. Firstly, the cleaned substrates were placed in the chamber upon the substrate holder. Then the substrate holder is fixed on the anode and kept at a constant distance from the anode during the coating. The anode section is a spoon-like tungsten (W) or Molybdenum (Mo)-included material for holding the coated material on the substrate. In our case, the boron-doped WO_3 powder as a pellet was poured inside the anode gently. The vacuum chamber was closed and the evacuation process started. Initially, the rotary pump and the turbo-molecular pump started. This process was continued until the pressure value achieved base pressure means $7x10^{-6}$ Torr. All processes such as evacuation, coating, amount of current, and voltage applied were monitored and controlled by various and suitably mounted devices. The coating process was started by applying AC and DC currents to the cathode and anode parts [1]. The cathode is constructed of tungsten wire surrounded by the Wehnelt cylinder and serves as an electron gun. After applying the current and voltage to the cathode, the tungsten wire is thermally heated, leading to electron emission. The emitted electrons moved toward the anode while using the Wehnelt the random movement of these electrons was avoided [2]. The collisions between the electrons and pelletized WO_3:B powders cause energy transfer, then a change in the phase of powders to liquid and so gas phases. This procedure continues after reaching a stable plasma of WO_3:B. This plasma was moved onto the substrate holder and deposited layer by layer on the cleaned substrates. The significant parameters during the coating are listed in Table 1.

Table 1. The effective TVA parameters during the coating process.

Parameters	WO_3:B	
	1%	3%
Discharge current (A)	0.30	0.25
Deposition time (s)	60	180
Working pressure (Torr)	$1.8x10^{-4}$	$2.04x10^{-4}$
Applied voltage (V)	200	200
Filament current (A)	18.7	18.2

Thin films were analyzed by Ambios Q-scope Atomic Force Microscope (AFM) in non-contact mode using the Scan Atomic V 5.1.0 SPM control software at room temperature. Compositional characterization of WO_3:B thin films was analyzed with, using Al source, X-ray photoelectron spectroscopy (XPS, Thermo Scientific K-Alpha, USA). The device works in a dual source light source utilizing ultra-low energy electron beam and Al Kα micro-focused condition. The structural properties of the films were measured through a X-ray diffraction (XRD, Malvern Panalytical Empyrean, UK). The optical features of the thin films were characterized using UV-VIS spectrophotometry (Unico Dual Beam, USA) and Filmetrics F20 devices. The UV-Vis spectrophotometry and Filmetrics were performed in 200-1100 nm and 400-1000 nm wavelength ranges, respectively. Both optical devices work at room temperature. The surface properties of the produced films were investigated with scanning electron microscopy (SEM, Zeiss Supra 40VP, Germany).

3. Results and Discussion

The three-dimensional (3D) images and crystallite distribution of the particles upon the surface of the boron-doped WO_3 thin films are shown in Figure 2. Using AFM, roughness, crystallite sizes, and symmetric distribution of the crystals upon the surface after the coating was revealed, as seen in Table 2. According to the measurement results, an increase in the boron amount is not affected by the roughness values, while an increase in the boron percent leads to a decrease in the roughness. So, the roughness value is directly related to substrate and boron amount.

The skewness is an indication of the symmetric distribution of particles on the surface [2]. In both

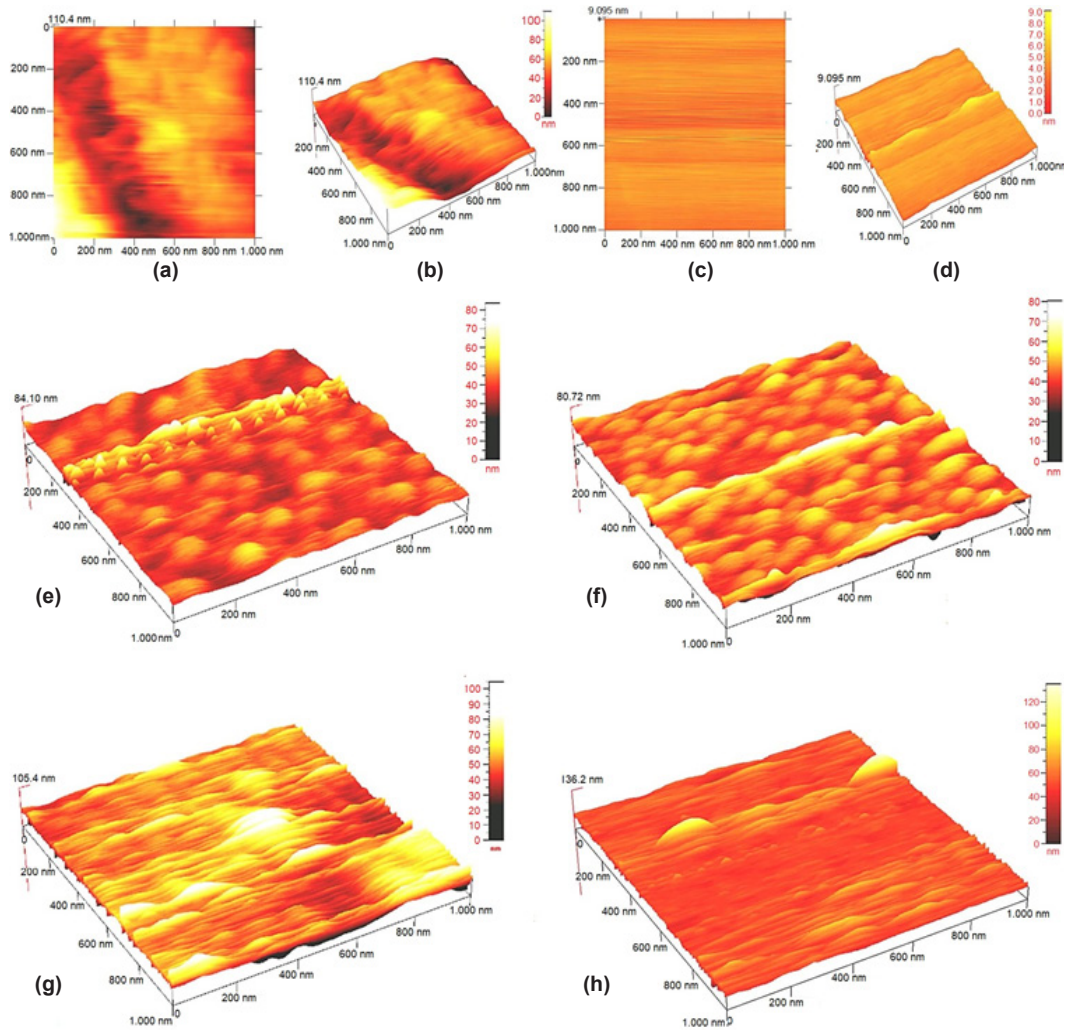

Figure 2. The AFM images of the a, b) bare glass substrate, c, d) bare Si wafer substrate, e) WO_3:B/glass (1%), f) WO_3:B (3%)/glass, g) WO_3:B (1%)/Si, h) WO_3:B (3%)/Si.

Table 2. The surface results obtained using the AFM device.

	RMS (nm)	Skewness (Ssk)	Kurtosis (Skr)
Bare glass substrate	13.1	0.97	0.74
Bare Si wafer substrate	0.33	3.78	40.88
WO_3:B (1%)/glass	5.01	0.08	4.1
WO_3:B (1%)/Si	9,39	0.16	1.96
WO_3:B (3%)/glass	5.13	0.24	3.12
WO_3:B (3%)/Si	6,48	0.70	11.56

cases, the highest symmetric distribution is measured at the films coated upon the glass substrate. This characteristic is not dependent on boron dopant percent.

The FESEM images of the coated films are shown in Figure 3. All images are portrayed in the 50,000X resolution. Regarding the images, there are no cracks on the surface. This feature is not related to the boron amount and substrate. Increasing the boron amount in the host material causes some agglomeration on the surface. The surfaces are compact and dense without pinholes. This characteristic shows the eligibility of the films for use in dye-synthesized solar cells [12]. The grains on the surface are spherical ball-like configurations that do not depend on the boron and substrate nature.

The micro-structural properties of the prepared films are performed and listed in Table 3. In the XRD patterns (Figure 4), WO_3 and B_2O_3 peaks demonstrate the polycrystalline nature of the prepared films. The result is not related to the structure of the substrate. According to the measurement, there are shifts in the WO_3 peaks, which show stress during the coating because of the boron dopant. This stress originated from adding dopant into the host structure, as reported by other researchers [1] and is responsible for the shift in the emerged peaks.

Regarding the patterns, the structure has no impurity, other phases, or bond between W and B. Significantly, in this case, the high-intensity peak is directly related to the amount of dopant. In the low dopant (1%) of the films, the high-intensity peak was WO_3 with (004) diffraction plane, while in the high dopant (3%), the highest peak was WO_3 with (222) diffraction plane.

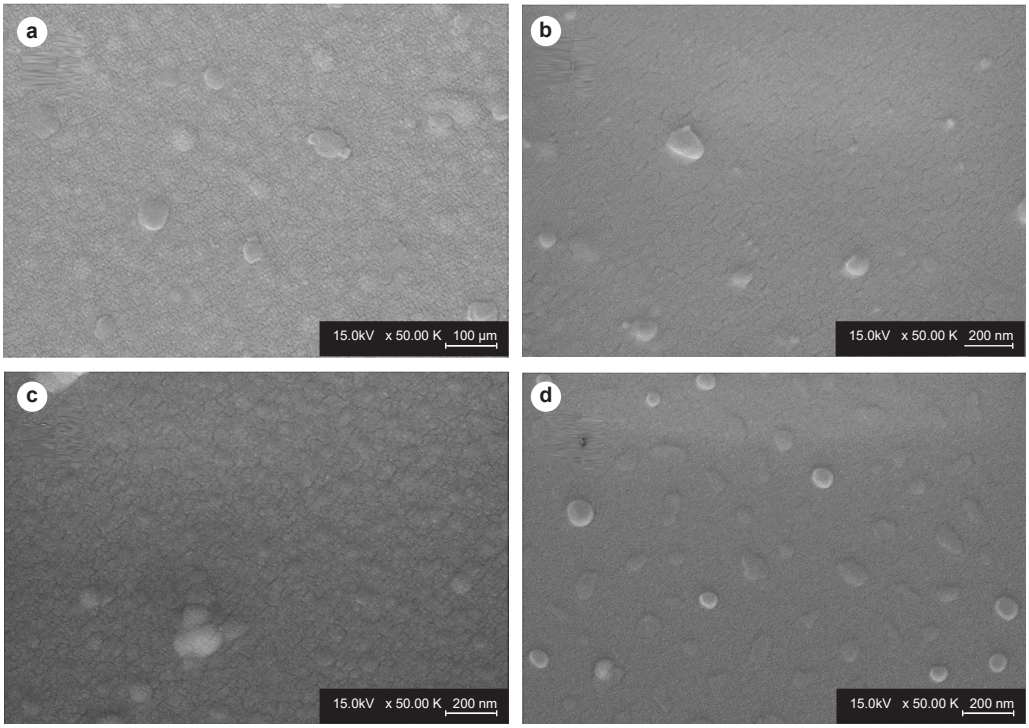

Figure 3. The FE-SEM images of the a) WO_3: B (1%)/glass, b) WO_3: B (1%)/Si, c) WO_3: B (3%)/glass, d) WO_3: B (3%)/Si (Scale bar: 1µm).

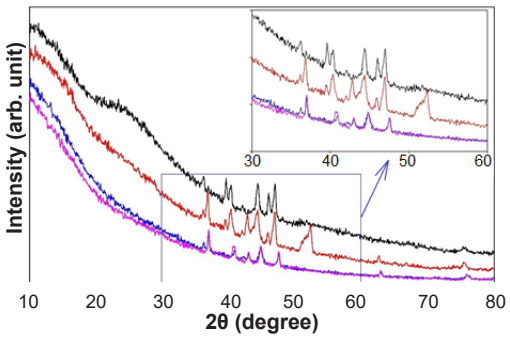

Figure 4. The XRD pattern of the Boron-doped WO_3 on glass and Si substrates, WO_3:B/glass (1%, black line), WO_3:B/Si (1%, red line), WO_3:B/glass (3%, blue line), and WO_3:B/Si (3%, pink line).

Therefore, increasing the boron amount causes a change in the WO_3 diffraction plane. This issue is not related to the nature of the utilized substrate. All emerging peaks show monoclinic WO_3 crystal structure and are compatible with ICDD card No: 43-1035 [2].

Using the patterns, for both substrates, the crystallite size (CS) of the films is calculated by the well-known Scherrer formula (Eq. 1) [3,4], where, the λ (=1.5406 Á), FWHM, and θ are the X-ray wavelength, full width at half maximum of a peak, and Bragg diffraction angle, respectively.

$$CS = \frac{0.94\,\lambda}{FWHM\cos\theta} \quad (1)$$

Respecting the results, the minimum and maximum grain sizes of the thin films coated on both substrates were altered between 14 and 49 nm, respectively. These results proved the eligibility of the TVA in the formation and growth of nanometer crystals on the various substrates. Despite the lack of thermal treatment application to produce the thin films, these values are comparable and, in some cases, smaller than the other coated WO_3 films in the literature [5-9].

Utilizing the above results, the dislocation density (δ) and microstrain (ε) residue in the coated thin films are calculated by Eq. (2) and (3) [4,10].

$$\delta = (CS)^{-2} \quad (2)$$

$$\varepsilon = \frac{FWHM\cos\theta}{4} \quad (3)$$

Considering the coating method, there are defects in the prepared thin film. In this situation, the defects during the coating process via TVA were computed and listed in the table. Also, the lattice strain (LS) due to pressure change during the coating, as well as the dopant effect, is evaluated by Eq. (4) [10-12].

$$LS = \frac{FWHM}{4\tan\theta} \quad (4)$$

These values are outlined in Table 3. The stress and strain values during the coating as well as dopant effects are comparable with other reported research in literature [1,6,13].

According to the calculated results, an increase in the boron dopant causes a reduction in the intensity of the maximum XRD peaks, replacement of (004) with (222) plane, and sharpening in the maximum emerged peak [1,7,14]. Amongst the various reasons for emerging the secondary phase, the existence of B_2O_3 in this structure is concluded owing to the large difference in

Table 3. The results of XRD measurement for the coated films on both substrates.

	Peak 2θ (˚)	Diffraction plane (hkl)	Phase	Crystal size (nm)	Dislocation density (δ) $(nm)^{-2}$	Microstrain (ε)	Lattice strain (LS)	ICCD card
WO_3:B/glass (1%)	36.15	122	WO_3	31	1.04×10^{-3}	7.44×10^{-2}	0.24	72-0199
	39.60	240	WO_3	48	4.34×10^{-4}	4.91×10^{-2}	0.14	72-0199
	40.33	021 103	WO_3 B_2O_3	27	1.37×10^{-3}	8.57×10^{-2}	0.25	98-008-9092 72-0199
	44.39	320	WO_3	23	1.89×10^{-3}	9.66×10^{-2}	0.26	72-0199
	46.01	123	WO_3	49	4.16×10^{-4}	4.80×10^{-2}	0.12	72-0199
	46.97	112 004	B_2O_3 WO_3	39	6.57×10^{-4}	5.98×10^{-2}	0.15	98-005-1575 72-0199
WO_3:B/Si (1%)	36.83	222	WO_3	37	7.30×10^{-4}	6.19×10^{-2}	0.20	43-1035
	40.32	103	B_2O_3	27	1.37×10^{-3}	8.57×10^{-2}	0.25	43-1035
	42.80	133	WO_3	23	1.89×10^{-3}	9.71×10^{-2}	0.27	43-1035
	44.34	320	WO_3	38	6.93×10^{-4}	6.04×10^{-2}	0.16	43-1035
	45.88	123	WO_3	38	6.93×10^{-4}	6.00×10^{-2}	0.15	43-1035
	46.93	112 004	B_2O_3 WO_3	39	6.57×10^{-4}	5.98×10^{-2}	0.15	98-007-4774 43-1035
	52.31	420	WO_3	50	4.00×10^{-4}	4.68×10^{-2}	0.11	43-1035
	62.58	143	WO_3	34	8.65×10^{-4}	6.68×10^{-2}	0.13	43-1035
	75.49	030	B_2O_3	18	3.09×10^{-3}	1.24×10^{-1}	0.20	98-007-4774
WO_3:B/glass (3%)	36.94	222	WO_3	48	4.34×10^{-4}	4.95×10^{-2}	0.16	43-1035
	40.87	103	B_2O_3	31	1.04×10^{-3}	7.33×10^{-2}	0.21	98-008-0829
	42.86	133	WO_3	15	4.44×10^{-3}	1.46×10^{-1}	0.40	43-1035
	44.81	123	WO_3	32	9.77×10^{-4}	7.23×10^{-2}	0.19	43-1035
	47.51	312	WO_3	39	6.57×10^{-4}	5.97×10^{-2}	0.15	43-1035
	62.88	143	WO_3	34	8.65×10^{-4}	6.67×10^{-2}	0.13	43-1035
	75.97	030	B_2O_3	14	5.10×10^{-3}	1.64×10^{-1}	0.27	96-151-0795
WO_3:B/Si (3%)	36.99	222	WO_3	48	4.34×10^{-4}	4.95×10^{-2}	0.16	43-1035
	40.77	103	B_2O_3	23	1.89×10^{-3}	9.78×10^{-2}	0.28	98-000-8217
	43.01	111 133	B_2O_3 WO_3	48	4.34×10^{-4}	4.85×10^{-2}	0.13	98-005-1575 43-1035
	44.85	123	WO_3	38	6.93×10^{-4}	6.03×10^{-2}	0.16	43-1035
	47.55	112 312	B_2O_3 WO_3	39	6.57×10^{-4}	5.97×10^{-2}	0.15	98-005-1575 43-1035
	62.91	143	WO_3	25	1.60×10^{-3}	8.90×10^{-2}	0.17	ICDD 20-1324
	75.89	030	B_2O_3	22	2.07×10^{-3}	1.03×10^{-1}	0.17	98-005-1575

the ionic radii of W^{6+} (0.62Å) and B^{3+} (0.2Å) [1]. Since this large difference between dopant and host atoms, i.e., tungsten and oxygen, the dopant tends to bond with oxygen [15,16] instead of aggregation in the grain boundary or being substituted into the tungsten location inside the WO_3 structure. The emerging B_2O_3 was crystalline, and the origin of the extra peak that emerged in the thin film that was produced is not obviously understandable.

XPS is widely utilized for determining the chemical composition of a surface. The elemental results of the films coated onto both substrates are illustrated in Figure 5. Regarding the patterns, there are W and O peaks in the spectrum. Meanwhile, the resulting patterns have C, N, Si, and B impurities. The Si peak gives rise to the substrate and the C and N are originated from the environment [6]. The doublet peaks in Figure 5a show the W4f valence state in the coated films. Only one state in the films demonstrates the one oxidation state in the tungsten atom. The W4f peak centers emerged at 35.3 eV and 37.4 eV, respectively, identifying this structure's 4f7/2 and 4f5/2 for W^{6+} [7,17]. The absorbance and transmittance of the films upon both substrates are shown in Figure 5 c-f. There are two regions in the absorbance spectrum; the first covers 200-320 nm and 320-1100 nm. There is an electronic transition in the thin film deposited onto the glass substrates for both cases.

The optical band gap (E_g) value of the thin films coated on glass substrates is shown in Figure 6d. The E_g of

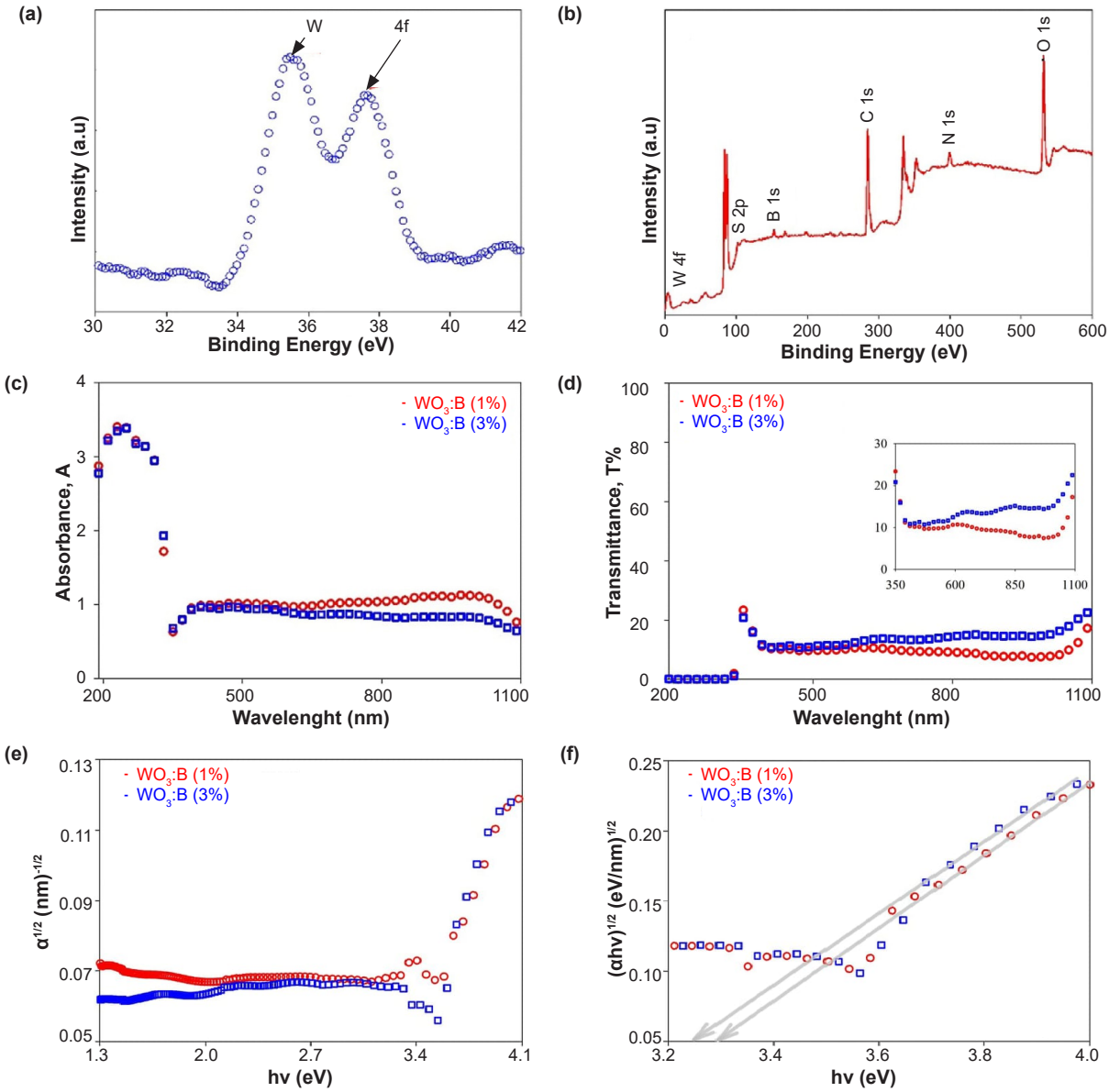

Figure 5. The a) narrow scan of W, and b) wide scan of the coated films. The optical results of the coated boron-doped WO_3 upon glass substrates, c) absorbance, d) transmittance, e) absorption coefficient, and f) optical band gap (E_g).

the thin films is computed using Eq. (5) [18]:

$$(\alpha hv)^n = A\,(hv - E_g) \tag{5}$$

the α, hv, and A are absorption coefficients, photon energy, and a constant. The A is defined as the band-band transition well-known as tailing values. This parameter also presented the coated film quality. In the above formula, the n describes the nature of transition and, in this case, is equal to 2 and 1/2 for direct and indirect optical band gap situations. In the present study, the electronic transition equals ½, which shows the indirect allowed transition of WO_3. The absorption coefficient (α) of the films is calculated by Eq. (6), where T is the transmittance of the coated films, and d is the thickness of films measured by Filmetrics. The E_g values of the WO_3:B films for both 1% and 3% on glass substrates were 3.23 [19] and 3.25 eV [20], respectively.

$$\alpha = \frac{Ln\,(1/T)}{d} \tag{6}$$

The optical parameters such as refraction index (n), reflectance (R), real (ε_{real}), and imaginary ($\varepsilon_{imaginary}$) dielectric constants and optical loss factor (tan δ) of the prepared films on both substrates are illustrated in Figure 6. The parameters show normal distribution in the given wavelength range. The refractive index of the films is in the range of 2.10-2.45. The measured values coincide well with the literature [7,21,22]. The higher refractive index shows a higher packing density and is related to the lower amount of voids and lattice defects [8]. Regardless of the substrate nature, the increase in the dopant value leads to higher packing density.

The real and imaginary parts of dielectric constants and loss function of the films are calculated according to Eq. (7):

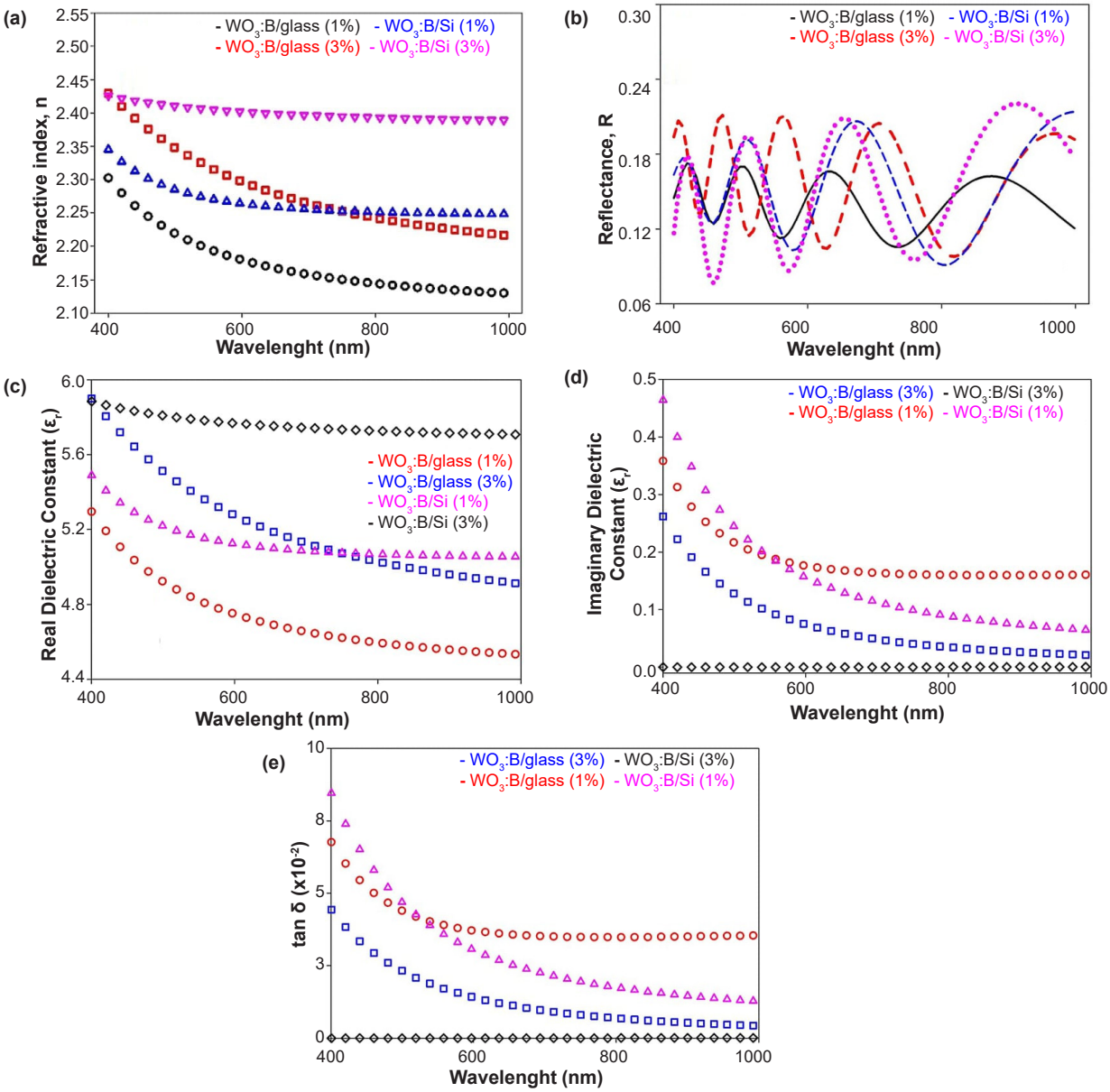

Figure 6. The a) refractive index, b) reflectance, c, d) Real and imaginary dielectric constant, and e) optical loss factor of the films coated onto the glass substrate.

$$\varepsilon(\lambda) = \varepsilon_{real}(\lambda) + \varepsilon_{imaginary}(\lambda) \quad (7)$$

Those are defined in Eq. (8-10):

$$\varepsilon_{real}(\lambda) = n^2 - k^2 \quad (8)$$

$$\varepsilon_{imaginary}(\lambda) = 2nk \quad (9)$$

$$\tan\delta = {}^{\varepsilon_{imaginary}}/_{\varepsilon_{real}} \quad (10)$$

Increasing the wavelength reduces this trend, which causes normal distribution [23]. The optical loss factor of the WO_3:B with different boron dopant amounts is shown minimum value compared to other published reports [19]. The lower optical loss factor originated from lower grain size [24]. This phenomenon is proved by crystallite size computed by the Scherrer equation which may cause a higher conductivity by increasing the amount of crystallite and lowering the defect in the structure [25].

4. Conclusions

In this research, boron-doped WO_3 was successfully coated on the glass and Si substrates using a plasma-based PVD system. Respecting the surface characterization, the roughness of the films directly depends on the boron amount and nature of the substrate. The structural results proved the formation of WO_3 phases on both substrates. An increase in the dopant amount causes a shift in the dominant peak in the XRD patterns. The calculated crystalline sizes for both films confirmed nanometer dimensions ranging from 14 to 49 nm. According to the optical results, the optical band gap (E_g) of the WO_3:B (1%) and WO_3:B (3%) films were obtained as 3.23 and 3.25 eV, respectively. The increase in the boron leads to an increase in the packing density of the films. There is no relationship between the substrate structure nature and packing density. Respecting this research results, there is a direct relationship between crystallite size

and lower optical loss function. The elemental analysis shows the presence of W and O in the spectrum.

5. Acknowledgements

The author would like to thank Kocaeli Health and Technology University for supporting the project (KOSTU BAP 2023/1).

References

[1]. Al-Kuhaili, M. F., & Drmosh, Q. A. (2022). Investigating the structural and optoelectronic properties of co-sputtered Fe-doped WO3 thin films and their suitability for photocatalytic applications. *Materials Chemistry and Physics*, *281*, 125897. https://doi.org/10.1016/j.matchemphys.2022.125897.

[2]. Thakur, A. K., Limaye, M. V., Rakshit, S., Maity, K. N., Gupta, V., Sharma, P. K., & Singh, S. B. (2018). Controlled synthesis of WO3 nanostructures: optical, structural and electrochemical properties. *Materials Research Express*, *6*(2), 025006. https://doi.org/10.1088/2053-1591/aae991.

[3]. Patterson, A. L. (1939). The Scherrer formula for X-ray particle size determination. *Physical Review*, *56*(10), 978. https://doi.org/10.1103/PhysRev.56.978.

[4]. Demirkol, U., Pat, S., Mohammadigharehbagh, R., Musaoğlu, C., Özgür, M., Elmas, S., ... & Korkmaz, Ş. (2019). Determination of the structural, morphological and optical properties of graphene doped SnO thin films deposited by using thermionic vacuum arc technique. *Physica B: Condensed Matter*, *569*, 14-19. https://doi.org/10.1016/j.physb.2019.05.035.

[5]. Ammar, A. U., Stan, M., Popa, A., Toloman, D., Macavei, S., Leostean, C., ... & Rostas, A. M. (2023). All-in-one supercapacitor devices based on nanosized Mn4+-doped WO3. *Journal of Energy Storage*, *72*, 108599. https://doi.org/10.1016/j.est.2023.108599.

[6]. Gupta, D., Chauhan, V., Mahajan, A., Gupta, R., Ali, S. A., & Kumar, R. (2023). Influence of gamma radiation on optical, structural and surface morphological properties of WO3 thin films grown by RF sputtering. *Radiation Physics and Chemistry*, *202*, 110554. https://doi.org/10.1016/j.radphyschem.2022.110554.

[7]. Kavitha, V. S., Krishnan, R. R., Sreedharan, R. S., Suresh, K., Jayasankar, C. K., & Pillai, V. M. (2019). Tb3+-doped WO3 thin films: A potential candidate in white light emitting devices. *Journal of Alloys and Compounds*, *788*, 429-445. https://doi.org/10.1016/j.jallcom.2019.02.222.

[8]. Jain, R. K., & Khanna, A. (2021). CuO-doped WO3 thin film H2S sensors. *Sensors and Actuators B: Chemical*, *343*, 130153. https://doi.org/10.1016/j.snb.2021.130153.

[9]. Reddy G V, A., Kumar, K. N., Sattar, S. A., Shetty, H. D., Prakash, N. G., Jafri, R. I., ... & Ansar, S. (2023). Effect of post annealing on DC magnetron sputtered tungsten oxide (WO3) thin films for smartwindow applications. *Physica B: Condensed Matter*, *664*, 414996. https://doi.org/10.1016/j.physb.2023.414996.

[10]. Elmas, S., Pat, S., Mohammadigharehbagh, R., Musaoğlu, C., Özgür, M., Demirkol, U., ... & Korkmaz, Ş. (2019). Determination of physical properties of graphene doped ZnO (ZnO: Gr) nanocomposite thin films deposited by a thermionic vacuum arc technique. *Physica B: Condensed Matter*, *557*, 27-33. https://doi.org/10.1016/j.physb.2018.12.039.

[11]. Özgür, M., Pat, S., Mohammadigharehbagh, R., Musaoğlu, C., Demirkol, U., Elmas, S., ... & Korkmaz, Ş. (2019). Sn doped ZnO thin film deposition using thermionic vacuum arc technique. *Journal of Alloys and Compounds*, *774*, 1017-1023. https://doi.org/10.1016/j.jallcom.2018.10.020.

[12]. Alsaad, A. M., Al-Bataineh, Q. M., Ahmad, A. A., Albataineh, Z., & Telfah, A. (2020). Optical band gap and refractive index dispersion parameters of boron-doped ZnO thin films: A novel derived mathematical model from the experimental transmission spectra. *Optik*, *211*, 164641. https://doi.org/10.1016/j.ijleo.2020.164641.

[13]. Eskalen, H., Kavun, Y., Kerli, S., & Eken, S. (2020). An investigation of radiation shielding properties of boron doped ZnO thin films. *Optical Materials*, *105*, 109871. https://doi.org/10.1016/j.optmat.2020.109871

[14]. Wong, L. H., & Lai, Y. S. (2021). Substrate temperature dependence of material, optical, and electronic properties of boron-doped ZnO thin films. *Optical Materials*, *115*, 111052. https://doi.org/10.1016/j.optmat.2021.111052.

[15]. Özgür, M., Pat, S., Mohammadigharehbagh, R., Musaoğlu, C., Demirkol, U., Elmas, S., ... & Korkmaz, Ş. (2019). Al doped ZnO thin film deposition by thermionic vacuum arc. *Journal of Materials Science: Materials in Electronics*, *30*, 624-630. https://doi.org/10.1007/s10854-018-0329-x.

[16]. Raja, M., Marnadu, R., Balaji, M., Ravikumar, K., Krishna, V. G., Kumar, M., & Massoud, E. E. S. (2022). Fabrication and characterization of novel Ga-doped WO3 films and n-Ga@ WO3/p-Si junction diode for optoelectronic device applications. *Inorganic Chemistry Communications*, *139*, 109291. https://doi.org/10.1016/j.inoche.2022.109291.

[17]. Mohan, L., Avani, A. V., Kathirvel, P., Marnadu, R., Packiaraj, R., Joshua, J. R., ... & Saravanakumar, S. (2021). Investigation on structural, morphological and electrochemical properties of Mn doped WO3 nanoparticles synthesized by co-precipitation method for supercapacitor applications. *Journal of Alloys and Compounds*, *882*, 160670. https://doi.org/10.1016/j.jallcom.2021.160670.

[18]. Lokhande, B. J., Patil, P. S., & Uplane, M. D. (2001). Studies on structural, optical and electrical properties of boron doped zinc oxide films prepared by spray pyrolysis technique. *Physica B: Condensed Matter*, *302*, 59-63. https://doi.org/10.1016/S0921-4526(01)00405-7.

[19]. Xu, X. G., Yang, H. L., Wu, Y., Zhang, D. L., Wu, S. Z., Miao, J., ... & Wang, B. Y. (2010). Intrinsic room temperature ferromagnetism in boron-doped ZnO. *Applied Physics Letters*, *97*(23) 1-9. https://doi.org/10.1063/1.3524493.

[20]. Thalji, M. R., Ali, G. A., Algarni, H., & Chong, K. F. (2019). Al3+ ion intercalation pseudocapacitance study of W18O49 nanostructure. *Journal of Power Sources*, *438*, 227028. https://doi.org/10.1016/j.jpowsour.2019.227028.

[21]. Tauc, J., Grigorovici, R., & Vancu, A. (1966). Optical properties and electronic structure of amorphous germanium. *Physica Status Solidi (b)*, *15*(2), 627-637. https://doi.org/10.1002/pssb.19660150224.

[22]. Kavitha, V. S., Suresh, S., Chalana, S. R., & Pillai, V. M. (2019). Luminescent Ta doped WO3 thin films as a probable candidate for excitonic solar cell applications. *Applied Surface Science*, *466*, 289-300. https://doi.org/10.1016/j.apsusc.2018.10.007.

[23]. Sriram, S. R., Parne, S. R., Pothukanuri, N., & Edla, D. R. (2023). Synthesis and characterization of pure and Cu-doped WO3 thin films for high performance of toxic gas sensing applications. *Applied Surface Science Advances*, *15*, 100411. https://doi.org/10.1016/j.apsadv.2023.100411.

[24]. Charles, C., Martin, N., Devel, M., Ollitrault, J., & Billard, A. (2013). Correlation between structural and optical properties of WO3 thin films sputter deposited by glancing angle deposition. *Thin Solid Films*, *534*, 275-281. https://doi.org/10.1016/j.tsf.2013.03.004.

[25]. Hutchins, M. G., Abu-Alkhair, O., El-Nahass, M. M., & Abd El-Hady, K. (2006). Structural and optical characterisation of thermally evaporated tungsten trioxide (WO3) thin films. *Materials Chemistry and Physics*, *98*(2-3), 401-405. https://doi.org/10.1016/j.matchemphys.2005.09.052.

[26]. Al-Salami, A. E., Dahshan, A., & Shaaban, E. R. (2017). Effect of film thickness on structural and optical properties of Cd-Zn-Te grown on glass and ITO substrates using electron beam evaporation. *Optik*, *150*, 34-47. https://doi.org/10.1016/j.ijleo.2017.09.062.

[27]. Huang, X., Zhang, H., Lai, Y., & Li, J. (2017). The lowered dielectric loss tangent and grain boundary effects in fluorine-doped calcium copper titanate ceramics. *Applied Physics A*, *123*, 1-7. https://doi.org/10.1007/s00339-017-0947-9.

[28]. Sangwong, N., Somphan, W., Thongbai, P., Yamwong, T., & Meansiri, S. (2012). Electrical responses and dielectric relaxations in giant permittivity NaCu3 Ti3 TaO12 ceramics. *Applied Physics A*, *108*, 385-392. https://doi.org/10.1007/s00339-012-6897-3.

BOR DERGİSİ
JOURNAL OF BORON
https://dergipark.org.tr/boron

Boraks dekahidrat çözeltilerinin faz değiştiren malzeme olarak ön soğutma işlemi yapılan soğuk depolama sisteminde kullanımı

Berçem Kıran Yıldırım [1,*], **Ebru Mançuhan** [1], **Sibel Titiz Sargut** [1]

[1]*Marmara Üniversitesi, Mühendislik Fakültesi, Kimya Mühendisliği Bölümü, 34854, Türkiye*

MAKALE BİLGİSİ

Makale Geçmişi:
İlk gönderi 14 Aralık 2023
Kabul 10 Nisan 2024
Online 28 Haziran 2024

Araştırma Makalesi

DOI: 10.30728/boron.1405029

Anahtar kelimeler:
Boraks dekahidrat
Enerji tasarrufu
Faz değiştiren malzemeler
Ön soğutma
Soğuk depolama

ÖZET

Ön soğutma işlemi taze sebze ve meyvelerin hasattan kısa süre sonra meydana gelen bozulmalarının önüne geçmek amacıyla yürütülen soğuk depolamanın önemli basamaklarından biridir. Bu çalışmada, laboratuvar ölçekli bir soğutma sistemi ön soğutma işlem koşullarında faz değiştiren malzemesiz (FDM'siz) ve FDM'lerle test edilmiştir. FDM olarak sisteme su ve farklı konsantrasyonlarda hazırlanan $Na_2B_4O_7.10H_2O$ çözeltileri entegre edilmiştir. Kompresör çalışma süresinin (%) tüm FDM'lerle azaldığı tespit edilmiştir. FDM'siz durumda %21,05 olarak belirlenen bu değerin ağ. %1,0 $Na_2B_4O_7.10H_2O$ çözeltisi ile %12,12 değerine kadar düştüğü belirlenmiştir. Dolayısıyla, toplam enerji tüketiminde maksimum azalma, ağ. %1,0 $Na_2B_4O_7.10H_2O$ çözeltisi ile %41,7 oranında hesaplanmıştır. Elektrik kesintisi esnasında ise, kabin iç hava sıcaklığının ortam sıcaklığına ulaşma süresi FDM'siz duruma göre ağ. %1,0 $Na_2B_4O_7.10H_2O$ çözeltisi ile yaklaşık 4,3 kat uzadığı belirlenmiştir. Sonuç olarak, ön soğutma işleminde kullanılan soğutma sistemlerinde kullanmak üzere ağ. %1,0 $Na_2B_4O_7.10H_2O$ çözeltisi alternatif FDM olarak önerilmektedir.

Utilization of borax dekahydrate solutions as a phase change material in a cold storage system for precooling process

ARTICLE INFO

Article History:
Received December 14, 2023
Accepted April 10, 2024
Available online June 28, 2024

Research Article

DOI: 10.30728/boron.1405029

Keywords:
Borax decahydrate
Energy saving
Phase change materials
Pre-cooling
Cold storage

ABSTRACT

The pre-cooling process is one of the important stages of cold storage, conducted to prevent the spoilage of fresh vegetables and fruits shortly after harvesting. In this study, a cooling system operating under the conditions of the precooling process was tested with and without phase change materials (PCMs). Water and $Na_2B_4O_7.10H_2O$ solutions at different concentrations were integrated into the system as PCMs. It was revealed that the compressor running time (%) decreased with all PCMs. This value, determined to be 21.05% without PCM, decreased to a value of 12.12% with 1.0 wt.% $Na_2B_4O_7.10H_2O$ solution. Therefore, the maximum reduction in total energy consumption was calculated to be 41.7% with 1.0 wt.% $Na_2B_4O_7.10H_2O$ solution. Additionally, it was observed that the time to reach the internal cabin air temperature to the ambient temperature was approximately 4.3 times longer with 1.0 wt.% $Na_2B_4O_7.10H_2O$ solution than that of the case without PCM during a power failure period. Consequently, 1.0 wt.% $Na_2B_4O_7.10H_2O$ solution is recommended as an alternative PCM to be used in cooling systems employed in the precooling process.

1. Giriş (Introduction)

Gıda ürünlerinin üretimlerinden son tüketiciye ulaşana kadar ki süreçlerde bozunmadan muhafaza edilmeleri çok önemlidir. Bu sebeple, tedarik zincir yönetimi türlerinden biri de soğuk zincir yönetimidir. Soğuk zincir yönetimi, süt, et, gıda, sebze, mantar, meyve, çiçek vb. gibi bozulabilir ürünlerin belirli bir süre içinde dağıtılmasını ve uygun koşullar altında saklanmasını sağlayan bir sistemdir [1]. Dolayısıyla, soğuk depolama bu tedarik zincirinin önemli bir basamağıdır.

Soğuk depolamanın önemli aşamalarından biri ön soğutma işlemi olarak bilinmektedir. Taze sebze ve meyvelerin kalitesinin korunması, hasat süreci sonrası, hasat koşullarına bağlı olarak barındırdıkları tarla ısısı olarak da bilinen ısının depolanma öncesinde hızlı bir şekilde alınmasına oldukça bağlıdır. Bu süreç ön soğutma işlemi olarak adlandırılmakta ve 0-10 ºC sıcaklık aralığında uygulanmaktadır [2]. Literatürde çok farklı ön soğutma uygulamasından bahsedilmiştir [3]. Ön soğutma yöntemleri; soğuk odada ön soğutma, hidro-soğutma, zorlanmış havayla ön soğutma, paket buzlama, vakumla ön soğutma ve kriyojenik soğutma

*Corresponding author: bercem.kiran@marmara.edu.tr

olmak üzere altı başlık altında sınıflandırılabildiği belirtilmiştir [4]. Bu yöntemlerden en bilinen ve yaygın olarak kullanılan uygulamalardan biri, soğuk hava deposunda veya ön soğutma odasında ürünlerin soğutulmasıdır [4]. Ön soğutmanın, ürün kalitesinin uzun süre korunması açısından avantaj sağladığı açıktır, ancak bu amaçla kullanılan sistemlerin tükettikleri enerjinin azaltılmasının da önemli olduğu bilinmektedir. Bu işlem yürütülürken tüketilen enerji miktarını azaltmanın alternatif yollarından biri, soğutma sistemlerinin termal enerji depolamasının en önemli örneklerinden biri olan faz değiştiren malzemeler (FDM'ler) ile çalıştırılmalarıdır. Tüm termofiziksel özelliklerinin bilinmesi, yüksek gizli ısısı ve kararlığı sebebiyle su, FDM olarak tercih edilirken [5,6], literatürde farklı ötektik tuz-su çözeltileri de önerilmektedir [7]. Bir evtipi buzdolabı performansı FDM'siz ve FDM olarak su (H_2O) ve bir ötektik çözeltinin sisteme entegre edildiği durumlarda deneysel olarak incelenmiştir. Ötektik çözelti olarak, faz değişim sıcaklığı -5ºC olan bir sodyum klorür (NaCl) çözeltisi (%90 H_2O+%10 NaCl) hazırlanmıştır. Sonuçlar FDM entegrasyonun performans katsayısını (coefficeint of performance, COP) önemli ölçüde arttırdığını ortaya koyarken ötektik çözeltinin suya göre daha etkin olduğu da belirtilmiştir [8]. Ev tipi bir buzdolabının FDM olarak su ve iki farklı faz değişim sıcaklığına (-2ºC ve -6ºC) sahip ötektik çözeltilerle teorik olarak modellendiği bir çalışmada, deneysel olarak da bir prototip buzdolabı test edilmiştir. Hem simülasyon hem de denklem sonuçları ile kompartman sıcaklığını kabul edilebilir sınırlar içinde tutmak için faz değişim sıcaklığı 0°C'nin altında olan bir ötektik FDM kullanılması gerektiği ortaya konulmuştur [9]. Dolayısıyla, bir soğutma sistemine FDM entegrasyonunda göz önünde bulundururulması gereken en önemli parametrelerden biri FDM'nin faz değişim sıcaklığıdır. Ötektik su-tuz çözeltilerinin FDM olarak tercih edilmelerinin en önemli sebeplerinden biri de faz değişim sıcaklıklarının hazırlanan çözelti konsantrasyonuna bağlı olarak ayarlanabilmesidir. Ancak, FDM'nin faz değişim sıcaklığı yanı sıra, miktarı, konumu ve kalınlığı vb. gibi çeşitli paramtrelerin de dikkate alınması gerekmektedir [10]. Literatürde, çeşitli FDM'lerin özelliklerinin sunulduğu ve FDM'lerin soğutma sistemlerinde kullanımının irdelendiği farklı çalışmaların derlemeleri sunulmuştur [11,12]. Örneğin, Joybari vd. (2015) tarafından sunulan çalışmada, literatürde sunulan çalışmalar göz önünde bulundurularak FDM özelliklerinin yanı sıra, ortam sıcaklığı, kabinin açılıp-kapanma sıklığı vb. gibi dikkate alınan diğer parametrelerde listelenmiştir [12]. Tüm parametreler göz önünde bulundurularak, belirli koşullarda çalışan soğutma sistemlerinin enerji tüketimini minimize edilebildiği uygun FDM'lerin önerilmesi, enerji kaynaklarının korunması ve enerji maliyetlerinin düşürülmesi açısından önemlidir. FDM'lerin soğutma sistemlerinde kullanımlarının sağladığı avantajların sunulduğu kapsamlı çalışmalar literatürde mevcuttur [13,14]. Rocha vd. (2023) 2007-2023 yılları arasında küçük ölçekli soğutma sistemlerinde FDM'lerin kullanımının deneysel olarak incelendiği çalışmalarda kullanılan FDM'ler ve FDM konumlarına bağlı olarak elde edilen önemli sonuçların bir listesini sunmuştur. FDM'lerin sistemlere entegre edildiği durumlarda sağlanan enerji tasarrufları değerlendirildiğinde minimum %4,4 [15] ile maksimum %18,6 [16] arasında değiştiği görülmektedir [14]. Sonuç olarak, soğutma sistemlerine FDM entegrasyonun enerji tasarrufu sağlayacağı açıktır.

Soğutma sistemlerinde FDM kullanımının sağlayacağı enerji tasarrufu göz önünde bulundurularak, bu çalışmada ön soğutma işlemi koşullarında çalıştırılan bir soğutma sistemi FDM'siz ve FDM'li durumlarda test edilmiştir. FDM olarak, su ve Türkiye'de yaygın olarak bulunan bor minerallerinden biri olan tinkalin (boraks dekahidrat, $Na_2B_4O_7.10H_2O$) farklı konsantrasyonlarda hazırlanan çözeltileri kullanılmıştır. Literatürde çeşitli çalışmalarda FDM'ler, aşırı soğuma problemlerine çözüm olması için sodyum tetraborat dekahidrat (boraks dekahidrat) [17,18] gibi nükleasyon ajanlarıyla, faz ayrımının önüne geçilmesi amacıyla ise karboksimetil selüloz (CMC) gibi jelleştirici ajanlarla modifiye edilmiştir [19,20]. Ancak FDM olarak boraks dekahidrat çözeltilerinin soğutma sistemlerine entegre edildiği bir çalışma literatürde sunulmamıştır. Belirtildiği gibi Ülkemizde yaygın olarak bulunması dolaysıyla kolay erişebilir olması ve ucuz olması göz önünde bulunudurularak çalışmamızda ilk olarak boraks dekahidrat çözeltileri FDM olarak bir soğutma sistemine entegre edilmiştir. FDM entegrasyonun çalışma periyodunda kompresör çalışma süresine (%) ve toplam enerji tüketimine etkileri incelenmiştir. İlaveten elektrik kesintisi durumu simüle edilmiş ve kabin iç hava sıcaklığının FDM'siz ve FDM'li durumlarda ortam sıcaklığına ulaşma süreleri kıyaslamalı olarak değerlendirilmiştir. Tüm değerlendirmeler sonucu, ön soğutma amacıyla kullanılan bir soğutma odasının enerji tüketimini minimize eden ve elektrik kesintisi esnasında soğutma odasında ürünlerin uzun süre bozunmadan korunmasını sağlayacak olan uygun FDM belirlenmiştir.

2. Malzemeler ve Yöntemler (*Materials and Methods*)

2.1. Malzemeler (Materials)

Ön soğutma işleminin simüle edildiği laboratuvar ölçekli bir soğutma sistemine entegre edilmek üzere FDM olarak distile su ve Eti Maden Bandırma bor ve asit fabrikalarında üretilen boraks dekahidrat ($Na_2B_4O_7.10H_2O$) rafine bor ürününden farklı konsantrasyonlarda (ağ. %1,0-ağ. %3,0) hazırlanan çözeltiler kullanılmıştır.

2.2. Yöntemler (Methods)

Laboratuvar ölçekli bir soğutma sistemi [21], ön soğutma işlemini simüle etmek üzere 0-10 ºC sıcaklık aralığında FDM'siz ve FDM'li olarak test edilmiştir. Sisteme FDM olarak, su ve $Na_2B_4O_7.10H_2O$ çözeltileri entegre edilmiştir. Boraks dekahidratın ajan olarak eklendiği çalışmalarda ağırlıkça düşük yüzdelerde FDM'lere

ilave edildiği görülmektedir [17,18,20]. Çalışmamızda da boraks dekahidratın çözünürlük verileri de [22,23] dikkate alınarak düşük konsantrasyonlarda (ağ. %1,0-ağ. %3,0) çözeltiler hazırlanmıştır. $Na_2B_4O_7.10H_2O$ çözeltilerinin pH değerinde konsantrasyon artışıyla belirgin bir değişim olmadığı, ağ. %1,0 ve %2,0 $Na_2B_4O_7.10H_2O$ çözeltilerinin pH değerleri 9,2 iken ağ. %4,0 $Na_2B_4O_7.10H_2O$ çözeltisi pH değeri 9,3 olarak ölçüldüğü literatürde belirtilmiştir [23]. FDM çözelti miktarı, literatürde uygun miktar olarak belirtilen 600 mL hacminde [7] hazırlanmıştır. Çözeltiler aluminyum kaplara yerleştirilmiş ve şarj etmek üzere dondurucuda (-18ºC) yatay olarak dondurulmuştur.

Soğutma sistem komponentleri kabin içine yerleştirilmiş bir evaporatör, bir kompresör, bir kondenser, bir genleşme valfidir. Şarj edilen FDM paketleri evaporatör yüzeyine entegre edilmiştir. Soğutucu akışkan olarak R404A sistemde sirküle edilmiştir. Sistemin bulunduğu ortam klimatize edilerek 20ºC'de kararlı rejim şartları sağlanmıştır. Soğutucu akışkanın sistem komponentlerine giriş-çıkış sıcaklıkları, anlık güç tüketim verileri ölçülmüş ve kaydedilmiştir. Her bir deney en az üç defa tekrar edilmiş ve ortalama değerler dikkate alınarak değerlendirmeler yapılmıştır. Deneysel çalışma sonunda elde edilen verilerden kompresör çalışma süresi (%) (Eş. 1), toplam güç tüketimi (Eş. 2) ve enerji tasarrufu (%) (Eş. 3) değerleri hesaplanmıştır. Eş. 1'de, $t_{açık}$ kompresörün açık kalma süresi (dakika), $t_{kapalı}$ kapalı kalma süresini (dakika) göstermektedir. *W(t)* çalışma periyodu boyunca (4 saat) toplam güç enerji tüketim değeri (kJ), *W(t)* ise anlık güç tüketim değeridir (kW). *W* FDM'siz durumda, W_{FDM} ise FDM'li durumda toplam enerji tüketim değerleridir. Soğutma sistemi, çalışma periyodunun ardından, elektrik kesintisinin simüle edildiği durum için de FDM'siz ve FDM'li olarak test edilmiştir. Her iki durumda da elektrik kesintisi esnasında kabin iç hava sıcaklığının, ortam sıcaklığına ulaşma süreleri tespit edilmiştir.

$$\text{Çalışma Süresi}(\%) = \frac{t_{açık}}{t_{açık}+t_{kapalı}} \text{ x } 100 \quad (1)$$

$$W(t) = \int_{t=0\ saat}^{t=4\ saat} \dot{W}(t)dt \quad (2)$$

$$\text{Eneji Tasarrufu}(\%) = \frac{W_{FDM}-W}{W} \text{ x } 100 \quad (3)$$

3. Sonuçlar ve Tartışma (Results and Discussion)

Laboratuvar ölçekli bir soğutma sistemi, ön soğutma amaçlı kullanılan bir soğutma sistemini simüle etmek üzere 0-10 ºC sıcaklık aralığında FDM'siz ve FDM olarak, su ve ağ. %1,0-ağ. %3,0 konsantrasyonlarında hazırlanan $Na_2B_4O_7.10H_2O$ çözeltileri ile test edilmiştir. Kabin iç hava sıcaklığının 2 saatlik çalışma periyodu için FDM'siz ve FDM'lerin sisteme entegre edildiği durumlarda zamanla değişmi Şekil 1'de sunulmuştur. Şekil 1'de sunulan 2 saatlik çalışma periyodunda, FDM'siz durumda 6,3 olan döngü sayısının tüm FDM'lerle azaltıldığı görülmektedir. Döngü sayısı, su, ağ. %1,0 $Na_2B_4O_7.10H_2O$, ağ. %2,0 $Na_2B_4O_7.10H_2O$ ve ağ. %3,0 $Na_2B_4O_7.10H_2O$ çözeltileri ile sırasıyla, 4,4, 3,6, 4,3 ve 4,6 olarak belirlenmiştir. Minimum döngü sayısının ağ. %1,0 $Na_2B_4O_7.10H_2O$ çözeltisi ile elde edildiği görülmektedir. Döngü sayısında ki azalmanın kompresör açık ya da kapalı kalma süresinin uzaması ile ilişkili olabileceği bilinmektedir. Sistem toplam enerji tüketimi ise kompresör kapalı kalma süresinin uzaması ile sağlanacaktır.

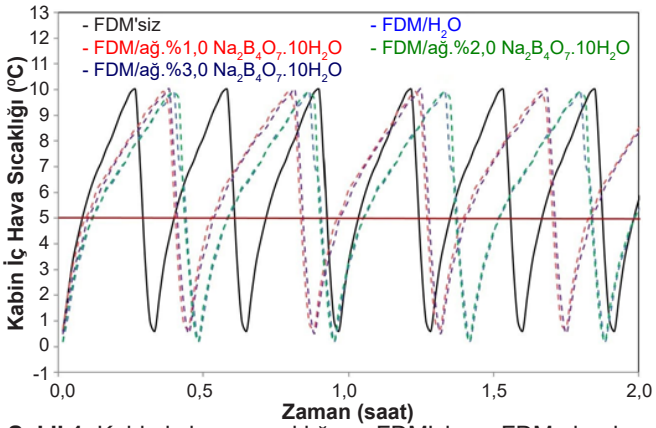

Şekil 1. Kabin iç hava sıcaklığının FDM'siz ve FDM olarak su ve $Na_2B_4O_7.10H_2O$ çözeltileri ile değişimi (2 saat) (Variation of cabin air temperature without PCM and with water and $Na_2B_4O_7.10H_2O$ solutions as PCM (2 hours)).

FDM'lerin entegre edildiği durumlarda belirlenen döngü sayılarında ki kompresör kapalı kalma süreleri Tablo 1'de sunulmuştur. Tablo 1 incelendiğinde FDM'siz ve FDM'li durumlarda kompresör açık kalma süresinin değişmediği, ancak FDM'siz durumda tespit edilen kapalı kalma süresinin FDM'li durumlarda arttığı görülmektedir. Kompresör açık ve kapalı kalma süreleri, Eş. 1 kullanılarak, çalışma süresi (%) değerlerinin hesaplanılması için kullanılmıştır. FDM'siz durumda %21,05 olarak hesaplanan çalışma süresinin, tüm FDM'lerle azaldığı görülmektedir. Kapalı kalma süresinde ki uzama FDM'lerle kompresör çalışma süresi (%) değerlerinin azalmasını sağlanmaktadır. Çalışma süresi değeri su, ağ. %1,0 $Na_2B_4O_7.10H_2O$, ağ. %2,0 $Na_2B_4O_7.10H_2O$ ve ağ. %3,0 $Na_2B_4O_7.10H_2O$ çözeltileri ile sırasıyla, 14,81, 12,12, 14,29, 15,38 olarak hesaplanmıştır. Çalışma süresi değeri ağ. %1,0 $Na_2B_4O_7.10H_2O$ çözeltisi ile minimum değerine ulaştığı tespit edilmiştir.

Tablo 1. FDM'siz ve FDM'li durumlarda kompresör çalışma süresi (%) değerleri (The running time (%) values.in the cases of with and without PCM).

FDM	Konsantrasyon (ağ. %)	$t_{açık}$ (dk)	$t_{kapalı}$ (dk)	Döngü Süresi (dk)	Çalışma Süresi (%)
-	-	4	15	19	21,05
Su	-	4	23	27	14,81
$Na_2B_4O_7.10H_2O$ Çözeltisi	1,0	4	29	33	12,12
	2,0	4	24	28	14,29
	3,0	4	22	26	15,38

Soğutma sisteminde anlık olarak kompresör güç tüketim değerleri de kaydedilmiş ve değerler FDM'siz ve FDM'li durumlar için Şekil 2'de sunulmuştur.

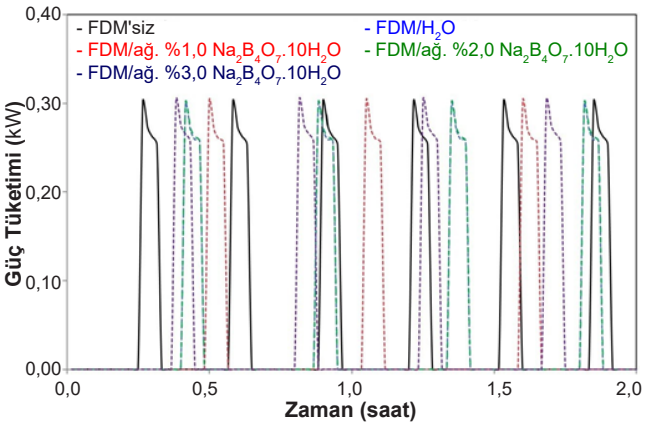

Şekil 2. Kompresör güç tüketiminin FDM'siz ve FDM olarak su ve $Na_2B_4O_7.10H_2O$ çözeltilerinin entegre edildiği durumlarda değişimi (2 saat) (Variation of compressor power consumption without PCM and with water and $Na_2B_4O_7.10H_2O$ solutions as PCM (2 hours)).

Kompresör anlık güç tüketim değeri incelendiğinde, FDM'siz durumda güç tüketim değerleri 0,301 kW ve 0,253 kW arasında değişirken, FDM olarak suyun kullanıldığı durumda 0,298 kW ve 0,258 kW arasında değiştiği tespit edilmiştir. FDM olarak ağ. %1,0, ağ. %2,0 ve ağ. %3,0 $Na_2B_4O_7.10H_2O$ çözeltileri kullanıldığında maksimum ve minimum güç tüketim değerleri ise sırasıyla, 0,302 kW-0,256 kW, 0,300 kW-0,257 kW, 0,303 kW-0,256 kW olarak tespit edilmiştir. Anlık güç tüketim değerlerinden Eş. 2 kullanılarak, çalışma periyodu için toplam güç tüketim değerleri hesaplanmıştır. FDM'siz durumda 13,07 kJ olarak hesaplanan toplam enerji tüketim değerinin tüm FDM'lerle azaldığı belirlenmiştir. Bu değer, FDM olarak, su ve ağ. %1,0, ağ. %2,0, ağ. %3,0 $Na_2B_4O_7.10H_2O$ çözeltileri ile sırasıyla, 8,99 kJ, 7,62 kJ, 8,74 kJ ve 9,89 kJ olarak hesaplanmıştır. Elde edilen değerlerden Eş. 3 kullanılarak, FDM'lerle enerji tüketiminde ki düşüş (%) hesaplanmıştır. FDM olarak, su ve ağ. %1,0, ağ. %2,0, ağ. %3,0 $Na_2B_4O_7.10H_2O$ çözeltileri ile enerji tasarrufu sırasıyla, %31,2, %41,7, %33,1, %24,3 olarak hesaplanmıştır. Çalışma süresinin minimize edildiği durumda, ağ. %1,0 $Na_2B_4O_7.10H_2O$ çözeltisi ile, beklenildiği gibi enerji tasarrufunun maksimize edildiği belirlenmiştir.

Soğutma sisteminde, çalışma periyodunun ardından elektrik kesintisi durumu simüle edilmiştir. Elektrik kesintisi esnasında, FDM'siz ve FDM'li durumlarda kabin iç hava sıcaklığının ortam sıcaklığına ulaşma süreleri tespit edilmiş ve Şekil 3'de sunulmuştur. Şekil 3 incelendiğinde, kabin iç hava sıcaklığının ortam sıcaklığı 20 ºC'ye ulaşma süresi FDM'siz durumda 115 dakika iken, bu süre tüm FDM'lerle uzamıştır. FDM olarak, su, ağ. %1,0 ve ağ. %3,0 $Na_2B_4O_7.10H_2O$ çözeltileri ile kabin iç hava sıcaklığının ortam sıcaklığına ulaşma süresi sırasıyla 426 dakika, 490 dakika ve 420 dakika olarak tespit edilmiştir. Bu sürenin ağ. %1,0 $Na_2B_4O_7.10H_2O$ çözeltisi ile maksimize edildiği ve FDM'siz durumda belirlenen sürenin 4,3 katına çıktığı belirlenmiştir.

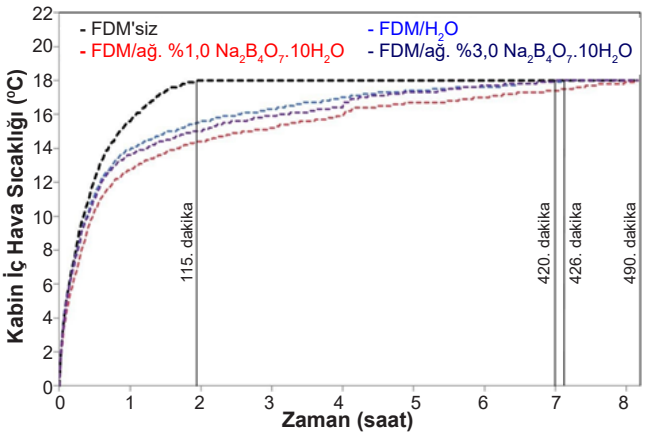

Şekil 3. Elektrik kesintisi periyodunda FDM'siz ve FDM olarak su ve $Na_2B_4O_7.10H_2O$ çözeltilerinin entegre edildiği durumlarda kabin iç hava sıcaklığının zamanla değişimi (Cabinet air temperature versus time in the cases of without PCM and with water and $Na_2B_4O_7.10H_2O$ solutions as PCMs during the power failure period).

Çalışma süresi (%), toplam enerji tüketimi ve enerji tasarrufu (%) değerleri ve elektrik kesintisi esnasında kabin iç hava sıcaklığının ortam sıcaklığına ulaşma süreleri, FDM'siz ve FDM'li durumlar için kıyaslamalı olarak, Tablo 2'de sunulmuştur. Tablo 2'de sunulan tüm sonuçlar değerlendirildiğinde, FDM olarak ağ. %1,0 $Na_2B_4O_7.10H_2O$ çözeltisi sisteme entegre edildiğinde çalışma süresinin (%) ve toplam enerji tüketiminin minimize edildiği, dolayısıyla enerji tasarrufu maksimize edildiği görülmektedir. Buna ek olarak, elektirik kesintisi esnasında kabin iç hava sıcaklığının ortam sıcaklığına ulaşma süresinin FDM'siz duruma göre ağ. %1,0 $Na_2B_4O_7.10H_2O$ çözeltisi ile maksimize edildiği belirlenmiştir. Dolayısıyla, ağ. %1,0 $Na_2B_4O_7.10H_2O$ çözeltisi sisteme entegre edildiğinde kabin içinde ki ürünler daha uzun süre bozunmadan korunabilecektir. Ön soğutma işlemi yürütülen bir soğutma sistemine FDM olarak, bor minerallerinden borik asitin iki farklı konsantrasyonunda (ağ. %2,0 ve ağ. %4,0) hazırlanan çözeltilerin test edildiği çalışmada da FDM'siz duruma kıyasla toplam enerji tüketiminin FDM'lerle azaltıldığı tespit edilmiştir. Kompresör çalışma süresi ağ. %2,0 borik asit çözeltisi sisteme entegre edildiğinde minimize (%13,79) edilirken, sağladığı enerji tasarrufunun (%33,8) maksimum değere ulaştığı belirlenmiştir. Elektrik kesintisinin simüle edildiği durumda ise kabin iç hava sıcaklığının ortam sıcaklığına (20 ºC) ulaşma süresinin 429 dakika olduğu tespit edilmiştir. Tüm sonuçlar değerlendirildiğinde ağ. %2,0 borik asit çözeltisinin uygun bir FDM olduğu ortaya konulmuştur [24]. Önerilen ağ. %2,0 borik asit çözeltisi ile belirlenen kompresör çalışma süresi, çalışmamızda kullanılan $Na_2B_4O_7.10H_2O$ çözeltileriyle elde edilen sonuçlarla kıyaslandığında ağ. %1,0 ve ağ. %2,0 $Na_2B_4O_7.10H_2O$ çözeltileri ile sırasıyla %12,12 ile %14,29 olarak

tespit edilen değerlerin arasındadır. Tüm sonuçlar değerlendirildiğinde, kompresör çalışma süresinin ağ. %1,0 $Na_2B_4O_7.10H_2O$ çözeltisi ile minimize edildiği görülmektedir. Böylelikle, bu FDM'nin sistemde kullanımının kompresör ömrünün arttırılmasına olanak sağlanacağı ortaya konulmuştur. FDM seçiminde faz değişim sıcaklığı ve gizli ısı değeri vb. gibi önemli özelliklerinin yanı sıra malzemenin çekirdeklenme hızı ve büyüme hızı yani kinetik özelliklerinin de dikkate alınması gerektiği bilinmektedir [25-27]. Tüm bu özelliklerin bileşik etkisi uygun FDM seçimini belirlemektedir. Elde edilen tüm sonuçlar ağ. %1,0 $Na_2B_4O_7.10H_2O$ çözeltisi ile kompresör çalışma süresi minimize edilerek enerji tasarrufunun maksimize edildiğini ortaya koymuştur, dolayısıyla alternatif bir FDM olarak önerilmektedir. Elde edilen tüm deneysel sonuçlar incelendiğinde, ön soğutma prosesinde sisteme FDM olarak ağ. %1,0 $Na_2B_4O_7.10H_2O$ çözeltisinin entegrasyonuyla maksimum enerji tasarruf sağlanmasının yanı sıra elektrik kesintisi esnasında ürünlerin kalitesinin daha uzun süreli korunabileceği ortaya konulmuştur.

Tablo 2. Çalışma süresi (%), toplam enerji tüketimi ve enerji tasarrufu (%) değerlerinin FDM'siz ve FDM olarak $Na_2B_4O_7.10H_2O$ çözeltilerinin entegre edildiği durumlarda değişimleri (Variations of the running time (%), total energy consumption and energy saving values in the cases of without PCM and with $Na_2B_4O_7.10H_2O$ solutions as PCMs).

FDM	FDM'siz	H_2O/FDM	$Na_2B_4O_7.10H_2O$/ FDM		
			%1,0	%2,0	%3,0
Çalışma Süresi (%)	21,05	14,81	**12,12**	14,29	15,38
Toplam Enerji Tüketimi (kJ/4 saat)	13,07	8,99	**7,62**	8,74	9,89
Enerji Tasarrufu (%)	-	- 31,2	**- 41,7**	- 33,1	- 24,3
Elektrik Kesintisi Esnasında Kabin İç Hava Sıcaklığının Ortam Sıcaklığına Ulaşma Süresi (dk)	115	426	**490**	-	420s

4. Sonuçlar (Conclusions)

Laboratuvar ölçekli bir soğutma sisteminin ön soğutma amaçlı kullanılan bir soğutma sistemini simüle etmek üzere 0-10 ºC sıcaklık aralığında FDM'siz ve FDM olarak, su ve ağ. %1,0-ağ. %3,0 konsantrasyonlarında hazırlanan $Na_2B_4O_7.10H_2O$ çözeltileri ile test edilmiştir. FDM'siz durumda çalışma süresi %21,05 olarak belirlenirken, tüm FDM'lerle bu değerin azaldığı tespit edilmiştir. Çalışma süresi, FDM olarak, su ve ağ. %1,0 $Na_2B_4O_7.10H_2O$, ağ. %2,0 $Na_2B_4O_7.10H_2O$, ağ. %3,0 $Na_2B_4O_7.10H_2O$ çözeltileri sisteme entegre edildiğinde sırasıyla, 14,81, 12,12, 14,29, 15,38 olarak bulunmuştur. Çalışma süresi değerinin ağ. %1,0 $Na_2B_4O_7.10H_2O$ çözeltisi ile minimize edildiği tespit edilmiştir. Toplam güç tüketiminin tüm FDM'lerle, FDM'siz durumda belirlenen (13,07 kJ) değerden daha düşük olduğu belirlenmiştir. FDM olarak, su ve ağ. %1,0, ağ. %2,0, ağ. %3,0 $Na_2B_4O_7.10H_2O$ çözeltileri ile toplam güç tüketiminin sırasıyla, 8,99 kJ, 7,62 kJ, 8,74 kJ ve 9,89 kJ değerlerine düştüğü ortaya konulmuştur. Sonuç olarak, FDM'lerle sağlanan enerji tasarrufu değerleri ise sırasıyla, %31,2, %41,7, %33,1, %24,3 olarak hesaplanmıştır. Elektrik kesintisinin simüle edildiği durumda, FDM'siz durumda 115 dakika olan kabin iç hava sıcaklığının ortam sıcaklığına ulaşma süresinin FDM'lerle önemli ölçüde uzadığı belirlenmiştir. Bu süre, FDM olarak, su, ağ. %1,0 ve ağ. %3,0 $Na_2B_4O_7.10H_2O$ çözeltileri sisteme entegre edildiği durumlarda sırasıyla, 426 dakika, 490 dakika ve 420 dakika olarak tespit edilmiştir. Tüm sonuçlar incelendiğinde, ön soğutma işleminin yürütüldüğü soğutma sistemlerinde kullanılmak üzere alternatif bir FDM olarak ağ. %1,0 $Na_2B_4O_7.10H_2O$ çözeltisi önerilmektedir. Bu çözeltinin belirtilen koşullarda çalışan sistemlere entegre edilmesinin önemli ölçüde enerji tasarrufu (%41,7) sağlayacağı ortaya konulmuştur. Buna ek olarak, elektrik kesintisi esnasında kabin iç hava sıcaklığının ani yükselişinin ağ. %1,0 $Na_2B_4O_7.10H_2O$ çözeltisi ile engellenebileceği, dolayısıyla kabin içinde bulunan ürünlerin uzun süre bozunmadan korunmasına olanak sağlanabileceği ortaya konulmuştur.

Yazar Katkısı Beyanı (Author Contribution Statement)

Berçem Kıran Yıldırım: Deneysel çalışmanın planlanması ve tasarlanması, kaynak sağlama, deneylerin yürütülmesi, elde edilen verilerin analiz edilmesi ve yorumlanması, makalenin yazılması,

Ebru Mançuhan: Kaynak sağlama, deneysel verilerin analiz edilmesi ve yorumlanması, makale metninin incelenmesi ve düzenlenmesi,

Sibel Titiz Sargut: Kaynak sağlama, deneysel verilerin analiz edilmesi ve yorumlanması, makale metninin incelenmesi ve düzenlenmesi

konularında katkıda bulunmuşlardır.

Teşekkürler (Acknowledgements)

Eti Maden Bandırma Bor ve Asit Fabrikaları İşletme Müdürlüğü'ne boraks dekahidrat rafine bor numune temini için teşekkür ederiz.

Kaynaklar (References)

[1] Shabani, A., Saen, R. F., & Torabipour, S. M. R. (2012). A new benchmarking approach in Cold Chain. *Applied Mathematical Modelling*, *36*(1), 212-224. https://doi.org/10.1016/j.apm.2011.05.051.

[2]. Altun, Ö., Aslantaş K., & Sökmen, E. (2020). Design of a Cold Storage Depot Using R744 as Refrigerant with Two Evaporators in Eskisehir. *Soğutma Dünyası*, *23*(88), 50-57. https://drive.google.com/file/d/14L8goNN2k9vGXdr

5v0G41PareShHwV84/view.

[3]. Thakur, B. (2016). Advancement in harvesting, pre-cooling and grading of fruits. *Innovare Journal of Agricultural Science*, *4*(2), 13-23. ISSN 2321-6832. https://journals.innovareacademics.in/index.php/ijags/article/view/6802/4961.

[4]. Brosnan, T., & Sun, D. W. (2001). Precooling techniques and applications for horticultural products-a review. *International Journal of Refrigeration*, *24*(2), 154-170. https://doi.org/10.1016/S0140-7007(00)00017-7.

[5]. Azzouz, K., Leducq, D., & Gobin, D. (2009). Enhancing the performance of household refrigerators with latent heat storage: An experimental investigation. *International Journal of Refrigeration*, *32*(7), 1634-1644. https://doi.org/10.1016/j.ijrefrig.2009.03.012.

[6]. Yusufoglu, Y., Apaydin, T., Yilmaz, S., & Paksoy, H. O. (2015). Improving performance of household refrigerators by incorporating phase change materials. *International Journal of Refrigeration*, *57*, 173-185. https://doi.org/10.1016/j.ijrefrig.2015.04.020.

[7]. Kiran-Yildirim, B. (2022). Performance evaluation of a laboratory-scale cooling system as a household refrigerator with phase change materials. *Energy Sources, Part A: Recovery, Utilization, and Environmental Effects*, *44*(3), 5852-5867. https://doi.org/10.1080/15567036.2022.2089300.

[8]. Khan, M. I. H. & Afroz H. M. M. (2013). Effect of Phase Change Material on Performance of a Household Refrigerator. *Asian Journal of Applied Sciences*, *6*, 56-67. https://doi.org/10.3923/ajaps.2013.56.67

[9]. Marques, A. C., Davies, G. F., Evans, J. A., Maidment, G. G., & Wood, I. D. (2013). Theoretical modelling and experimental investigation of a thermal energy storage refrigerator. *Energy*, *55*, 457-465. https://doi.org/10.1016/j.energy.2013.03.091.

[10]. Khan, M. I. H. (2016). Conventional refrigeration systems using phase change material: a review. International *Journal of Air-Conditioning and Refrigeration*, *24*(03), 1630007. https://doi.org/10.1142/S201013251630007X.

[11]. Oró, E., De Gracia, A., Castell, A., Farid, M. M., & Cabeza, L. F. (2012). Review on phase change materials (PCMs) for cold thermal energy storage applications. *Applied Energy*, *99*, 513-533. https://doi.org/10.1016/j.apenergy.2012.03.058.

[12]. Joybari, M. M., Haghighat, F., Moffat, J., & Sra, P. (2015). Heat and cold storage using phase change materials in domestic refrigeration systems: The state-of-the-art review. Energy Buildings, 106, 111-124. https://doi.org/10.1016/j.enbuild.2015.06.016.

[13]. Le, T. L., Duong, X. Q., Nguyen, D. T., Nguyen, P. Q. P., Rajamohan, S., Vo, A. V., & Le, H. S. (2023). Application of phase change materials in improving the performance of refrigeration systems. *Sustainable Energy Technologies and Assessments*, *56*, 103097. https://doi.org/10.1016/j.seta.2023.103097.

[14]. Rocha, T. T. M., Teggar, M., Trevizoli, P. V., & de Oliveira, R. N. (2023). Potential of latent thermal energy storage for performance improvement in small-scale refrigeration units: A review. *Renewable and Sustainable Energy Reviews*, *187*, 113746. https://doi.org/10.1016/j.rser.2023.113746.

[15]. Sekhar, S. J., Raj, M. A. F., Raveendran, P. S., & Murugan, P. C. (2022). Cladding phase change materials in freezing and chilling zones of household refrigerator to improve thermal performance and environmental benefits. *Journal of Energy Storage*, *55*, 105476. https://doi.org/10.1016/j.est.2022.105476.

[16]. Yilmaz, D., Mancuhan, E., & Yılmaz, B. (2020). Experimental investigation of PCM location in a commercial display cabinet cooled by a transcritical CO2 system. *International Journal of Refrigeration*, *120*, 396-405. https://doi.org/10.1016/j.ijrefrig.2020.09.006.

[17]. Kalidasan, B., Pandey, A. K., Rahman, S., Khir, H., & Zaed, M. A. (2024). Experimental investigation on nucleating agent for low temperature binary eutectic salt hydrate phase change material. E3S *Web of Conferences*, *488*, 01004. https://doi.org/10.1051/e3sconf/202448801004.

[18]. Hou, P., Mao, J., Chen, F., Li, Y., & Dong, X. (2018). Preparation and thermal performance enhancement of low temperature eutectic composite phase change materials based on Na2SO4· 10H2O. *Materials*, *11*(11), 2230. https://doi.org/10.3390/ma11112230.

[19]. Zhao, L., Xing, Y., Liu, X., & Luo, Y. (2018). Thermal performance of sodium acetate trihydrate based composite phase change material for thermal energy storage. *Applied Thermal Engineering*, *143*, 172-181. https://doi.org/10.1016/j.applthermaleng.2018.07.094.

[20]. Liang, Q., Zhang, H., Li, Y., Zhang, X., & Pan, D. (2024). Multifunctional response of biomass carbon/sodium sulfate decahydrate composite phase change materials. *Journal of Energy Storage*, *83*, 110621. https://doi.org/10.1016/j.est.2024.110621.

[21]. Kiran-Yildirim, B., T. Noya, E. Mancuhan, & S. Titiz-Sargut. (2021). Investigation of Energy Consumption for a PCM Integrated Laboratory Scale Cooling System: An Experimental Study. *23rd Congress on Thermal Science and Technology with International Participation (ULIBTK 2021), Turkiye*. *1*, 1002-1008. https://drive.google.com/drive/folders/1dmF8npoQu3qAe3NCtv0xLElqJyi-jIRD.

[22]. Lide, D. R. (2009). *CRC handbook of chemistry and physics* (90th Edition). CRC press. ISBN 9781420090840.

[23]. Smith, R. A., & McBroom, R. B. (2000). Boron oxides, boric acid, and borates. *Kirk-Othmer Encyclopedia of Chemical Technology*. https://doi.org/10.1002/0471238961.0215181519130920.a01.

[24]. Kıran Yıldırım, B., Düzgün, E., Kül, B., Gök, S., Mançuhan, E., Sargut, S., & Ersoy, A. (2023). Ön Soğutma İşlemi Yapılan Bir Soğuk Depolama Sisteminde Enerji Tüketiminin Faz Değişim Malzemesi Kullanılarak İncelenmesi [Examination of Energy Consumption in a Cold Storage System used for the precooling process with Phase Change Material], 15. Ulusal Kimya Mühendisliği Kongresi (UKMK-15) [*15. National Chemical Engineering Congress (UKMK-15)], Türkiye*, *782-785*. https://drive.google.com/file/d/1NtbxaLs0CqKo9Z4nJNKk-mbrP_HVkx43/view.

[25]. Lane, G. A. (1983). *Solar Heat Storage* (Volume I: Latent Heat Material). CRC Press. https://doi.org/10.1201/9781351076753.

[26]. Garg, H. P., Mullick, S. C., & Bhargava, A. K. (1985). *Solar Thermal Energy Storage*. Springer Dordrecht. https://doi.org/10.1007/978-94-009-5301-7.

[27]. Tek, Y. (2009). *Synthesis, characterization and physicochemical properties of urea and thiourea-fatty acid condensation compounds* (Thesis No. 244875). [Master's thesis, Gaziosmanpaşa University]. Council of Higher Education.

BOR DERGİSİ
JOURNAL OF BORON
https://dergipark.org.tr/boron

Investigation of flexural properties of hexagonal boron nitride added thermoplastic composites

Özgür Demircan [1,*], **Adnan Kalaycı** [1]

[1]*Ondokuz Mayıs University, Faculty of Engineering, Department of Metallurgical and Materials Engineering, Samsun, 55139, Türkiye*

ARTICLE INFO

Article history:
Received December 6, 2023
Accepted May 8, 2024
Available online June 28, 2024

Research Article

DOI: 10.30728/boron.1401096

Keywords:
Flexural test
Hexagonal boron nitride (h-BN)
Short glass fiber reinforced polyamide 66
Thermoplastic composite

ABSTRACT

In this study, 0, 0.5 and 2 wt% hexagonal boron nitride (hBN) were added to 30 wt% short glass fiber reinforced polyamide 66 (PA 66) matrix (GF30) to fabricate the thermoplastic composite materials. The hBN additives were applied by coating of granules of GF30 materials. The hBN coated thermoplastic materials were produced by plastic injection method. The effect of various weight percentages of hBNs on the flexural properties of thermoplastic composites were examined in the produced samples. The produced samples were subjected to three-point bending tests. Fourier transform infrared spectroscopy (FTIR), X-ray diffraction (XRD) and Scanning electron microscopy (SEM) were used to analyse structural and physical properties of the composites. The highest enhancement of flexural properties was obtained from the sample of PA 66/GF30/2% hBN. The samples with 2 wt% hBN showed the best flexural properties with an improvement of 85 and 52% flexural modulus and strength, respectively, compared to the samples without hBN (PA 66/GF30). According to the obtained results of this study, as the percentage of the hBN weight contents increased, the flexural strengths and flexural modulus increased significantly. It was concluded that hBN coated thermoplastic composite samples demonstrated high improvements for flexural properties at optimum rates of hBN.

1. Introduction

Hexagonal boron nitride (hBN) nanomaterials have excellent mechanical and thermal properties. Nanomaterials of hBNs can be used in thermoplastic composites in order to increase their mechanical and thermal properties. Mechanical and thermal properties of hBN reinforced polymeric composites have been investigated by several researches as shown in Table 1.

A comparison of injection moulding, powder bed fusion and casting was studied by Andreassen et al. [1]. They found that addition of hBN increased the elastic modulus and strength at high hBN ratios. Effect of hBN on mechanical properties of polyamide 6/glass fibers (5 wt%) nanocomposites was reported by Pramanik et al. [2]. They found the overall mechanical properties of PA6/5GF/hBN nanocomposites at 1 wt% hBN, significantly increased compared to other developed PA6/5GF/hBN composites. Travas et al. [3]. studied tensile performance of high-density polyethylene by addition of expanded graphite and BN. They found that at a high percentage of additives, the elastic modulus increased by 105% and 91%. Producing polyamide/BN nanocomposites with high thermal conductivities and mechanical properties was reported by Park et al. [4]. They showed that enhanced mechanical properties for the composites were obtained by 20 wt% of hBN content. The structural and mechanical performance of boron nanoparticle reinforced nanocomposites and bonded joints exposed to an acid environment were studied by Gültekin et al. [5]. They found that boron nanoparticles reinforced composites showed higher mechanical properties.

Ashrafi et al. studied [6] multifunctional thermoplastic composite materials using BN and carbon nanotubes in different ratios (0.5%, 1%, 2%, 5 wt%). According to the results of the study, the elastic modulus of BN composites had a higher value than that of carbon nanotube composites. Ayrilmis et al. [7] examined the mechanical properties of thermoplastic matrix (high-density polyethylene (HDPE) and polypropylene (PP)) composite materials using poplar wood flour (50 wt%) and BN (2%, 4%, and 6 wt%). With the addition of BN, the flexural strength of poplar/PP composites increased from 28.2 MPa to 43.7 MPa and the flexural strength of poplar/HDPE composites increased from 25.5 MPa to 33 MPa. Cai et al. [8] examined the thermal stability, flame retardancy, and mechanical properties of composite materials with polyurethane matrix using the chemically functionalized form of inert hBN (cetyl-trimethylammonium bromide, 0-4 wt%). According to

*Corresponding author: ozgur.demircan@omu.edu.tr

Table 1. Some studies of hBN/polymer composites.

Nanomaterials	Integration Technique	Optimum Loading	Mechanical Properties	Reference
hBN	Coating with PA 66	0, 0.5, 2% wt% hBN	85 % increase in flexural modulus 52% increase in flexural strength	Ozgur et al. [this research]
	Dry mixing with PA 66	0.5, 1, 3 wt% hBN	13.6% increase in hardness, 13.8% increase in tensile strength	Pramanik et al. [2]
	Mixing the components with PA 66 withplasmaassisted mechanochemistry (PMC)	1, 5, 10, 20 wt% hBN	Enhanced mechanical properties for the composites were obtained by 20 wt% of h-BN content	Park et al. [4]
Expanded graphite (EG), BN	Mixing the components with high-density polyethylene (HDPE) in heating	80-5-15, 70-8-22, 70-15-15, 60-25-15, 84-8-8	105% and 91% increase in elastic modulus at a high percentage of additives	Travas et al. [3]
BN and boron carbide (B_4C)	Mixing with epoxy	2 wt% of BN/B_4C	Boron nanoparticles reinforced composites showed higher mechanical properties	Gültekin et al. [5]
BN nanotubes, Carbon nanotubes	Mixing with epoxy	0.5, 1.0, 2.0, 5.0 wt% BNNT and 1.0, 2.0 wt% CNT	2.40 GPa of elastic modulus in epoxy 2 wt% BNNT 2.08 GPa of elastic modulus in epoxy 2 wt% CNT	Ashrafis et al. [6]
Cetyl-trimethylammonium bromide-BN	Solvent blending and co-coagulation of thermoplastic polyurethane-based composites	0, 1, 2, 4 wt% hBN	79.3% increase in tensile strength	Cai et al. [8]
BN	Mixing with vinylester resins	0, 0.5, 1, 1.5, 2% wt% hBN	The ideal values were obtained with the addition of 1% BN	Boztoprak et al. [10]
BN (1-2 µm) **BN (7-10 µm)**	Compression molding with PP	15, 21 and 29 vol% byBN	The thermal conductivity and storage modulus of BN with large particles increased	Cheewawuttipong et al. [16]

the results, the heat dissipation rate of polyurethane composites with nano-filler addition of 4.0% hBN and the maximum value of total heat dissipation decreased by 57.5% and 17.8%, respectively. In addition, the tensile strength of the polyurethane composite increased by 79.3% compared to that of the pure polyurethane composites with the addition of 2.0 wt% hBN. Yu et al. [9] examined the thermal conductivity of epoxy matrix composites by using vertically oriented hBN (10-30 µm, 12-44 vol%). With the increase in hBN content, an increase in thermal conductivity was observed. When 44% hBN was used, the thermal conductivity was 9W/m.K. However, there was a significant decrease in tensile strength when 44% hBN was used. Boztoprak et al. [10] studied the mechanical properties of composite materials with vinyl ester matrix and BN particles. As a result of the research, there was an increase in the hardness of composite samples and the abrasion resistance and impact strengths were improved. Göncü et al. [11] investigated the effect of hBN addition on composite materials with alumina matrix. It was determined that hBN additive reduced the density of composite samples. It was also concluded that hBN additives acted as a lubricant. Owing to having a similar crystal structure to hydroxyapatite, the addition of hBN improves the mechanical properties of the host materials. Such improvements in the contribution of boron compounds in biomedical applications would increase in the future.

Furthermore, Taşdelen et al. [12] investigated the mechanical properties of PA 66 material. It was found that the tensile strength of PA 6 material was 82 MPa. Kaştan et al. [13] examined the mechanical properties of nanoclay-integrated PA thermoplastic composite materials. It was determined a maximum of 30 MPa of the flexural strength for the PA material. Karslı et al. [14] investigated the choice of polymer composite material for light weapons. In their research, it was stated that the tensile strength of PA 66 GF30 material was 155 MPa.

Oz et al. studied the thermal behaviour of hBN in an open atmosphere [15]. It was shown that BN was like the carbon structure, but it showed resistance to higher temperatures compared to similar carbon allotropes. It was mentioned that BN can be used as an additive in polymers and in other industrial applications. It has been explained that the crystal sizes of BNs were different from each other. Cheewawuttipong et al. [16] examined the thermal conductivity of composites with PP matrix using BN in different ratios (15%, 21%, and 29 vol%) and sizes (1-2 μm and 7-10 μm). According to their results, the thermal conductivity of BNs with large particles increased compared to small particles. Isarn et al. [17] examined the thermal conductivity of BN-filled (0%, 10, 20, 30, 40, (6 μm) and 40 wt% (80 μm (batch)) and thiol-epoxy matrix thermoset composites. Composites with a size of 6 μm and containing 40 wt% BN increased thermal conductivity by 400% from 0.2 W/K.m to 0.97 W/K.m, and when a bulk BN containing 40 wt% BN was used, the thermal conductivity values of the composites increased by 775% from 0.2 W/K.m to 1.75 W/K.m. Harrison et al. examined [18] the radiation protection of polyethylene matrix composites with BN (15 vol%) in the application of spacecraft. According to the results, using 2 wt% BN showed high radiation protection compared to the pure PP composite material. Zhou et al. [19] examined the thermal and electrical properties of epoxy matrix composites using intermittent hBN (0.5 μm, 50 wt%). Composites treated with silane-modified BN showed high thermal conductivity compared to the silane-free state. A low dielectric permeability (less than 5.4) and dielectric loss (less than 0.02), high volume resistivity ($6.3x10^{14}$ Ω.cm), high dielectric strength (16 kV/mm) in the frequency range of 10^{-1} to 10^{-7} Hz were obtained with increased boron content (it was added to epoxy by 50 wt%).

Moreover, Madakbas et al. [20] examined the thermal stability and flame retardancy of composites using polyacrylonitrile and 10 wt% hBN. It was found that glass transition temperatures increased with increasing h-BN percentage. The limiting oxygen index (LOI) value reached from 18% to 27%. Muratov et al. [21] studied the thermal conductivity of composites by using two types of hBN (sizes 2-5 μm and 120-140 nm) in the HDPE polymer matrix. hBN was modified with 3-aminopropyl, triethoxysilane, binder (KR TTS and LICA 12) chemicals. The composite materials were fabricated by adding HDPE and hBN in a 1:1 volume ratio. Composite material showed a thermal conductivity of 2 W/m.K without any binding material. Pure hBN showed a thermal conductivity of 0.35 W/m.K. Wang et al. [22] measured the planar thermal conductivity of films with polyvinylidene fluoride (PVDF) matrix by converting hBN (lateral size 7 μm) into boron nitride nanosheet (BNNS) and blending it with chemicals of NaOH, KOH, DMF. According to the results, the planar thermal conductivity of the PVDF/BNNS composite with 4% BNNS reached 4.69 W/mK and the thermal conductivity of the PVDF/BNNS composite increased 2297% compared to pure PVDF. Pan et al. [23] investigated the thermal conductivity of composites with polytetra fluorine ethylene (PTFE) matrix using hBN (diameter 1.5 μm) and aluminum nitride (AlN) particles (diameter 2.5 μm). The thermal conductivity of AlN and hBN-integrated PTFE composites was measured at 1.04 W/mK. This was 3.8 times higher compared than that of pure PTFE.

Currently, 30 wt.% short glass fiber reinforced PA 66 matrix (GF30) thermoplastic composites are used in some parts such as diesel filters and brake pedals in automotive. Especially brake pedals can be subjected to different foot loads during driving of the cars. Therefore, it is important to fabricate brake pedals with increased flexural strength by using hBN additives in the composites. Since increasing of the weight percentages of nanomaterials, agglomerations have increased as well. Hence, the low number of the targeted weight percentages of hBNs (0, 0.5, and 2 wt%) were chosen in this research. The literature search shows that certain rates of hBN material added composites had enhanced mechanical, thermal, and electrical properties compared to the composites without boron additives. The flexural properties of hBN (0, 0.5, and 2 wt%) added GF30 thermoplastic composites have not yet been investigated. During this research, the experiments are designed to answer questions such as which rate of boron material can be used in thermoplastic composite material, and how much the flexural properties of the composite material can be increased by using boron material.

2. Materials and Methods

2.1. Materials

Polyamide thermoplastics are semi-crystalline polymers. Polyamides with excellent mechanical properties can be hard and tight or soft and flexible. The slip and wear properties of polyamides are very good. They could absorb moisture. Polyamides are frequently used in fields such as automotive, electrical, electronics, and textiles. Polyamides are usually produced by plastic injection and extrusion and they can be completely recycled mechanically. Neat PA 66 and 30 wt.% short fiber reinforced PA 66 granules (Mat Polymer, Türkiye) were used as matrix materials (Table 2).

hBN is a type of non-toxic non-porous material of white colour, known for its chemical stability, electrical conductivity, thermal conductivity, and lubricating properties. BN is used in many areas due to its low reactive and superior physical and chemical properties. They are preferred due to their electrical insulation and thermal conductivity properties. hBN was obtained from Boron Research Institute of the Turkish Energy, Nuclear and Mineral Research Agency. The particle sizes of hBN was 250-300 nm (Table 3).

Table 2. Properties of neat PA 66 and 30 wt.% short fiber reinforced PA 66.

Mechanical Properties	PA 66	30 wt.% short fiber reinforced PA 66
Elastic modulus (MPa)	3200	10000
Yield stress (MPa)	85	185
Izod notched impact strength (kJ/m²)	5	13
Melting temperature (°C)	262	262
Density (Kg/m³)	1140	1360

Table 3. Properties of hBN.

Parameter	Value
Particle size (nm)	250-300
Form	Powder
Density (g/cm³)	2.3
Elastic modulus (GPa)	865
Melting point (°C)	3000

2.2. Methods

In this study 0, 0.5, and 2 wt % hBNs were added into thermoplastic composites. hBN nano-scale powders were added to 500 ml of ethanol in the required amounts and the solutions were prepared. After mixing the solutions for 150 min in the magnetic mixer, 30 min in the ultrasonic mixer, and 3 min in the mechanical mixer, homogenization of the solutions was achieved. Homogenized hBN-doped ethanol solutions were mixed with 500 mg PA 66/GF30 granules. In order to mix the solutions in homogeneously, the solutions were divided into equal quantities and each mixture was mixed ultrasonically and mechanically for 10 minutes. Later, they were left to dry for 3 days to remove ethanol in the mixed solutions (Figure 1).

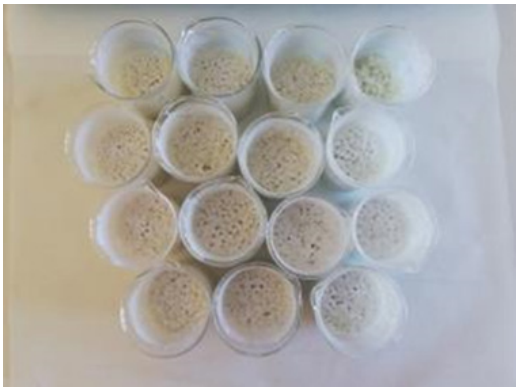

Figure 1. hBN coated PA 66/GF30 granules.

The samples were produced by the plastic injection molding machine (10 Tonnes, Permak Makina, Türkiye) and they were cooled down for three days. Three-point bending tests were applied to the samples that came to the appropriate conditions. The three-point flexural tests were performed on GF30 reinforced hBN added thermoplastic composites with PA 66 matrix in accordance with the ISO 178 Standards. The samples of PA 66, PA 66/GF30, PA 66/GF30/0.5% hBN and PA 66/GF30/2% hBN composites are 80 mm x 15 mm x 4 mm in size. Bending tests were applied on specimens with Instron 5982 100 KN universal test device (USA) at Ondokuz Mayıs University (OMU) KITAM Central Laboratory. The flexural strength (σ_f), modulus (E_B), and strain (ε_f) were calculated using Equ. 1 to 3, where, P is the flexural load (N); L is the support span (mm); b and d are the width (mm) and the thickness (mm) of the sample; m is the slope of the tangent to the initial straight-line portion of the load-deflection curve; D is the maximum deflection of the center of the sample (mm) [24].

$$\sigma_f = \frac{3PL}{2bd^2} \quad (1)$$

$$E_B = \frac{L^3 m}{4bd^3} \quad (2)$$

$$\varepsilon_f = \frac{6Dd}{L^2} \quad (3)$$

Composite void volumes are found by performing burn-out tests according to ASTM D3171 standard. Fourier transform infrared (FTIR, Bruker Tensor 27, Germany) spectroscopy analysis was performed. The specimens were pelletized before FTIR analysis. FTIR spectra were in the range of 650 to 4000 cm^{-1} of wavenumber. Scanning electron microscopy (SEM) images were obtained in an analytical field-emission SEM (JEOL JSM-7001 F, Japan). Before performing SEM, the cross sections of the specimen were coated with gold. X-ray diffraction analysis (XRD, Rigaku Smart Lab, Japan) was done. The Bragg's angle, 2θ, was ranged from 10° to 60° with a scan rate of 1°/min.

3. Results and Discussion

The measured densities and void volumes of the composites with PA 66/GF30/2% hBN were 1.374 g/cm^3 and 0.64 cm^3. These were 1.374 g/cm^3 and 0.18 cm^3 for the PA 66/GF30 specimens.

The measured densities and void volumes of the composites with PA 66/GF30/2% hBN were 1.374 g/cm^3 and 0.64 cm^3. These were 1.374 g/cm^3 and 0.18 cm^3 for the PA 66/GF30 specimens. Figure 2a and Figure 2b depict the Fourier Transform Infrared (FTIR) spectra of the PA 66/GF30/2% hBN composite and hBN powder. The absorption bands at 2934 cm^{-1} and 2859 cm^{-1} attributed to the symmetric and asymmetric C-H stretching vibrations and C-H twisting (Figure 2a). The peaks at 1635 cm^{-1} and 1534 cm^{-1} are attributed to the stretching vibration of the C=O group of amide I and the N-H bending and C-N stretching vibration of amide II. The peak at 1271 cm^{-1} indicates C-N-H coupling vibration of amide III. The peaks at 935 cm^{-1} and 1197 cm^{-1} are attributed to Si-OH and Si-O-Si groups. Typical peaks of hBN at 1353 cm^{-1} and 803 cm^{-1} can be related to in-plane B-N stretching and out-of-plane B-N bending vibrations of hBN (Figure 2b) [2].

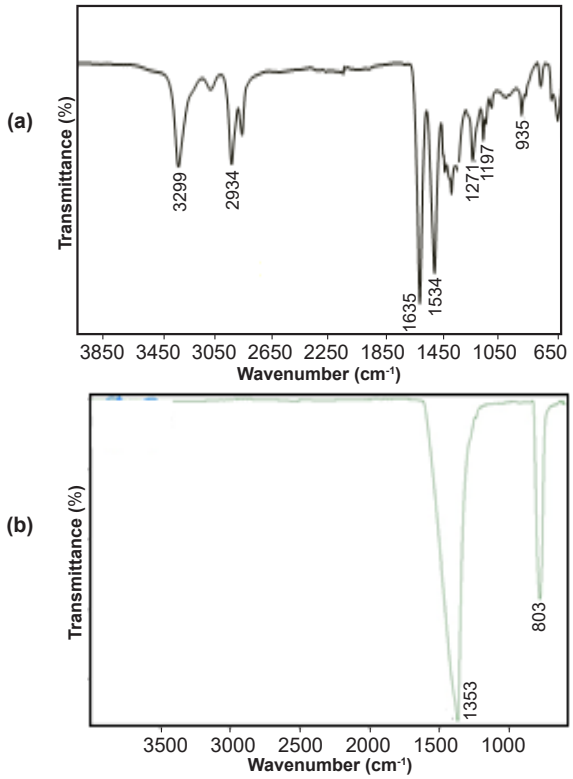

Figure 2. FTIR spectra of the specimens: a) PA 66/GF30/2% hBN composite and b) hBN powder.

Three-point bending test results are demonstrated in Figure 3 and Table 4. According to the results of the flexural tests of the composites with PA 66 matrix (Figure 3 and Table 4), the polymer consisting of pure PA 66 granules showed a ductile behaviour. PA 66/GF30, PA 66/GF30/0.5% hBN and PA 66/GF30/2% hBN composites exhibited higher flexural strength compared to pure PA 66. In the composites, samples with 2wt% hBN showed the best flexural properties with an improvement of 85% and 52% flexural modulus and strength, respectively, compared to the samples without hBN (PA 66/GF30).

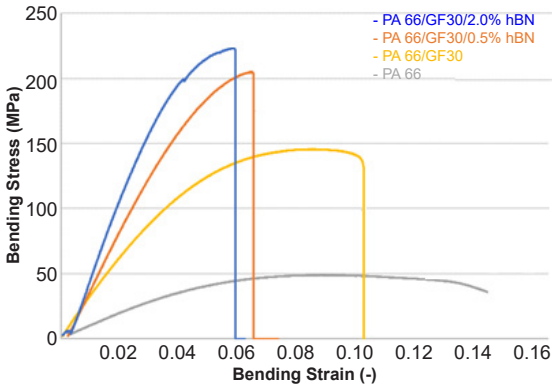

Figure 3. Three-point bending test plots.

Brittle fractures were detected in Figure 4 in hBN-added samples. These brittle fractures are due to the existence of the hBN in the structure of the composites In this study, compared to the literature, hBN-added PA 66 composites with PA 66 matrix showed a significant.

Table 4. Bending test results with standard deviations of PA 66 matrix composites.

Sample	Bending Modulus (GPa)	Bending Strength (MPa)
PA66	1.04±0.10	65.20±5.22
PA66/GF30	3.30±0.11	144.00±2.26
PA66/GF30/%0.5 hBN	3.89±0.82	165.00±34.0
PA66/GF30/%2 hBN	5.24±0.21	218.42±8.93

increase in flexural strength compared to PA 66 and PA 66/GF30 thermoplastics. According to the results, high improvements in bending properties were obtained from hBN particles added PA 66/GF30 thermoplastic composites. The flexural strength of PA 66/GF30/2% hBN increased by 235% when compared to pure PA 66 polymer, by 52% compared to PA 66/GF30 composite, and by 39.5% when compared to PA 66/GF30/0.5% hBN composite. PA 66/GF30/2% hBN samples also showed an increase in bending modulus. The Flexural modulus of PA 66/GF30/2% hBN composite with the addition of hBN achieved the highest value of 5.24 GPa, an increase of 404% compared to pure PA 66 polymer and an increase of 58% compared to PA 66/GF30 composite. Due to the obtained higher mechanical properties from hBN-added composites, which proofs that the coating of the nanomaterials of polymers was homogeneous. When the mechanical properties reduce, in non-uniform coating of nanomaterials into polymers increase. Furthermore, the flexural properties of the composites were compared with the literature. In the work of Pramanik et al. [2], the mechanical (13.6% hardness, 13.8% tensile strength, and 1300% elongation increased) properties of PA 6/5GF/hBN hybrid nanocomposites with 1 wt% hBN were significantly higher than those of PA 6/5GF composites. In the work of Taşdelen et al. [12] tensile strength of PA 6 material was 82 MPa. In the work of Autay et al. [25] flexural strengths of PA 66 and PA 66/GF30 materials were 42.66 MPa and 80.7 MPa, respectively.

Figure 4. PA 66 matrix composites after flexural test.

Figure 5 represents the SEM image of the surface morphology of the fractured specimen from the bending tests. In that figure, the broken glass fibers and embedded hBN nano-particles into the PA 66 matrix can be seen. There is a certain amount of hBN to absorb the fracture energy and stop the crack propagation [26]

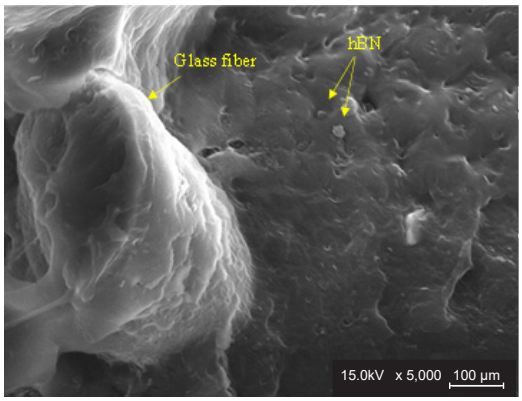

Figure 5. SEM image of hBN particles in fractured specimen from the bending tests.

Figure 6 represents the results of the XRD pattern of the PA 66/GF30 and PA 66/GF30/2% hBN composites. The International Centre for Diffraction Data (ICDD) card number of the hBN particles was 34-421. These XRD results agreed well with the literature. It was observed that PA 66 exhibited strong crystalline diffraction peaks at 2θs = 20.9° and 24.0° [27]. The hBN nanoparticles in the composite exhibited distinct and sharp peaks at 2θ = 26.8° [2]. In the subsequent studies, during the development and fabrication of new designs of composites, the obtained information on different weight contributions of hBN particles in composites will provide the optimization of materials.

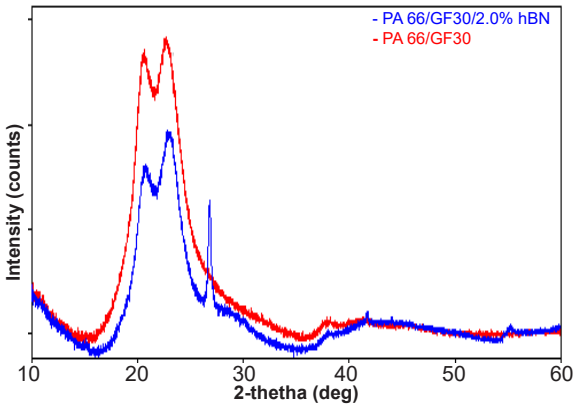

Figure 6. XRD spectra of the PA 66/GF30 and PA 66/GF30/2% hBN composites.

4. Conclusions

The hBN additives were applied by coating granules of PA 66/GF30 materials and the hBN-coated thermoplastic materials were produced successfully by plastic injection method. This study shows that the addition of hBN particles to PA 66/GF30 materials increased the flexural strength and modulus of the composites. The optimum amount of addition of hBN in composites was 2 wt%. Samples with 2 wt% hBN showed the best flexural properties with an improvement of 85 and 52% flexural modulus and strength compared to the samples without hBN (PA 66/GF30). It was concluded that hBN-coated thermoplastic composite samples exhibited very high improvements in flexural strength at low weight rates.

5. Acknowledgements

Authors would like to thank the Boron Research Institute of the Turkish Energy, Nuclear and Mineral Research Agency for supporting this work with the project number 2019-30-06-30-003 and the Research fund of Ondokuz Mayıs University with the project numbers of PYO.TIP.1908.20.001 and PYO.MUH.1901.18.008.

References

[1]. Do, N. B. D., Imenes, K., Aasmundtveit, K. E., Nguyen, H. V., & Andreassen, E. (2023). Thermal conductivity and mechanical properties of polymer composites with hexagonal boron nitride-A comparison of three processing methods: Injection moulding, powder bed fusion and casting. *Polymers*, *15*(6), 1552. https://doi.org/10.3390/polym15061552.

[2]. Vikram, K., Pramanik, S., & Bhaumik, S. (2023). Effect of hexagonal boron nitride on structural, mechanical, and tribological behavior of polyamide 6/glass fibers (5 wt%) hybrid nanocomposites. *Iran Polymer Journal*, *33*, 551-530. https://doi.org/10.1007/s13726-023-01261-x.

[3]. Travas, L., Rujnic H. M., & Pilipovic A. (2023). Optimization of thermal conductivity and tensile properties of high-density polyethylene by addition of expanded graphite and boron nitride. *Polymers*, *15*(17), 3645. https://doi.org/10.3390/polym15173645.

[4]. You, J., Choi, H. H, Lee, Y. M., Cho, J., Park, M., Lee, S. S., & Park, J. H. (2019). Plasma-assisted mechanochemistry to produce polyamide/boron nitride nanocomposites with high thermal conductivities and mechanical properties, *Composites Part B: Engineering*, *164*, 710-719. https://doi.org/10.1016/j.compositesb.2019.01.100.

[5]. Gültekin, K., & Korkmaz, Y. (2022). The effect of boron nanoparticle reinforcement on the structural and mechanical performance of nanocomposites and bonded joints exposed to an acid environment, *International Journal of Adhesion and Adhesives*, *118*, 103244, https://doi.org/10.1016/j.ijadhadh.2022.103244.

[6]. Ashrafi, B., Jakubinek, M. B., Martinez-Rubi, Y., Rahmat, M., Djokic, D., Laquas, K., Park D., Kim, K., Simard, B., & Yousefpour, A. (2017). Multifunctional fiber reinforced polymer composites using carbon and boron nitride nanotubes. *Acta Astronautica*, *141*, 57-63. https://doi.org/10.1016/j.actaastro.2017.09.023.

[7]. Ayrilmis, N., Dundar, T., Kaymakci, A., Ozdemir, F., & Kwon, J.H. (2014). Mechanical and thermal properties of wood-plastic composites reinforced with hexagonal boron nitride. *Polymer Composites*, *35*, 194-200. https://doi.org/10.1002/pc.22650.

[8]. Cai, W., Mu, X., Pan, Y., Guo, W., Wang, J., Yuan, B., Feng, X., Tai, Q., & Hu, Y. (2018). Facile fabrication of organically modified boron nitride nanosheets and its effect on the thermal stability, flame retardant, and mechanical properties of thermoplastic polyurethane. *Polymers for Advanced Technologies*, *29*, 2545-2552. https://doi.org/10.1002/pat.4366.

[9]. Yu, C., Zhang, J., Li, Z., Tian, W., Wang, L., Luo, J., Li, O., Fan, X., & Yao, Y. (2017). Enhanced through-plane thermal conductivity of boron nitride/epoxy composites. *Composites: Part A*, *98*, 25-31. https://doi.org/10.1016/j.compositesa.2017.03.012.

[10]. Boztoprak, Y., & Kartal, İ. (2019). Investigation of the mechanical properties of vinyl ester matrix composites reinforced with boron nitride particles. *El-Cezeri Journal of Science and Engineering*, *6*(1), 43-50. https://doi.org/10.31202/ecjse.450790.

[11]. Göncü, Y., Onar, İ. C., & Ay, N. (2020). The effect of hexagonal boron nitride addition on presureless sintered alumina matrix composites. *Journal of Boron*, *5*(1), 40-47. https://doi.org/10.30728/boron.633242.

[12]. Taşdelen, M. A., & Yılmaz, İ. N. (2018). Preparation of glass fiber doped polyamide 66/polythalamide mixtures. *Uludag University Journal of Engineering Faculty*, *23*(1), 285-294. http://dx.doi.org/10.17482/Uumfd.350589.

[13]. Kaştan, A., Yalçın, Y., Ünal, H., & Talanut, Ş. (2015). Investigation of mechanical properties of PA 6 / YYPE / nanoclay composites. *Afyon Kocatepe University Journal of Science and Engineering*, *15*(1), 9-20. http://hdl.handle.net/11630/4083.

[14]. Karslı, M. (2016). *Selection of polymer composite material for light weapons* (Publication No. 456251) [Master Thesis, Karadeniz Technical University]. Council of Higher Education.

[15]. Oz, M. (2016). Thermal behavior of hexagonal boron nitride in the open atmosphere. *Cumhuriyet Science Journal*, *37*(1), 57-64. http://dx.doi.org/10.17776/csj.38616.

[16]. Cheewawuttipong, W., Fuoka, D., Tanoue, S., Uematsu, H., & Iemoto, Y. (2013). Thermal and mechanical properties of polypropylene/ boron nitride composites. *Energy Procedia*, *34*, 808-817. https://doi.org/10.1016/j.egypro.2013.06.817.

[17]. Isarn, I., Ramis X., Ferrando, F., & Serra, A. (2018). Thermoconductive thermosetting composites based on boron nitride fillers and thiol-epoxy matrices. *Polymers*, *10*(3), 277-293. https://doi.org/10.3390/polym10030277.

[18]. Harrison, C., Weaver, S., Bertelsen, C., Burgett, E., Hertel, N., & Grulke, E. (2008). Polyethylene/boron nitride composites for space radiation shielding. *Journal of Applied Polymer Science*, *109*, 2529-2538. https://doi.org/10.1002/app.27949.

[19]. Zhou, W., Zuo, J., Zhang, X., & Zhou, A. (2014). Thermal, electrical, and mechanical properties of hexagonal boron nitride-reinforced epoxy composites. *Journal of Composite Materials*, *48*(20), 2517-2526. https://doi.org/10.1177/0021998313499953.

[20]. Madakbas, S.¸ Çakmakçı, E., & Kahraman, M.V. (2013). Preparation and thermal properties of polyacrylonitrile/hexagonal boron nitride composites. *Thermochimica Acta*, *552*, 1-4. https://doi.org/10.1016/j.tca.2012.11.011.

[21]. Muratov, D. S., Stepashkin, A. A., Anshin, M. S., & Kuznetsov, V. D. (2018). Controlling thermal conductivity of high density polyethylene filled with modified hexagonal boron nitride (hBN). *Journal of Alloys and Compounds*, *735*, 1200-1205. https://doi.org/10.1016/j.jallcom.2017.11.234.

[22]. Wang, E., Jiao, Z., Chen, Y., Hou, X., Fu, L., Wu, Y., … & Yu, J. (2018). Enhanced thermal conductivity of poly(vinylidene fluoride)/boron nitride nanosheet composites at low filler content. *Composites Part A*, *109*, 321-329. https://doi.org/10.1016/j.compositesa.2018.03.023.

[23]. Pan, C., Kou, K., Zhang, Y., Li, Z., Wu, G. (2018). Enhanced through-plane thermal conductivity of PTFE composites with hybrid fillers of hexagonal boron nitride platelets and aluminum nitride particles. *Composites Part B*, *153*, 1-8. https://doi.org/10.1016/j.compositesb.2018.07.019.

[24]. Bilisik, K., Karaduman, N.S., Sapanci E. (2019). Flexural characterization of 3sD prepreg/stitched carbon/epoxy/multiwalled carbon nanotube preforms and composites. *Journal of Composite Materials*, *53*(5), 563-577. https://doi:10.1177/0021998318787861.

[25]. Autay, R., Missaoui, S., Mars, J., Dammak, F. (2019). Mechanical and tribological study of short glass fiber-reinforced PA 66. *Polymers and Polymer Composites*, *27*(9), 587-596. https://doi:10.1177/0967391119853956.

[26]. Mortazavi, B., Cuniberti, G. (2014). Mechanical properties of polycrystalline boron-nitride nanosheets. *RSC Advances*, *4*(37), 19137-43. https://doi.org/10.1039/C4RA01103A.

[27]. Fang, H., Li, G., Wang, K., Wu, F. (2023). Significant improvement of thermal conductivity of polyamide 6/boron nitride composites by adding a small amount of stearic acid. *Polymers*, *15*, 1887, 1-12. https://doi.org/10.3390/polym15081887.

BOR DERGİSİ
JOURNAL OF BORON
https://dergipark.org.tr/boron

Specification of lethal concentration (LC_{50}) of boron effect on *Daphnia pulex* (Leydig, 1860) using probit model

Burcu Yeşilbudak [1,*]

[1]*Çukurova University, Department of Biology, Faculty of Science and Letters, Adana, 01330, Türkiye*

ARTICLE INFO

Article history:
Received January 6, 2024
Accepted March 11, 2024
Available online June 28, 2024

Research Article

DOI: 10.30728/boron.1415733

Keywords:
Boron toxicity
Daphnia pulex
Mortality
Regression estimate

ABSTRACT

Statistical models used in toxicity experiments have been quite useful tools in interpreting the organism's susceptibility, exposure response, amount of tolerable concentration, and function of tolerance time. In order to determine and evaluate the toxic effects of boron on *Daphnia pulex* (Leydig, 1860), different boron concentrations considered to be tolerable in aquatic ecosystems were tested for *D. pulex*. Percentage mortality rates at different boron concentrations and probit regression estimates at these concentrations were investigated through the static method. Probit analysis in this study revealed that rising boron concentrations led to mortality, and that finding was statistically significant with P value. These results indicate that the use of episodic boron, which enters the aquatic ecosystem through natural or unnatural means, should be planned due to its potential for stress or toxicity situations on organisms.

1. Introduction

Boron has many important industrial uses such as fiberglass insulation, borosilicate glass, cleaning products, fertilizer, metallurgy and nuclear protective material production [1,2]. However, it is also predicted that boron may become a drinking water contaminant in the next few years [3]. Despite such a risk, it is thought that the use of boron should be done with a planned and technical arrangement [3]. Boron is an important essential micronutrient, but has also been reported to create toxic conditions [4]. Various studies showing an increase its genotoxic effect on organisms have focused on boron as not being biodegradable in the aquatic ecosystem [5,6]. Boron levels can exceed toxic levels in the aquatic ecosystem through natural and unnatural metal corrosion and contamination processes [7]. Although surface waters are generally below the toxic level (0.01-1.5 mg/l) [8], it has been stated that the boron level for aquatic organisms should be below 1.2 mg/l [9]. The toxic properties of boric acid and borates (sodium borate, sodium tetraborate, or disodium tetraborate), especially against arthropods, are known; however [10-12], there is no specific information about their toxicity against water fleas, which have an important place in the food chain in the aquatic ecosystem. The use of invertebrates in monitoring the aquatic ecosystem health provides significant economic benefits [13,14]. As they are very sensitive creatures, invertebrates have become models for protecting public health by providing immediate warnings about unpredictable changes in the ecosystem in advance [13,14]. Water fleas, especially with their many practical features such as short life cycles, parthenogenetic reproductive features, and reduction of traditional animal tests, have provided significant benefit in determining the deviations in ecotoxicological, behavioral, ecophysiological and genetic profiles caused by environmental xenobiotics [15-18].

The invertebrate *Daphnia pulex* with its widespread presence in aquatic ecosystems has been an important animal model in both ecological and laboratory studies [19]. However, little is known about the ecotoxicological probit modeling of boron toxicity on *D. pulex*. Therefore, it is essential to perform different tests to understand the sensitivity variability between organisms along with regression models, which help to evaluate different protection levels of organisms in wildlife [20]. The first aim of our study is to estimate the mortality status and the corresponding lethal concentration of *D. pulex* at the ecotoxicological endpoints of different boron concentrations. It is also aimed to provide a perspective on the sensitivity and applicability of the secondarily applied probit estimation in toxicological tests.

2. Materials and Methods

2.1. Experiment Animals and Chemicals

Water fleas used as the experimental material, were transferred from shallow habitats in northern Anatolia to a culture medium with a stainless steel support

*Corresponding author: yesilbudak@gmail.com

frame along with freshwater samples of its own habitat. Light microscopy was used to identify water fleas and determine their vital characteristics such as mortality, color change and brightness (Omax Microscope, USA). The guide for the identification of micro-invertebrates in the world's continental waters was used for the species identification of water fleas [19], followed by their adaptation to the culture environment for 1 month. The culture tank was renewed with 20°C spring water and aerated. A 16-hour light/8-dark photoperiodism was maintained for the culture tank, and baker's yeast suspension was fed at 1 ml per tank once a day for one week before the experiments. $Na_2B_4O_7 \cdot 10H_2O$ (Eti Maden®, Turkey) was used in the experiments to determine the effect of boron on mortality in water fleas.

2.2. Experimental Design

The boron concentrations tested in the experiment were selected according to the prerequisite of performing at least five tests for the toxic substance in the limit determination tests recommended by the Environmental Protection Agency (EPA) [21] and the availability limits of boron in surface waters [22]. Depending on these prerequisites, deaths in daphnia were monitored during 48-hour exposure periods in jars containing different concentrations of boron (0.05, 0.10, 0.20, 0.40, 0.80, 1.60, 3.20, 6.40 mg/l) compared to the jar containing no boron in the control group. The median lethal concentration (LC_{50} values) for *D. pulex* were determined by using 48h static bioassay experiment [23-25]. It is stated and recommended that 20 test organisms are suitable for each toxicity application in probit toxicity studies [26]. Since there were a total of 9 test jars with 20 *D. pulex* for each boron concentration in the probit prediction experiment, in total 180 *D. pulex* were observed in the entire experiment. The preparation of the stock solution was made according to the stock preparation procedures of the APHA methods [27], and the chemical at the specified concentrations was diluted into the test aquarium and injected into the experimental environment. The mean and standard error of the carapax length and carapax width of neonatal *D. pulex* (~24h) at the beginning of the experiment were determined as 0.721±0.01 mm, 0.092±0.01 mm. By adding 100 ml of the organisms' culture medium and 100 ml of spring water to the experimental environments, each experimental area was created sequentially in 200 ml of medium. Under the light microscope, the *D. pulex* color change, inability to move, and cessation of heartbeat were noted for each group as indicators of its mortality.

2.3. Instrumentations

Inductively coupled plasma mass spectrometry was used to determine boron concentrations in application aquariums (ICP-MS Agilent 7500ce series, Octopole Reaction Systems, Agilent Technologies, Japan). The recovery percentage of the boron limit determined in the spectrophotometer was determined as 95.7%. In the validation parameters of the analytical method for the analyte, the detection limit (LOD) value was 1.45 $ng.g^{-1}$; limit of quantification (LOQ) value was 5.25 $ng.g^{-1}$; the relative standard deviation (RSD, %) and the coefficient of determination (R^2) values were determined as 1.07% and 0.99, respectively.

The physical-chemical properties of the experimental environments and the methods used to determine these properties are given in Table 1. Analyzes were performed three times to determine the physical and chemical properties of the experimental tank ambiance.

Table 1. Physical and chemical properties of the tank

Parameters, Unit	Analytical method	Mean ± Std. Error
Water temperature, °C	Temperature probe	20.10±0.91
Dissolved oxygen, mg/l	Oxygen meter probe	7.83±0.09
pH	pH probe	7.12±0.13
Total hardness, mg/l	Titrimetric method	98.75±2.23

2.4. Statistical Analysis

Statistical analyses were performed using the SPSS statistical software (V 27.0.1.0, IBM, Corp., USA) to determine the effects of boron on the *D. pulex* population [28]. The relationship between boron concentrations applied to *D. pulex* and mortality and the direction of the relationship were determined by regression-correlation analysis. The level of significance was set to be at least $P \leq 0.01$. Depending on the significance determined, probit analysis estimates were made [29,26]. The sigmoidal mortality chart of the population was drawn, and the lethal concentration (LC_{50}) value was checked with the calculated value [30].

3. Results and Discussion

In this study examining boron toxicity, the direction of the relationship between boron concentrations applied to a total of 180 *D. pulex* exposed to boron and their mortality rates is shown in Figure 1, and Pearson correlation matrices are given in Table 2. As boron concentration increased, the average mortality level similarly increased; thus, a strong positive correlation was observed ($P \leq 0.01$) (Pearson's $R=0.802$; $df=7$; $p=0.005$). In a study examining boron toxicity, it was observed that high concentrations of boron potentially affected the weight of Diptera larvae [31]. In another study where the water quality parameters of water samples taken from different drainage channels were examined seasonally, the Pearson correlation coefficient between boron concentrations in the spring season and the mortality rate of *Daphnia magna* was found to be positively significant with 0.71 ($p = 0.003$) [32]. The high positive correlation levels indicated that boron derivatives had toxic effects on macroinvertebrate populations.

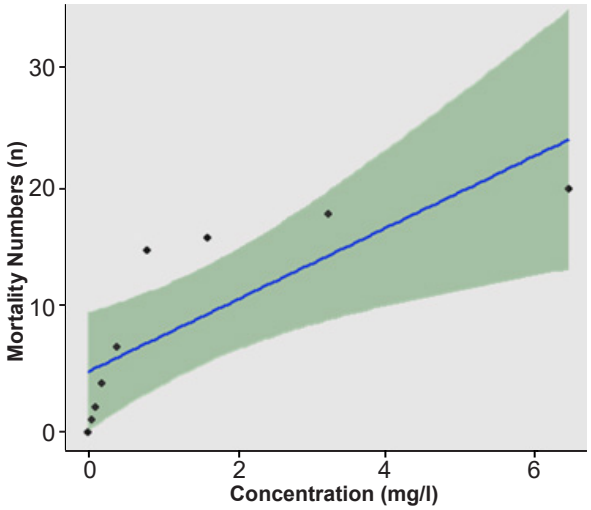

Figure 1. Pearson correlation between boron concentrations and mortality.

Table 2. Pearson correlation matrix between exposed concentrations of boron and mortality of *D. pulex*.

	Pearson's *R* matrix	Concentration (mg/l)
Number of Mortality (n)	Pearson's *R*	0.80 (*P*<0.01)*
	df	7
	p-value	0.005
	95% Confidence Interval Upper	0.965
	95% Confidence Interval Lower	0.394

The results of estimating the probit line plots (with confidence limits) and probit analyses of cladocerans are given in Figure 2 and Table 3. The probit regression results of *D. pulex* exposed to boron for 48 hours were found to be R^2=0.73; y= -0.96+0.85x. Accordingly, as a result of probit analysis in this study, the effect of boron application doses on survival was found to be statistically significant with p values. Since the estimated coefficient was a positive value (1.002), it indicated that the effects were positive i.e. the number of deaths occurred more frequently as the dose increased. As seen from the relevant chi-square values and the corresponding p values, the established probit regression model was found to be significant.

The probit analysis is used extensively in ecotoxicology to determine the relative toxicity of toxic substances on organisms and assumes that the relationship between the concentration and response state is normally distributed [33]. In this study, the acute toxic effects of boron on *D. pulex* were determined using the probit analysis with LC_{50} determination method due to the cumulative normal distribution. In the analysis, the dose-response curve was visualized as a straight line, providing maximum probabilities and least squares or regression estimates. The concentration values that caused 50% mortality at the end of the 48-hour period were analyzed, and the results are shown in Table 3. LC_{50} was found only at 0.51 mg/l boron concentrations.

The percentage mortality in the *D. pulex* population determined as a response to boron toxicity yielded an upward sloping sigmoidal curve (Figure 3). Basically, the probit cumulative standard is inverse to the normal distribution [34,25]. It is seen that the values of the fit hypothesis (Pearson Goodness of Fit Test) were significant for regression (Table 3). Moreover, probit regression seems more suitable for this study as it shows the 95% extreme values of the chemical.

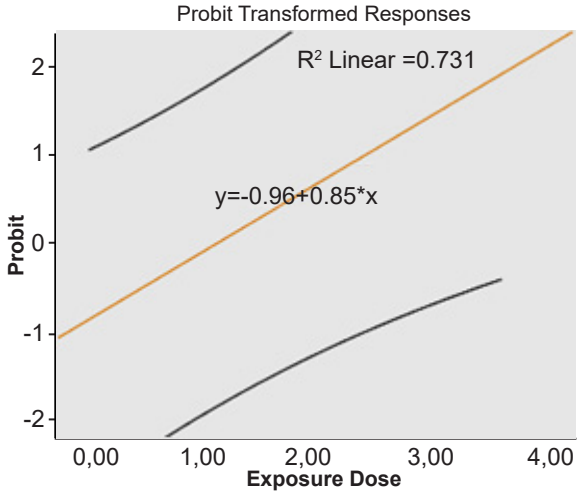

Figure 2. Result of probit regression estimation.

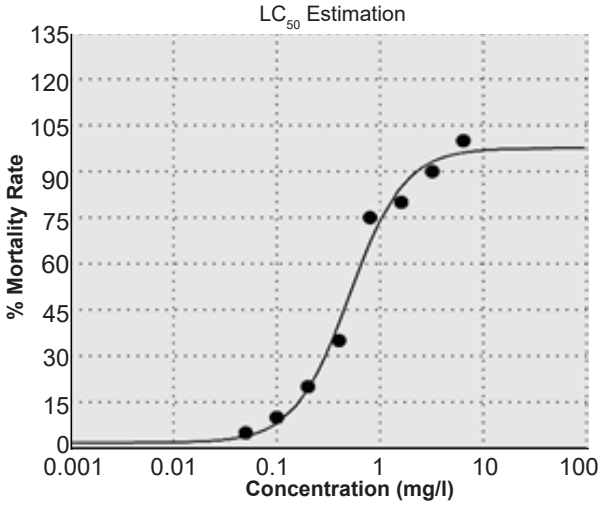

Figure 3. Lethal concentration (LC_{50}) of *D. pulex*.

4. Conclusions

The results revealed that environmental increases in boron may affect *D. pulex* mortality. The increase in the concentration of boron compounds such as boron and borate, especially in domestic and agricultural areas, causes the extinction of key species in the food chain as well as the destruction of harmful species. Planned use should be ensured, taking into account that increased concentrations of boron for various reasons may cause a negative situation in the welfare of aquatic organisms. In addition, it is thought that the sensitivity of *D. pulex* determined in this study to the effect of boron concentrations and the suitability

Table 3. Probit regression parameters of *D. pulex* under boron exposure.

Parameter Estimates							
						95% Confidence Interval	
PROBIT[a]	Parameter	Estimate	Std. Error	Z	Sig.	Lower Bound	Upper Bound
	Exposure Dose	1.002	0.15	6.56	0.00	0.70	1.30
	Intercept	-1.034	0.15	-6.76	0.00	-1.19	-0.88

[a.] PROBIT model: PROBIT(p) = Intercept + BX

Chi-Square Tests				
		Chi-Square	df[b]	Sig.
PROBIT	Pearson Goodness-of-Fit Test	27.20	7	0.00[a]

[a.] Since the significance level is greater than 0.150, no heterogeneity factor is used in the calculation of confidence limits.

[b.] Statistics based on individual cases differ from statistics based on aggregated cases.

95% Confidence Limits for Exposed								
PROBIT	Probability	Estimate	Lower Bound	Upper Bound	Probability	Estimate	Lower Bound	Upper Bound
	0.01	-1.29	-6.14	-0.38	0.55	1.16	0.61	2.76
	0.05	-0.61	-3.84	0.07	0.60	1.28	0.73	3.15
	0.10	-0.25	-2.65	0.34	0.65	1.41	0.85	3.57
	0.15	-0.00	-1.87	0.55	0.70	1.56	0.96	4.01
	0.20	0.19	-1.28	0.74	0.75	1.71	1.08	4.51
	0.25	0.36	-0.81	0.95	0.80	1.87	1.20	5.06
	0.30	0.51	-0.43	1.17	0.85	2.07	1.33	5.71
	0.35	0.65	-0.12	1.43	0.90	2.31	1.49	6.54
	0.40	0.78	0.12	1.72	0.95	2.67	1.73	7.77
	0.45	0.91	0.31	2.04	0.97	2.91	1.87	8.57
	0.50	1.03	0.47	2.40	0.99	3.35	2.15	10.10

LC_{50} Regression Results	Value
LC_{50}	0.51
Equation Form	$Y = \text{Min} + \frac{\text{Max} - \text{Min}}{1 + \left(\frac{X}{LC_{50}}\right)^{\text{Hill coefficient}}}$

of the applied probit model for the study will provide importance in the use of both, preferably for different ecotoxicological studies.

5. Contribution Statement

The author declares that she has contributed to 100% of the article.

6. Conflict of Interest

The author has no conflicts of interest to declare.

References

[1]. Power, P. P., & Woods, W. G. (1997). The chemistry of boron and its speciation in plants. *Plant and Soil*, *193*, 1-13. https://doi.org/10.1023/A:1004231922434.

[2]. Řezanka, T., & Sigler, K. (2008). Biologically active compounds of semi-metals. *Studies in Natural Products Chemistry*, *35*, 835-921. https://doi.org/10.1016/S1572-5995(08)80018-X.

[3]. U.S. Environmental Protection Agency (US EPA). (2003). *Drinking water contaminant candidate list*. http://www.epa.gov/safewater/ccl.

[4]. Scorei, R. (2006). *Boron, essential micronutrient for animal nutrition* (Analele IBNA, Vol. 22, pp. 75-85). The National Research - Development Institute for Animal Biology and Nutrition. https://ibna.ro/anale/Anale_22_2006%20pdf/Anale%20IBNA%2022_11%20Scorei.pdf.

[5]. Acar, Ü., İnanan, B. E., Zemheri, F., Kesbiç, O. S., & Yılmaz, S. (2018). Acute exposure to boron in Nile tilapia (Oreochromis niloticus): Median-lethal concentration (LC50), blood parameters, DNA fragmentation of blood and sperm cells. *Chemosphere*, *213*, 345-350. https://doi.org/10.1016/j.chemosphere.2018.09.063.

[6]. Konuk, M., Liman, R., & Cigerci, I. H. (2007). Determination of genotoxic effect of boron on Allium cepa root meristematic cells. *Pakistan Journal of Botany*, *39*(1), 73-79. https://www.pakbs.org/pjbot/PDFs/39(1)/PJB39(1)073.pdf.

[7]. Kot, F. S. (2015). Boron in the environment. In: Kabay, N., Bryjak, M., & Hilal, N. (Eds.), *Boron Separation Processes* (pp. 1- 33). Elsevier. ISBN 9780444634542.

[8]. Sokmen, N., & Buyukakinci, B. Y. (2018). The usage of boron/boron compounds in the textile industry and its situation in Turkey. *CBU International Conference Proceedings*, *6*, 1158-1165. https://doi.org/10.12955/cbup.v6.1309.

[9]. Moss, S. A., & Nagpal, N. K. (2003). *Ambient Water Quality Guidelines for Boron-Full Report*. British Columbia. Water Protection Section, Ministry of Water, Land and Air Protection. https://www2.gov.bc.ca/assets/gov/environment/air-land-water/water/waterquality/water-quality-guidelines/approved-wqgs/boron/boron-tech-appnx.pdf.

[10]. National Center for Biotechnology Information (2023). *PubChem Compound Summary for CID 16211214*, Borax. https://pubchem.ncbi.nlm.nih.gov/compound/Borax.

[11]. Klotz, J. H., Moss, J., Zhao, R., Davis Jr, L. R., & Patterson, R. S. (1994). Oral toxicity of boric acid and other boron compounds to immature cat fleas (Siphonaptera: Pulicidae). *Journal of Eeconomic Entomology*, *87*(6), 1534-1536. https://doi.org/10.1093/jee/87.6.1534.

[12]. Gersich, F. M. (1984). Evaluation of a static renewal chronic toxicity test method for *Daphnia magna straus using boric acid. Environmental Toxicology and Chemistry: An International Journal*, *3*(1), 89-94. https://doi.org/10.1002/etc.5620030111.

[13]. Yeşilbudak, B. (2022). Mini Bio-Ecological Scale Indicators Used in Comparison of Water Quality Criteria of Wetlands. *International Multilingual Journal of Science and Technology*, *7*(8): 5358-5362. ISSN: 2528-9810.

[14]. Yeşilbudak, B. (2022). Some morphological traits and heavy metal accumulation in muscle tissue of Ruditapes decussatus (Linnaeus, 1758). *Eskişehir Technical University Journal of Science and Technology C-Life Sciences and Biotechnology*, *11*(2), 39-49. https://doi.org/10.18036/estubtdc.1045591.

[15]. Martins, J., Teles, L. O., & Vasconcelos, V. (2007). Assays with Daphnia magna and Danio rerio as alert systems in aquatic toxicology. *Environment International*, *33*(3), 414-425. https://doi.org/10.1016/j.envint.2006.12.006.

[16]. Luo, T., Chen, J., Song, B., Ma, H., Fu, Z., & Peijnenburg, W. J. G. M. (2017). Time-gated luminescence imaging of singlet oxygen photoinduced by fluoroquinolones and functionalized graphenes in Daphnia magna. *Aquatic Toxicology*, *191*, 105-112. https://doi.org/10.1016/j.aquatox.2017.07.016.

[17]. Bownik, A. (2017). Daphnia swimming behaviour as a biomarker in toxicity assessment: a review. *Science of the Total Environment, 601-602*, 194-205. https://doi.org/10.1016/j.scitotenv.2017.05.199.

[18]. Colbourne, J. K., Shaw, J. R., Sostare, E., Rivetti, C., Derelle, R., Barnett, R., Campos, B., LaLone, C., Viant M. R., & Hodges, G. (2022). Toxicity by descent: A comparative approach for chemical hazard assessment. *Environmental Advances*, *9*, 100287. https://doi.org/10.1016/j.envadv.2022.100287.

[19]. Benzie, J. A. H. (2005). *Guides to the identification of the microinvertebrates of the continental waters of the world*. Backhuys Pub. ISBN: 90-5782-151-6.

[20]. DeForest, D. K., Brix, K. V., & Adams, W. J. (1999). Critical review of proposed residue-based selenium toxicity thresholds for freshwater fish. *Human and Ecological Risk Assessment: An International Journal*, *5*(6), 1187-1228. https://doi.org/10.1080/10807039.1999.10518886.

[21]. U.S. Environmental Protection Agency (2002). *Short-term Methods for Estimating the Chronic Toxicity of Effluents and Receiving Waters to Freshwater Organisms* (EPA-821-R-02-013). https://www.epa.gov/sites/default/files/2015-08/documents/short-term-chronic-freshwater-wet-manual_2002.pdf.

[22]. Howe, P. D. (1998). A review of boron effects in the environment. *Biological Trace Element Research*, *66*, 153-166. https://doi.org/10.1007/BF02783135.

[23]. Sprague, J. B. (1970). Measurement of pollutant toxicity to fish. II. Utilizing and applying bioassay results. *Water Research*, *4*(1), 3-32. https://doi.org/10.1016/0043-1354(70)90018-7.

[24]. Eaton, A. D., & Franson, M. A. H. (Eds.). (1981). *Standard methods for the examination of water and waste water* (Vol. 6). American Public Health Association. ISBN 087553287X.

[25]. Stephan, C. E. (1977). Methods for calculating an LC50. In Mayer, F. L., & Hamelink, J. L. (Eds.), *Aquatic Toxicology and Hazard Evaluation: Proceedings of the First Annual Symposium on Aquatic Toxicology: A Symposium* (pp. 65-84). ASTM International.

[26]. Finney, D. J. (Eds.). (2009). *Probit Analysis*. London: Cambridge University Press. ISBN: 9780521135900.

[27]. Rice, E. W., & Bridgewater, L. (Eds.). (2012). *Standard methods for the examination of water and wastewater* (Vol. 10). American Public Health Association. ISBN 9780875532875.

[28]. IBM Corp. (2016). IBM SPSS Statistics for Windows (Version 24.0) [Computer Software]. Armonk, NY: IBM Corp. https://www-01.ibm.com/support/docview.wss?uid=swg21476197.

[29]. Kobayashi, K., Pillai, K. S. (Eds.). (2003). *Applied Statistics in Toxicology and Pharmacology*. Science Pub Inc. ISBN: 9781578083046.

[30]. AAT Bioquest, Inc. (2023). *Quest Graph™ LC50 Calculator*. AAT Bioquest. https://www.aatbio.com/tools/lc50-calculator.

[31]. Cai, M., Hu, R., Zhang, K., Ma, S., Zheng, L., Yu, Z., & Zhang, J. (2018). Resistance of black soldier fly (Diptera: Stratiomyidae) larvae to combined heavy metals and potential application in municipal sewage sludge treatment. *Environmental Science and Pollution Research, 25*, 1559-1567. https://doi.org/10.1007/s11356-017-0541-x.

[32]. Higgins, D., & Miesner, J. F. (1995). *Assessment of*

Aquatic Toxicity in Irrigation Drain-Water, Newlands Project Area, Carson Desert, Nevada, March-August 1995 (Final Report EC 30.14.6). Nevada Fish and Wildlife Office Division of Environmental Quality. https://ecos.fws.gov/ServCat/DownloadFile/7576?Reference=7827

[33]. Hassan, J., & Tabarraei, H. (2015). Toxicity of copper on rainbow trout: lethal concentration or lethal dose evaluation. *Environmental Science: An Indian Journal, 11*(3), 98-102. https://www.tsijournals.com/articles/toxicity-of-copper-on-rainbow-trout-lethal-concentration-or-lethal-dose-evaluation.pdf.

[34]. Topcu, Y. (2008). Effective Factors' Analysis on Willingness to Utilize from Farmers' Agricultural Support Policies: The Case Study of Erzurum Province. *Akdeniz University Journal of the Faculty of Agriculture*, *21*(2), 205-212. https://dergipark.org.tr/en/download/article-file/18080.

BOR DERGİSİ
JOURNAL OF BORON
https://dergipark.org.tr/boron

Review of properties, synthesis, and energy applications of borophene, a novel boron-based 2D material

Gülbahar Bilgiç Tüzemen [1,*]

[1]*Nevşehir Haci Bektas Veli University, Faculty of Engineering-Architecture, Department of Metallurgical and Materials Engineering, Nevşehir, 50300, Türkiye*

ARTICLE INFO

Article history:
Received February24, 2024
Accepted May 31, 2024
Available online June 28, 2024

Review Article

DOI: 10.30728/boron.1442569

Keywords:
Boron
Borophene
Energy applications
Two-dimensional material

ABSTRACT

At least 16 bulk polymorphs of linked icosahedrons exist in boron that are not found in other materials, due to the low covalent radius and sp^2 hybridization capacity of boron atoms. One of them is borophene, an exciting new nanomaterial with a wide range of possible energy uses. The existence of borophene, a two-dimensional (2D) material, has been proven by both theoretical and experimental studies. Borophene's high magnetic conductivity, theoretical specific capacities, and ion transport properties make it a promising candidate in energy applications (EAs). In this study, firstly, the structure, chemical, and physical properties of borophene were mentioned. Then, in terms of synthesis approaches, both top-down and bottom-up techniques such as ultra-high vacuum (UHV), chemical vapor deposition (CVD), exfoliation by sonochemistry (ExS), molecular beam epitaxy (MBE) and multi-step thermal decomposition (MTD) were discussed. Finally, its use as a catalyst in high-metal-ion batteries, hydrogen storage (HS), nanoelectronics applications hydrogen evolution reaction (HER) was mentioned.

1. Introduction

Over the past ten years, active energetic elements including, sulfur, nitrogen, zinc, molybdenum, phosphorus, halogens, and boron have caught the attention of researchers. Due to the increasing need for green chemistry and renewable energy, boron is becoming increasingly important in energy research. Boron's adaptable chemistry makes energy applications (EAs) easier [1,2]. Atomic, physiochemical, and other properties of boron are listed in Table 1. Figure 1 depicts the location of boron in the periodic table [2-5]. A boron atom has three valence electrons in its outermost layers, scattered in the $2s^2$ and $2p^1$ orbitals. The boron atom has an electron deficiency because it possesses four bonding orbitals, one more than the valence electron. Therefore, boron is capable of sp^2 hybridization, which facilitates the development of low-dimensional structures and produces a wide range of characteristics. Moreover, boron may form various compounds due to its location halfway between metals and nonmetals [5-7]. Boron atom, due to its similarity to nearby carbon, fullerenes, nanotubes, and 2D films can develop as well as other low-dimensional allotropes. It is sensitive to chemical reactions that saturate the valence shell and coordination sphere. Due to the many ways that boron may be bound, at least 16 bulk polymorphs consisting of linked icosahedrons exist in boron that are not present in other base materials [8]. The capacity of boron to create stable molecular networks with covalent bonds makes it comparable to carbon. Regular boron icosahedra are seen in amorphous boron. Crystalline boron forms four primary allotropes: γ-orthorhombic, β-tetragonal, α-rhombohedral, and β-rhombohedral [5].

Table 1. Structural properties of boron.

	B
Atomic number	5
Phase	Solid
Atomic weight	10.81
Allotropes	α-tetragonal, α-rhombohedral, β-rhombohedral, γ orthorhombic, β-tetragonal, borophene, cubic boron, borospherene, amorphous boron
Isotope	^{10}B, ^{11}B
Melting point	2076°C
Density (liquid)	2.08 g/cm^3
Molar heat capacity	11.087 J/(mol·K)
Thermal conductivity	27.4 W/(mK)
Electronegativity	2.04

*Corresponding author: glbhrblg@nevsehir.edu.tr

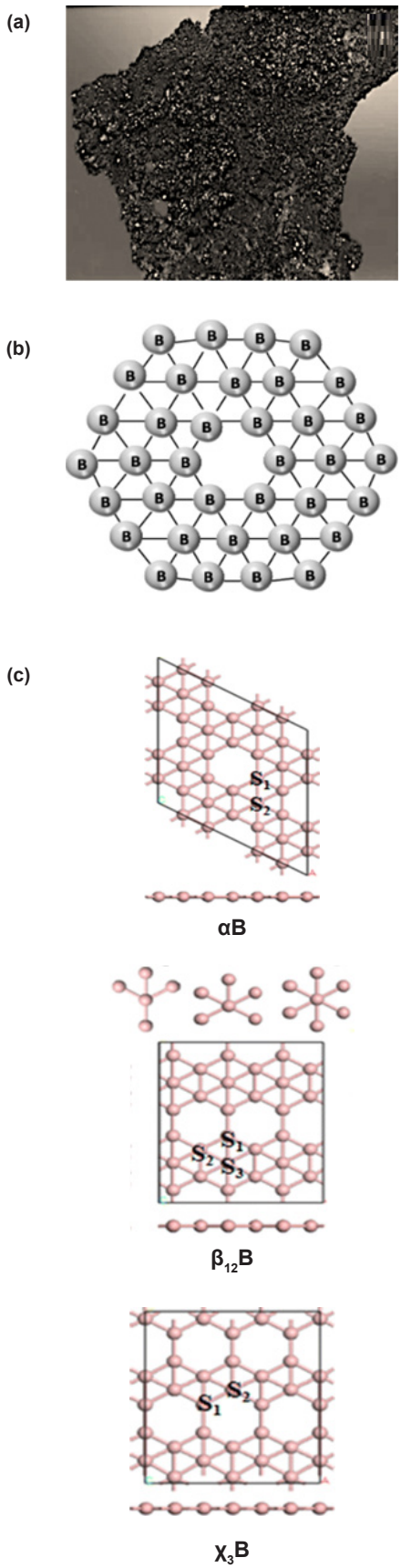

Figure 1. a) The real image of borophene, b) Structure of smallest atomic-cluster scale borophene (B_{36}), c) Top and side views of atomic structures of αB, β_{12}B, and χ_3B [Open access 27].

At room temperature, the most prevalent and stable phase is β-rhombohedral. In 2014, it was discovered that elemental boron has new allotropes called borospherene (B40 molecules similar to fullerene) and borophene (a structure similar to graphene) icosahedra [9]. Due to their extremely 2D electron quantum confinement, these 2D nanomaterials have considerable promise for many uses, including biomedicine, electronics, catalysis, and energy storage [10]. Of these nanomaterials, graphene is one of the most well-known. Its zero-band gap and semi-metallic structure, however, restrict its application, especially in semiconductor apparatuses that need a suitable energy gap. Recent research has focused on black phosphorus and antimony because of their low thermal conductivities, high carrier mobilities, and adjustable band gaps. However, these materials degrade rapidly when exposed to air, limiting their use in photoelectric and photovoltaic devices [11]. It has become possible to artificially synthesize 2D borophene from boron atoms recently. Unlike 3D objects generated by specific production processes, pure bulk boron clusters such as B7, B13, or B36 are planar or quasi-planar structures that may form 2D nanostructures like borophene [10].

Borophene and its 2D materials display a wide range of electronic features, including topology, superconductivity, charge density wave, magnetism, and other rich physical properties [13]. Both graphene and borophene have a huge specific surface area and a 2D planar structure. Furthermore, the B atom has a lower relative atomic mass than the C atom. This fact makes borophene superior to graphene in applications such as hydrogen storage (HS) [14]. In brief, the crystalline form of boron's atomic monolayer is called borophene. This current review of borophene research focuses on new developments in EAs. Firstly, the chemical and physical characteristics of borophene were covered. The thermal, optical, mechanical, electrical, elastic, and mobile characteristics of borophene have been compared with those of other 2D materials. Then, recent advancements in the synthesis of borophene are explained in various stages. Subsequently, the possible uses of borophene were explored, including supercapacitors, metal ion batteries, catalytic behavior, and HS. Large-scale applications in the fields of energy, green chemistry, catalysis, nanocomposites, nanohybrids, heterolayer devices, and sensors can all benefit from this review. Lastly, a summary of borophene is provided, considering its significant contribution to materials science and applications. Even after borophene was realized experimentally, most of the literature on the subject still focuses on theoretical studies. More work is needed to uncover more novel and intriguing physical features of crystalline and semiconductor borophene [15]. This brief analysis will lead to a fresh perspective on the matter.

2. Structure, Chemical and Physical Properties of Borophene

Comprehensive research of 2D boron materials was prompted by the proposal of Boustani et al. [16,17] that the most stable boron structure might form by bucking triangular motifs. Lau and Pandey [18] demonstrated that the buckled triangular boron may be stabilized by combining delocalized three-center-two-electron bonds and localized two-center-two-electron σ bonds. In a study conducted by Yakobson et al. in 2007 [19], the B80 buckyball, consisting of 20 hexagons and 12 pentagons, was found to be similar to the well-known C60 fullerene in terms of form and symmetry. Figure 1a displays the real image of borophene. Whereas the next element of boron, carbon, favors a bulk two-dimensional layered graphite, borophene is well-known for the presence of B12 icosahedral lattices, which serve as the building blocks for several boron compounds. Since there are only three electrons in the outer shell of borophene, and since the electrons are highly confined, and limited to each boron atom and its neighbor, the honeycomb of borophene is unstable. However, both the basic unit of the bulk boron molecule and the icosahedral B12 cluster [20-22] are very reactive. In addition to the above structures, three more pure B, B7, B13, and B36, have been reported, but their existence is still entirely hypothetical. B7, B13, or B36 (see Figure 1b) are planar or quasi-planar structures that can form 2D nanostructures like borophene. Planar and quasi-planar structures, usually constructed as pentagonal pyramid B6 or hexagonal pyramid B7 units, have been experimentally proven [17]. Unlike graphene, which has a higher relative atomic quality, borophene has an anisotropic structure that gives it outstanding mechanical qualities. Furthermore, borophene outperforms Pt and MoS_2, which are readily accessible on the market, as a feasible choice for hydrogen evolution reaction (HER) in H_2 fuel batteries, according to recent research. Graphene is not as efficient at storing H_2 gravimetrically as borophene [23]. The atomic structure, typical of electron-deficient elements like boron, is created via polycentric and bicentric in-plane bonding. The two-dimensional boron sheet borophene also exhibits this structural diversity. A further examination reveals that the borophene synthesizes in three phases, specifically 2Pmmn, β12, and χ3 [24]. Furthermore, χ3 and β12 both show a triangular lattice that is identified by various periodic hole configurations. Scanning tunneling microscopy has demonstrated that they are likewise flat, lacking any observable vertical undulation. Finally, the hole densities of the β12 and χ3 sheets are quite close together [4]. The borophenes β12 and χ3 are metallic. Tight hole densities in the β12 and χ3 sheets explain the simple exchanges between the two structures during annealing. They are both flat and free of vertical undulation [4]. One of these is the fully flat χ3 phase, whereas β12 is an atomic sheet with atomic ridges [24-27]. Figure 1c shows the atomic structures of αB, β12B, and χ3B borophene. Higher electron densities are observed along the ridges with the χ3 phase [25,26]. The gaps between the ridge lines can serve as ion transport channels in use for energy storage. It is predicted that the atomic bonding of gaseous molecules on the borophene surface will be better at the ridge line, as this may provide better stabilization. In a similar vein, more catalytic activity is anticipated [24]. Borophene is a remarkable material because of its special qualities and enormous potential for technological applications. Nevertheless, before it can be marketed, more research on its structural traits and qualities is needed. A vacancy defect in borophene that affects the mechanical characteristics was proposed by Zhou and Jiang [28]. The synthesized χ3 and sheets were found to have Young's modulus up to 198.5 N/m and 179.0 along the armchair direction. Additionally, 2-Pmmn displays a negative Poisson's ratio that is entirely distinct from all known 2D materials. The Young's modulus of the 2-Pmmn phase is 398 N/m. This value is larger than that of β12 and χ3. According to Penev et al.'s [29] prediction, the 2px and 2py states gave rise to the metallic states of β12 and χ3 sheets, which caused a band gap to develop in the boron sheets at η=10~15%, almost exactly at the Fermi level. Further theoretical calculations show that borophenes such as α, β12, χ3 and δ6, boron layers can achieve structural planarity and greater stability by intermixing hollow hexagons and triangular lattice instead of just triangular lattice [7]. Interestingly, the hollow hexagons of the triangular lattice contribute significantly to the structural diversity of borophene. After hydrogenation, the γ-B28 and α′-borophene have been effectively studied by Hou et al. [30], who discovered that the boron may widen up the bandgap to generate semiconducting materials. In the meantime, photoluminescence spectroscopy and UV-vis absorption were also studied to work the optical characteristics of the boron sheets. In borophene, thermal conductivity has been investigated as an additional significant physical characteristic. The many kinds of thermal conductivity are a result of the diversity of borophene structures. The heat conductivity of α-sheet borophene was found to be 1.43 $nWK^{-1}nm^{-2}$ [13]. Furthermore, the majority of other borophenes have anisotropic heat conduction. In the zigzag and armchair directions, the thermal conductivities of β12 are approximately 10.97 and 3.30 $nWK^{-1}nm^{-2}$, respectively. As a result, it was discovered that borophene has almost as remarkable thermal conductivity as graphene. Furthermore, employing first-principles calculations, Yakobson et al. [31,32] have methodically examined the superconducting property of borophene. Amazingly, they discovered that superconductivity was present in every kind of stable borophene. Nonetheless, there are currently few experimental studies on the advantageous characteristics of borophenes. It is critically anticipated that further impacts on experimental realization would enhance and validate the features of borophene [31-34]. Figure 2 shows the top view of χ3-borophene along the (a) c-axis (b) a-axis and (c) b-axis [25].

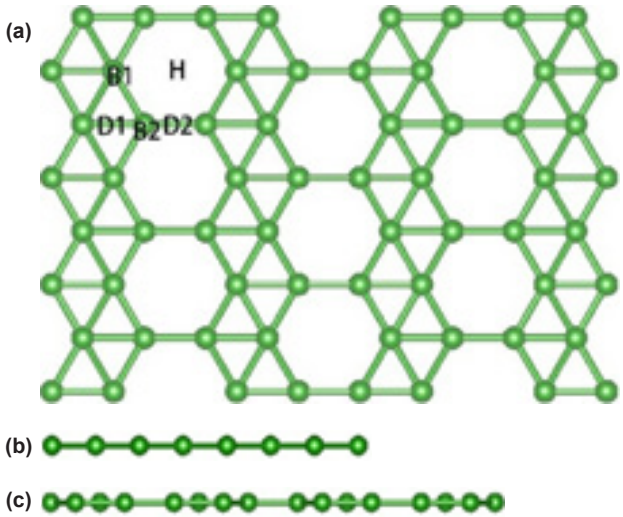

Figure 2. Top view of χ_3-borophene along the (a) c-axis (b) a-axis, and (c) b-axis (Open access [25]).

3. Synthesis of Borophene

Because of its distinct chemical and physical characteristics, borophene has accelerated many applications in optoelectronics, nanoelectronics, energy conversion, and energy storage [32].

However, because of the material's reactivity, borophene is prone to oxidation. These factors make borophene costly to produce and challenging to handle. This makes borophene less useful in general. A few review papers on the synthesis and uses of borophene have surfaced recently. Their primary synthesis methods are ultra-high vacuum (UHV), chemical vapor deposition (CVD), exfoliation by sonochemistry (ExS), and molecular beam epitaxy (MBE) for borophene. What is important in the structure and quality of the synthesized borophene are the materials that provide the kinetically preferred growth. A suitable metal substrate, such as Cu or Ag stabilizes the formation of 2D boron clusters. Second, the temperature needs to be carefully regulated, as extremely low temperatures prevent boron growth from exceeding the nucleation barrier of the 2D structure. In such cases, boron aggregates are formed. When temperatures are very high, growth is encouraged to overcome the 3D boron nucleation barrier, resulting in the development of 3D structures. As a result, the temperature must be maintained at the temperature between the development of 2D and 3D structures [12,30]

3.1. Ultra High Vacuum Conditions

By forcing the gas out of a UHV chamber, ultra-high vacuum conditions are produced. The gas is in free molecular flow at these low pressures. Before a gas molecule collides with another gas molecule, it will collide with the chamber walls several times. As a result, nearly every molecular interaction occurs on different chamber surfaces. The focus of borophene has been on its varied polymorphism and anticipated characteristics, such as phonon-mediated high mechanical strength, superconductivity, and flexibility. However, borophene oxidizes quickly in air, making it difficult to integrate borophene into useful devices and restricting experimental characterization to UHV conditions. Liu et al.'s [34] work involved hydrogenating borophene with atomic hydrogen under an extremely high vacuum to create "borophene" polymorphs. Borophene was hydrogenated by subjecting it to atomic hydrogen under UHV conditions. In an ultrahigh vacuum preparation room (~1×10^{-10} mbar), a solid boron rod was evaporated onto Ag (111) sheets on mica. The pristine Ag (111) surface was prepared for borophene development by repeatedly sputtering Ar ions for 30 minutes at 1×10^{-5} mbar and then annealing for 30 minutes at 550°C. According to the findings, the most prevalent borophene polymorph has a mixture of three-center-two-electron boron-hydrogen-boron and two-center-two-electron boron-hydrogen connections. Kiraly et al. [22] synthesized and characterized nanoscale borophene structures on Au (111) at UHV. Spectroscopic measurements revealed that borophene grown on Au (111) has a metallic electronic structure. A statistical examination of island size revealed that, at low boron concentration, borophene islands were composed of one to eight rhombohedral units with a typical area of 1 nm2. It was verified that borophene on Au (111) had metallic electrical characteristics. Mannix et al. [35] produced thin borophene layers on the inert Ag (111) single-crystal surface. Solid boron was used as a source of atoms under an extremely high vacuum to create the sheets. To circumvent the difficulties presented by hazardous precursors, it was produced as atomically thin sheets of borophene under UHV conditions utilizing a solid supply of boron atoms. The findings demonstrated that at the substrate temperature of 550°C, three phases of borophene the scrapped phase, the homogenous phase, and the nanoribbons were produced. The substrate was kept at between 450°C and 700°C during development, with a boron flow rate of between 0.01 and 0.1 monolayers per minute. The conjugated striped phase appeared as the temperature rose; however, both phases exhibited metallic characteristics. However, due to significant material consumption and energy loss, maintaining UHV conditions in laboratories is expensive and difficult. It also takes a lot of time.

3.2. Molecular Beam Epitaxy

Recently, boron nanosheets on an Ag substrate were successfully manufactured using MBE, as shown above. However, the method's applicability as a manufacturing technique was constrained by the poor yield, which led to a tiny sample at a high cost. MBE is a concentrated kind of physical vapor deposition or vacuum evaporation that allows for exact control over doping concentrations, alloy compositions, material cleanliness, and interface formation [36]. To confirm the 2D structure of borophene, Feng et al. [37] grew atomic borophene layers on silver substrates with the UHV chamber combining an MBE. Elemental boron,

used as a precursor to borophene, was evaporated on a pure silver substrate at temperatures ranging from 550 to 800 K. As a result, β12 and χ3 phase borophene were obtained. Zhu and colleagues [38] used ab initio calculations to evaluate the enhanced stability of the MBE method for effectively producing honeycomb borophene onto an aluminum substrate. Analysis of the structural, electrical, and lattice energy factors yielded results indicating a strong adhesion between the metal substrate and honeycomb borophene that was significantly higher than that of graphene and metal. Li et al. [39] have successfully synthesized graphene-like borophene, a pure honeycomb, by growing MBE in an ultrahigh vacuum on an Al (111) surface. Images obtained using scanning tunneling microscopy show that borophene is a perfect monolayer with a flat, non-buckled honeycomb structure, similar to graphene. Liu et al. [40] experimentally demonstrated the synthesis of an atomically well-defined borophene on Ag (111) via MBE in a UHV. The structure of this bilayer (BL) borophene is consistent with two covalently bonded α-phase layers (referred to as BL-α borophene), according to the results of its characterization. A heightened local work function surpassing 5 eV and significant interfacial charge transfer doping are shown by field-emission resonance spectroscopy, whereas the electronic density of states around the Fermi level of BL-α borophene is identical to that of SL borophene polymorphs. Van der Waals epitaxy is considered to be a highly effective method for growing perfect 2D materials on large functional substrates; however, there are currently no reports on the stable and controlled synthesis of borophene on non-metallic substrates. Wu et al. [41] have formed borophene films on a mica substrate using van der Waals epitaxy, where H_2 and sodium borohydride ($NaBH_4$) served as carrier gases and boron sources. The lattice structure of the synthesized borophene was found to match the expected α′-boron layer. Under the light of a 625 nm light-emitting diode, the borophene photodetector exhibits good photosensitivity of 1.04 A W^{-1} at a reverse bias of 4 V.

3.3. Chemical Vapor Deposition

CVD is a technique commonly used to produce graphene. It has been tried to use this technique to produce more 2D borophene at a reduced cost while also increasing its efficiency and yield. However, the substrates selected, and the various conditions used for various applications remain to be studied extensively. Therefore, more research into borophene synthesis techniques and related circumstances is crucial. The vacuum deposition method, known as CVD, is used to produce solid materials with excellent performance. In the semiconductor sector, this process is widely used to make thin sheets. In conventional CVD, one or more volatile precursors are introduced to the wafer (substrate); thereafter, they react and/or decompose to generate the target deposit on the substrate surface. Gas passage across the reaction chamber regularly produces and eliminates volatile byproducts. In microfabrication procedures, CVD is commonly utilized to deposit materials in a range of morphologies, including amorphous, polycrystalline, and monocrystalline. Borophene, carbon nanotubes, diamond, graphene, tungsten, filaments, fluorocarbons, titanium nitride, and various high dielectrics are among these materials [42]. Tai et al. [43] successfully grew a borophene-like material on Cu using the CVD technique. The process was performed at 1100°C with a B: B_2O_3 ratio of 1:1, conditions like those utilized in the production of graphene. To create borophene, the CVD process involves injecting diborane onto a flat surface that has been warmed, cleaned atomically, and subjected to a high vacuum. The surface was then selectively filtered from borazine using a liquid nitrogen-cold trap in a freeze-thaw cycle. Hou et al. [30] used a handmade CVD to build the boron monolayer. Throughout the experiment, hydrogen gas was utilized as a carrier gas, and a combination of B and B_2O_3 powders as a boron source to create diboron dioxide vapor. A temperature of 1100°C was set. A big area of boron monolayer was produced on Cu foil at 1000°C for one hour. The analysis results unmistakably demonstrated that the monolayer structure consisted of icosahedral B12 units and B2. Furthermore, considerable photoluminescence was seen, suggesting that the monolayer is a promising semiconductor. The optical band gap of the produced borophene determined by UV-vis was found to be around 2.25 eV, which is close to the predicted value (2.07 eV).

3.4. Exfoliation via Sonochemistry or Liquid Phase Exfoliation

2D materials can be ultrasonically prepared, cleaned, and diluted using sonochemistry [44]. It is difficult to produce borophene sheets without defects, as they generally require extremely low pressure and highly advanced production equipment. ExS synthesis can result in the production of the desired layer, depending on the solvent type and sonication period. Figure 3 shows illustrates the sonication-assisted liquid-phase exfoliation process of borophene. Massive lateral monolayer sheets may emerge if the solvent interacts with the material in the right way. If it does not interact properly, it sonicates for the same length of time and forms sheets with many stacking layers; on the other hand, extended sonication causes fragmentation and little borophene dots. Due to the inherent limitation of borophene growth via UHV and MBE to tiny regions, industrial-scale production is challenging and expensive [21]. Chowdhury and colleagues [45] investigated the electrochemical exfoliation approach used generally to produce graphene. Figure 3 shows borophene production by exfoliation via sonochemistry. This method was utilized to validate the creation of borophene from elemental boron. The generated borophene's Raman spectrum was assessed, and the zeta potential was used to gauge the borophene's stability. When compared to other methods in use, this one may be regarded as the most prospective

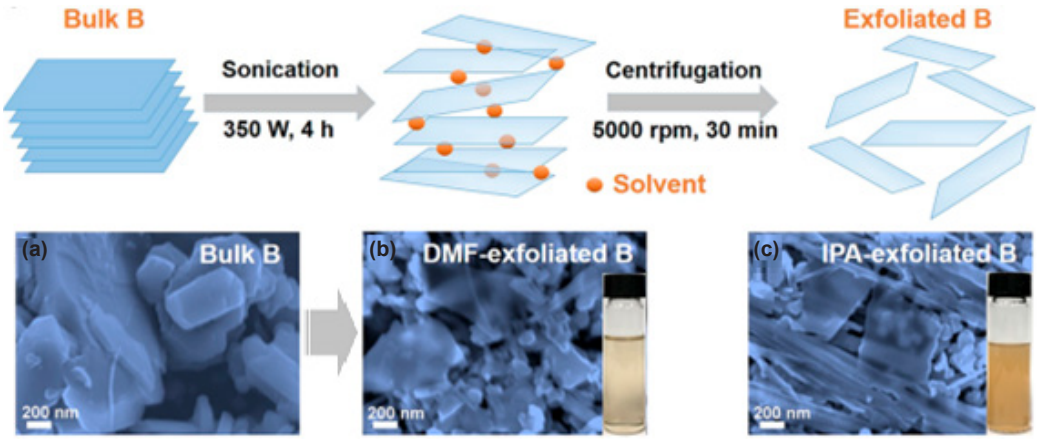

Figure 3. (a) Illustrates the sonication-assisted liquid-phase exfoliation process, (b) SEM images of bulk B. The insets of (c) and (d) show the corresponding photographs of a B sheet dispersion in DMF and IPA, respectively. Reproduced with permission from Ref. [46], ©American Chemical Society, 2018.

and promising approach. Li et al. [46] established a more efficient method of liquid-phase exfoliation for synthesizing high-grade boron sheets by adjusting the concentrations of the solvents dimethylformamide and isopropyl alcohol and the centrifugation rates. Exfoliated few-layer B sheets have been fabricated for the electrode materials of supercapacitors. Exceptional cycle stability with an energy retention of 88.7% was demonstrated by this capacitor, which also displayed exceptional energy density as high as 46.1 Wh/kg at a power density of 478.5 W/kg. It has also been proven to have excellent electrochemical performance with a wide potential of up to 3.0 V. Ranjan et al. [47] stated a simple and flexible technology for the synthesis of borophene utilizing an inventive ExS technique. In contrast to its reduction, which produces free-standing borophene, modification of Hummer's approach resulted in the chemical production of borophene oxide. By using ExS of boron powder in a variety of solvents, including, ethylene glycol, acetone, water, isopropyl alcohol, and dimethylformamide, freestanding borophene was created. The existence of interphases of β12, χ3, and borophene, phase purity, and metallic nature were supported by the analysis results. They found that borophene oxide has a specific capacity of ≈4941 mAh g^{-1}, which is far higher than that of current 2D materials and their hybrids.

Zhang et al. [48] produced a new borophene preparation methodology with several layers and large flake sizes using an ExS approach involving probe ultrasonic and ball milling-thinning. The surface tension of some solvents is correlated with the exfoliating action of B precursors. When utilizing solvents, a comparatively low surface tension is appropriate for exfoliating bulk B. Four thick layers of borophene with an average lateral dimension of 5.05 μm were created using acetone as the peeling solvent. Large-flake-size exfoliated few-layer borophene exhibits minimal surface composition change. On the other hand, surface contamination both before and during exfoliation causes a certain amount of chemical state

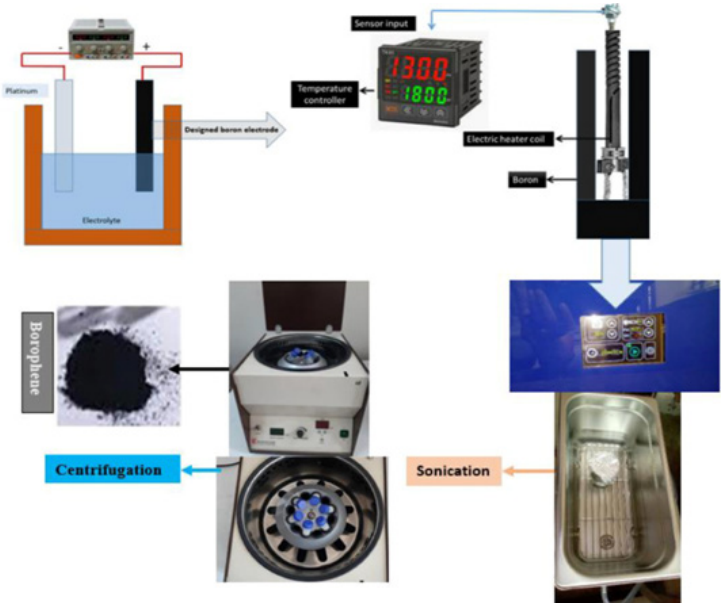

Figure 4. Borophene production by ExS (Open access [45]).

alteration in B. This liquid-phase-exfoliation process with acetone solvothermal assistance can provide enormous horizontal sizes of high-quality borophene. This is a straightforward and efficient way to create large-scale, few-layer borophene flakes, and it may be applied to other 2D materials without comparable bulk layer allotropes.

3.5. Multi-Step Thermal Decomposition

IIn recent years, the in-situ MTD of $NaBH_4$ has been used to manufacture freestanding, large-scale, ultra-stable hydrogenated borophene layers. By using in-situ MTD of $NaBH_4$ powder in an atmosphere rich in hydrogen, Wu et al. [49] created metal matrix composites consisting of borophene. By using spark plasma sintering, 3D borophene sheet network/ copper (BSN/Cu) composites have been created. The synthesized samples' structure and chemical bonding properties were assessed using a variety of analytical techniques. In conclusion, the addition of borophene greatly enhances the mechanical characteristics of the composites. Because borophene and copper have a greater interfacial attraction than graphene and copper, they can bond to the material without breaking [49]. Hou et al. [30] synthesized hydrogenated borophenes using in situ MTD of sodium borohydride. Crystalline borophenes rewritable memory devices, which become ultra-stable upon application of strong acid or base, have been found to have impressive switching properties such as a high ON/OFF current ratio, a low operating voltage, and strong stability. In the study, they showed that by using hydrogen as a carrier gas and gradually in situ MTD of sodium borohydride, hydrogenated borophenes can be produced in large quantities without the need for any metal substrate. Table 2 shows the comparison of borophene synthesis methods.

As the newest member of the 2D nanomaterial family, borophene still has a knowledge gap to fill. This can be achieved using an easy, cost-effective, scalable, and repeatable manufacturing process. Therefore, efforts are ongoing to obtain bulk quantities of several-layered borophene and produce bulk amounts of borophene for further fundamental studies and practical potential evaluation. For this purpose, a new method, different from the synthesis methods mentioned above, appears in the literature. Zielinkiewicz et al. [50] investigated the effectiveness of using mechanical energy in a planetary ball mill to exfoliate bulk boron into a few-layered borophene. The conditions under which β-rhombohedral, γ-orthorhombic, and τ-B structures occur have been characterized. It was discovered that the length of the ball-milling process, the mass rotation speed, and the bulk boron loading could all be used to regulate the thickness and distribution of the final flake. In-depth examinations employing microscopic and spectroscopic methods demonstrate that the phase shift brought about by mechanical energy during ball milling aids in the exfoliation process in the borophene sample that is produced. The XRD diffraction patterns of boron before and after ball milling are displayed in Figure 5. For an easy comparison, rotational speed (Figure 5a), time (Figure 5b), and mass loading (Figure 5c) are displayed. All samples exhibited the typical reflections of volumetric boron.

4. Using Borophene as an Energy Material

Applications of borophene in energy have gained a lot of interest due to its ionic conductivity, high surface activity, and metallic band structure suitable for electronic conductivity. Unlike graphene, which has a higher relative atomic quality, borophene has an anisotropic structure that gives it outstanding mechanical qualities. Borophene has been tested in applications related to chemical sensors, voltaic devices, supercapacitors, storage devices, photodetectors, and sensors. Furthermore, the ability to store energy makes borophene a potentially useful electrode material. This section will explain borophene's EAs, such as HS, electronic and optical devices, metal-ion batteries, oxygen, and hydrogen evolution reactions.

4.1. Storage of Hydrogen

Since, hydrogen is a renewable and clean energy source, its development and use are critical for society. One of the most significant technological issues facing the development of H_2 energy sources is HS. The optimal physical HS technique should have average adsorption energy that falls between physical and chemical adsorption energies (0.1-08 eV) [51]. Borophene has attracted attention among physical HS molecules due to its good adsorption kinetics and large specific surface areas. The enormous surface area of the atomic layers and the ease with which hydrogen atoms stick to borophene's monolayer structure make it a promising material for storing hydrogen. According to theoretical research, borophene outperforms other materials in its ability to store hydrogen, being able to store almost 15% of its weight in hydrogen [51-53].

Table 2. Comparison of borophene synthesis methods

Methods	Temperature (°C)	Boron Source	Structure of Borophene	Ref.
Ultrahigh vacuum	400-750	Solid boron	Freestanding monolayer	[35]
Chemical Vapor Deposition	500-1000	Boron rod, B, B_2O_3	γ-phase, rhombohedral	[22]
Exfoliation by Sonochemistry	5-100	Boron powder	β12, X3, and intermediate phases	[24]
Molecular beam epitaxy	150-500	Pure boron, Borax	β_{12} and X_3 phases	[41]
Multi-step thermal decomposition	490-800	$NaBH_4$ powder	3D-borophene network	[49]

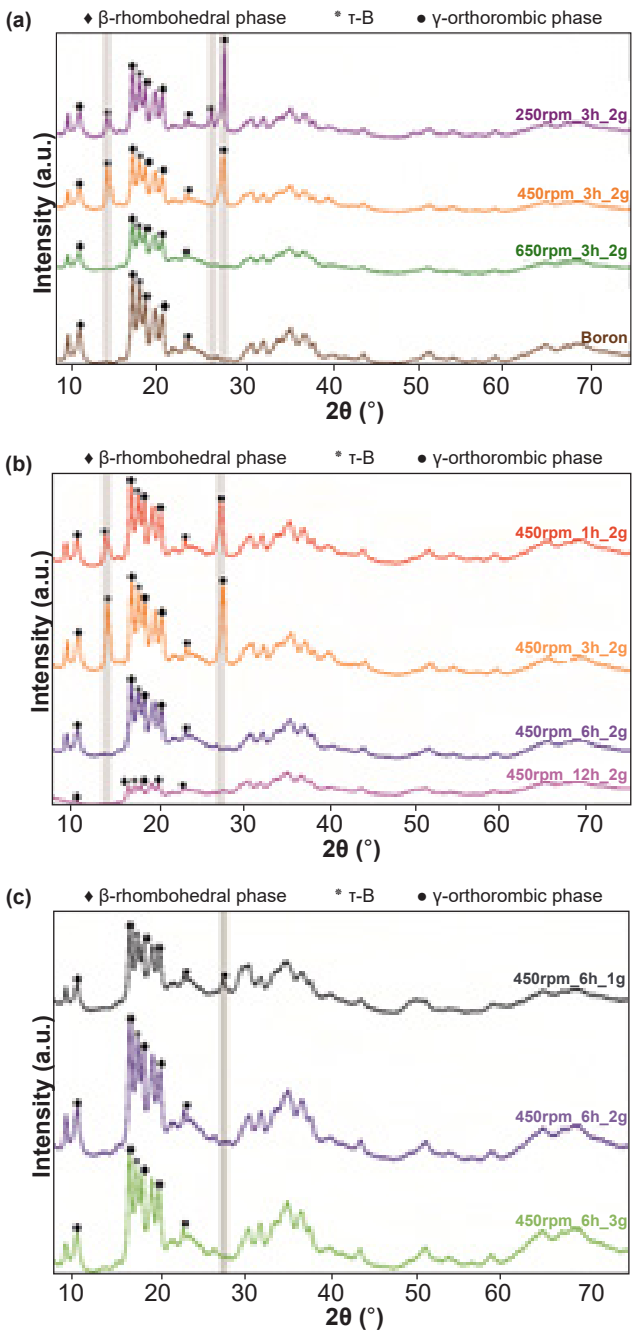

Figure 5. XRD of bulk boron and borophene flakes after the ball-milling process comparing (a) rotation speed, (b) time, and (c) mass loading (Open access [50]).

Baraiya and colleagues [23] utilized density functional theory (DFT)-based first-principles calculations to examine the HS capacity of nitrogen-doped and pure nitrogen-decorated borophene. The work includes a detailed discussion of the adsorption site, charge transfer, electronic structure, adsorption energy, and HS ability of borophene layers that are pristine, nitrogen-doped, and pure nitrogen-decorated. Without clustering, the N atom forms a strong bond with the borophene layer. When an N atom is added, the borophene layer's ability to adsorb H_2 is increased in comparison to its pure state. Nitrogen-doped and pure nitrogen-decorated layers attain gravimetric densities of 6.22 wt% and 1.51 wt%, respectively, according to calculations for HS. Cabria et al. [54] used a quantum thermodynamic model, and Van der Waals-corrected DFT performed the HS capacity of confined Li-decorated borophene layers in a stable configuration. They demonstrated the remarkable volumetric HS capacity, particularly at low temperatures, of borophene's small Li-decorated slit pores. Thus, in low-temperature applications, nanoboron sheets would be perfect for storing H_2. Liu et al. [51] conducted a theoretical investigation into the HS characteristics of β12-borophene and β12-borophene decorated with Li. The results show that H_2 molecules are first totally split into H atoms, which are then adsorbed on the B-B bridge areas. They then modified the HS capacity of β12-borophene and enhanced the HS performance using Li atoms. Numerical simulations show that the 2Li-β12 system has an HS capacity of 10.85 weight percent and can adsorb up to H_2 molecules, compared to the Li-β12 system's maximum capacity of seven H_2 molecules. Consequently, the reversible HS ability was enhanced, and the amount of hydrogen stored was greatly increased by the physical adsorption of H_2 on Li-β12. Using theoretical calculations, Wang et al. [55] looked into the HS characteristics of a novel Ca-decorated boron sheet. One Ca atom has been shown to be able to trap up to six H_2 molecules at 0 K, with an improved binding energy of -0.20 to -0.32 eV/H_2. When the boron plate is adsorbed with Ca on both sides, a gravimetric H_2 density of 12.68 weight percent is attained. It was also determined how temperature and pressure affected the Ca-decorated boron plate's ability to store H_2. The findings indicate that a possible HS medium for use in vehicles is the Ca-decorated boron layer.

4.2. Nanoelectronics Applications

Owing to the extraordinary qualities that were just discussed, borophene has available prospective uses in the many domains of optoelectronics, and nanoelectronics. For these applications, a useful technique to open the band gap of borophene and stabilize the structure of 2D materials is hydrogenation. For instance, graphene, silicene, and germanene can undergo hydrogenation to go from excellent conductors to semiconductors with a large bandgap. Similarly, theoretical studies have demonstrated that hydrogenation is a useful strategy for adjusting the electrical characteristics of boron layers and stabilizing their structure. Large-scale hydrogenated borophenes were successfully produced by Hou et al. [30] using hydrogen as the carrier gas. They created a process for the in situ MTD of $NaBH_4$ in order to generate borophenes under controlled circumstances without the need for a metal substrate. The memory device that was built showed good stability, a small working voltage of less than 0.35 V, and a high ON/OFF current ratio of 3×10^3 [30]. The tunability of the band gap of two-dimensional (2D) semiconductor few-layer borophene was experimentally investigated by Wang et al. [11]. Using EvS, functionalized borophene (borophene-OH)

was created for this purpose. Consequently, by adjusting the centrifugation rates, borophene-OH with the desired thickness was achieved. Smooth borophene was created during exfoliation by surface energy matching and breaking the B-B bond between boron and 2-butanol. Borophene-OH has an adjustable band gap ranging from 0.65 to 2.10 eV. When compared to other 2D monoelemental materials, it demonstrates a considerable increase in photosensitivity (58.5 μAW^{-1}) and photocurrent intensity (5.0 μAcm^{-2}) with the introduction of borophene-OH. As a result, borophene-OH has high optoelectronic potential and is a promising semiconductor. For usage in lasers, Ma et al. [56] looked into the photonic qualities of borophene. They used LPS to create 2D borophene. The produced borophene's shape and structure were thoroughly examined, and a Z-scan was utilized to quantify its nonlinear optical characteristics. It has been discovered that borophene is a highly effective broadband optical switch that is widely employed in mid-and near-infrared laser systems for mode-locking. At center wavelengths of 1560 and 1063 nm, respectively, pulses with durations as short as 693 and 792 fs have been effectively transmitted.

4.3. Catalytic Capabilities

The researchers claim that borophene's exceptional catalytic abilities in the CO_2 electroreduction process, as well as the evolution reactions of hydrogen and oxygen, possess the ability to bring forth a new era for water, including energy cycles. Numerous applications exist for borophene in the HER. The lightest HER catalyst is borophene [49]. There is an excessively strong contact between the H atom and borophene due to its high surface activity. Water splitting might be greatly accelerated by Ni-doped α-borophene, according to Wanga and Zheng's [27] calculations. They showed that decoration or doping with different transition metals, such as Ni or Co, has a profound effect on the catalytic activity of χ3, α, and β12 borophenes. Ni-doped α-borophene exhibited low Gibbs free hydrogen adsorption energy (ΔGH~0.055 eV) for the HER and a worthwhile overpotential (0.455 V) for the OER. According to Wang et al. [27], borophene is a good HER catalyst with many active sites, metallic conductivity, and almost negligible free energy resulting from hydrogen adsorption. However, the free energy of borophene hydrogen adsorption was found to be only 0.02 eV. This is considerably lower than the ΔGH on the mostly used Pt catalyst (0.09 eV). Moreover, a silver substrate has no effect on borophene's strong catalytic activity. Negatively charged borophene has a maximum CO_2 collection capacity of 6.731014 cm^2. Wang and others [26], investigated the catalytic performance of borophene nanoribbons (BNRs) using first-principles calculations. Calculations indicate that BNRs can be highly active edge-dependent catalysts for the hydrogen evolution reaction. The effects of nanoribbon width and strain engineering on the catalytic performance of BNRs were investigated and it was found that the width did not affect the catalytic activity of armchair BNRs (ABNRs). A Gibbs free energy of ΔGH ≈ 0 was reached at a critical pressure strain of εC = -2%. This concludes that ABNRs may be a catalyst for an ultrafast HER through modulation of strain engineering. Figure 6 a and b show the energy-strain diagram of ABNRs and the stress-strain diagram of ABNRs. The figure suggests that the elongation at break for ABNRs is above 5%.

The CO_2 electroreduction of Cu-supported borophene structures was studied by Shen, H., and collaborators. The lowering of the CO_2 electroreduction overpotential is mostly due to the distinct chain architectures of Cu atoms [57]. The researchers found that by offering secondary adsorption sites and producing tiny overpotentials in the favored reaction pathway CO_2-CH_3OH, borophene-based copper chains exhibit strong catalytic activity for CO_2 electroreduction. Cu's outstanding CO_2 consumption performance motivates the distribution of Cu's 2D characteristics for improved catalysis. They investigated the catalytic characteristics of Cu atom chains on β-borophene layers for the first time, motivated by cutting-edge research on novel 2D-protected B-layers. They discovered that by disrupting the cross-sectioning connection, the Cu-B layer would remain safe.

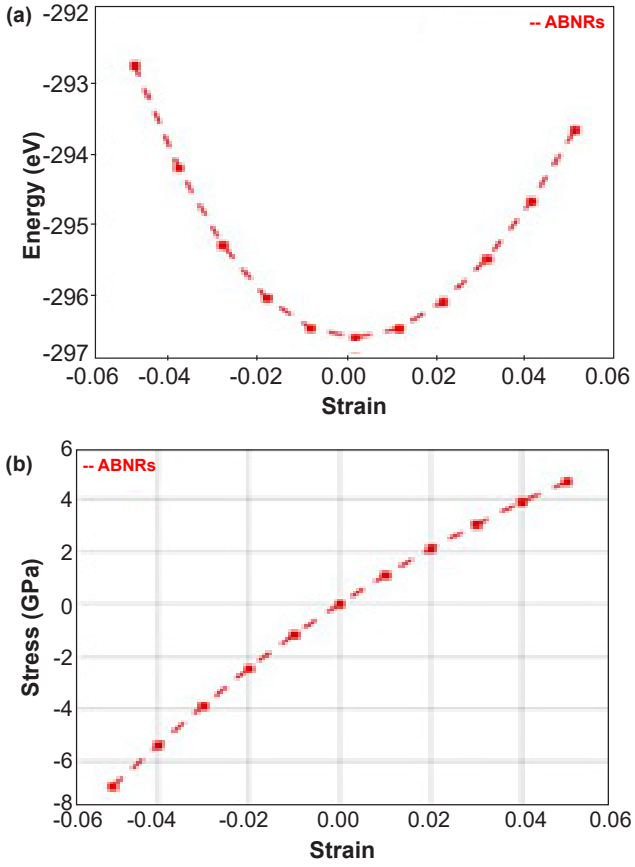

Figure 6. (a) The energy-strain diagram of ABNRs, and (b) the stress-strain diagram of ABNRs. Reproduced with permission from Ref. [26], ©American Chemical Society, 2021.

4.4. Metal-Ion Batteries

Borophene is considered a viable anode material for Na, Li, and Mg ion batteries because of its exceptional ion transport capabilities, high theoretical specific capacities, and good electrical conductivity. The outstanding electronic conductivity and ionic conductivity of borophene ensure the seamless operation of the charging and discharging processes. Borophene film studies in the literature have generally been done from a theoretical perspective. The use of flat borophene films (BFs) in the construction of lightweight, high-capacity, improved rechargeable ion batteries has been investigated [14,20]. Mortazavi et al. [58] investigated the use of distinct flat BFs as anode materials for Li-ion, Al, Mg, and Na batteries using comprehensive first-principles DFT simulations. The charge transfer between the BFs was assessed via Bader charge analysis. The study of ion diffusions was also conducted using the nudged elastic band approach. Profiles of open-circuit voltage and average atom adsorption energies as a function of adatoms coverage were calculated. The results imply that flat borophene films can serve as thermally stable, electrically conductive anode materials for Al, Li-ion, Mg, and Na batteries, with ultra-high capacities of 1640 mAh/g, 2480 mAh/g, and 2040 mAh/g, respectively. Xia and associates [59] suggested halogen decorating as an experimentally workable way to promote the Li-ion transition in χ3 borophene, using χ3 borophene as the prototype system. It is anticipated that borophenes, which are synthetic polymorphs of boron with three different forms (T, β12, and χ3), could one day be used as anode materials for Li-ion batteries that have extraordinary capacity. In the study, potential adsorption sites and binding interactions between halogens and χ3 borophene were examined. The most common diffusion paths have energy barriers of less than 0.2 eV, making iodine the ideal dopant. However, the use of these borophenes in the rapid charging area is hindered by their sluggish hopping of Li into β12 and χ3 borophenes with high energy barriers (about 0.6 eV). Strong binding of halogens to χ3borophene resulted in a large electron transfer from the second to the first, which caused a local electron shortage in χ3borophene. The findings suggest that in borophene-based anode materials, halogen inclusion can promote Li-ion intercalation and deintercalation.

4.5. Supercapacitors

Unlike other 2D materials, borophene's edges can regenerate at low temperatures and low chemical energies. The production of borophene nanomaterials with innovative morphologies, such as ultra-thin borophene nanoribbon, is now possible and is anticipated to enhance electronics performance for a range of applications [18]. It has been proposed that borophene might be a viable material for flexible electronics, such as supercapacitors, when combined with polymers and advanced composites [17]. α-borophene was synthesized by Göktuna and Taşaltın [60] using a simple and inexpensive ultrasonic exfoliation method. The synthesized α-borophene exhibited enough electrostatic repulsion, as indicated by the zeta potential profile, resulting in acceptable physical stability. It was observed that even after 1000 cycles, the synthesized borophene's specific capacitance remained at 95%, measuring 960 $F.g^{-1}$. This demonstrated that α-borophene might enhance polyaniline's functionality. It has been suggested that the developed PANI/Borophene electrode is a promising material for supercapacitors. Large-scale several-layer B sheets were made via sonication-assisted liquid-phase exfoliation by Hongling Li, Lin Jing, and others [61] and their capacitive performance was assessed.

Additionally, exfoliated few-layer B sheets showed exceptional stability and excellent dispersion in organic solvents without aggregates for more than 50 days under ambient conditions. This was made possible by the solvent residue shell that forms an excellent barrier against air oxidation on the B sheet surface. With an impressive energy density of up to 46.1 Wh/kg at a power density of 478.5 W/kg, an energy retention of 88.7%, and an extensive potential window up to 3.0 V, this device as designed delivers excellent electrochemical performance that is demonstrated steadily throughout the cycle. This work provided evidence of a successful method for the regulated synthesis of B-sheets. In addition, the synthesized B shows promise for energy storage and next-generation optoelectronics application. In addition to the energy applications mentioned above, borophene has rarely been studied in other applications. These include photoelectrochemical cells and water separation applications. For a type-II heterojunction, complementary surface-charged, nanoscale 0D-0D hybrids of borophene and phosphorous nitride dots with advantageous band alignments are suggested by Mohanta and Qureshi [62]. For improved photoelectrochemical water oxidation, this hybrid model offers quick carrier separation and resistance to carrier recombination. The two processes in the synthesis of borophene dots were hydrothermal and sonication. To create the 2D sheets, 30 mL of dimethylformamide solution containing 30 mg of boron powder was ultrasonically sonicated at 400 W for 5 hours. The findings demonstrate that improved photoelectrochemical performance is supported by surface charge-directed borophene phosphorous nitride nanodot heterojunction. Zhang et al. [63] studied the effects of two-dimensional boron sheets on solar thermal water evaporation. In this work, they hydrogel-based solar vapor generators enhanced with novel 2D boron nanosheets. Under 1 sun irradiation, the resultant solar vapor generators showed an exceptional evaporation rate of 4.03 $kg\ m^{-2}\ h^{-1}$. The remarkable enhancement is ascribed to the two-dimensional boron nanosheets, which resulted in an increased intermediate water content and a decreased water evaporation enthalpy of 845.11 $kJ\ kg^{-1}$. High salt

resistance and durability were also displayed by the solar vapor generators into which boron nanosheets were included, indicating their enormous potential for desalination applications.

5. Conclusion

In this review, theoretical and experimental progress in borophene research, especially the prospects for its chemical synthesis, was analyzed. Unlike others, research on borophene as a two-dimensional material was dominated by preliminary theoretical research. However, after more than ten years of persistent theory, the discovery of single-atom layer borophene, which has been successfully experimentally synthesized on silver substrates, has stimulated a great deal of research on borophene in the international academic community. There are inherent disadvantages to both top-down and bottom-up techniques in terms of synthesis approaches. Although borophene substrate growth synthesis is made possible by CVD and MBE technologies, which also provide hurdles for real-world borophene applications, these methods are costly, time-consuming, and produce materials that have little.

The further advancement of borophene energy applications inevitably requires many considerations. Previously mentioned methods have been tried to grow large-area, high-quality borophene, but there is still a big challenge in this field. More robust and effective methods must be created to boost production and quality. Phase stability analyses revealed that the 2-Pmmn, χ3, and β12 phases exhibited relatively greater stability on Ag substrates, whereas the production of honeycomb borophene was limited, especially when grown on an Al substrate. One can synthesize borophene in a single phase on a given metal substrate. On the other hand, the wet chemical process leads to the formation of β12 and χ3-phases. Qualitative analysis of the effects of substrate, growth temperature, growth precursors, and other factors on the nucleation of borophene and the inhibition of three-dimensional borophene nucleation needs to be investigated. Borophene's high surface activity is a major synthesis problem as well as a contributing factor to its instability. One way to stabilize them could be to alter their surface in a way that lowers the borophene's surface energy. Hydrogenation is a further strategy for borophene stabilization. Borophene can be used with other 2D materials to lower surface energy and provide a more stable solution. The author hopes that this article can stimulate further theoretical and experimental research and shed light on borophene research, which will ultimately help achieve large-area, high-quality results.

Authorship contribution statement

Gülbahar Bilgiç Tüzemen: Methodology, investigation, writing-original draft, review & editing.

References

[1]. Bilgiç, G., Şahin, M., & Kaplan, H. (2020). A system design for large scale production of elemental boron by electrochemical deposition. *Journal of The Electrochemical Society*, *167*(16), 162513. https://doi.org/10.1149/1945-7111/abd2d7.

[2]. Bilgiç, G. (2022). Investigation of boron-based ionic liquids for energy applications. In Wongchoosuk, C. (Ed.), *Characteristics and applications of boron*. IntechOpen. https://doi.org/10.5772/intechopen.105970.

[3]. Bilgiç, G., Korkmaz, N., Şahin, M., & Karadağ, A. (2022). Synthesis, structural, andelectrochemical properties of boron-based Ionic liquid. *Ionics*, *28*(7), 3289-3300. https://doi.org/10.1007/s11581-022-04575-7.

[4]. Fazilaty, M., Pourahmadi, M., Reza Shayesteh, M., & Hashemian, S. (2020). χ3 borophene-based detection of hydrogen sulfide via gas nanosensors. *Chemical Physics Letters*, *741*, 137066. https://doi.org/10.1016/j.cplett.2019.137066.

[5]. Oganov, A. R., Chen, J., Gatti, C., Ma, Y., Ma, Y., Glass, C. W., … & Solozhenko, V. L. (2009). Ionic high-pressure form of elemental boron. *Nature*, *457*(7231), 863-867. https://doi.org/10.1038/nature07736.

[6]. Biyik, S. (2019). Effect of cubic and hexagonal boron nitride additions on the synthesis of ag-SNO2 electrical contact material. *Journal of Nanoelectronics and Optoelectronics*, *14*(7), 1010-1015. https://doi.org/10.1166/jno.2019.2592.

[7]. Biyik, S., Arslan, F., & Aydin, M. (2014). Arc-erosion behavior of boric oxide-reinforced silver-based electrical contact materials produced by mechanical alloying. *Journal of Electronic Materials*, *44*(1), 457-466. https://doi.org/10.1007/s11664-014-3399-4.

[8]. Sahoo, B. B., Pandey, V. S., Dogonchi, A. S., Thatoi, D. N., Nayak, N., & Nayak, M. K. (2023). Exploring the potential of borophene-based materials for improving energy storage in supercapacitors. *Inorganic Chemistry Communications*, *154*, 110919. https://doi.org/10.1016/j.inoche.2023.110919.

[9]. Zarechnaya, E. Yu., Dubrovinsky, L., Dubrovinskaia, N., Filinchuk, Y., Chernyshov, D., Dmitriev, V., … Simak, S. I. (2009). Superhard semiconducting optically transparent high-pressure phase of boron. *Physical Review Letters*, *102*(18), 185501-185504. https:// doi.org/10.1103/PhysRevLett.102.185501.

[10]. Tang, X., Chen, H., & Ding, Y. (2018). Mechanical properties of double-layered borophene with Li-storage. *Materials Research Express*, *6*(3), 035010. https://doi.org/10.1088/2053-1591/aaf367.

[11]. Wang, X., Liang, J., You, Q., Zhu, J., Fang, F., Xiang, Y., & Song, J. (2020). Bandgap engineering of hydroxy-functionalized borophene for superior photo-electrochemical performance. *Angewandte Chemie International Edition*, *59*(52), 23559-23563. https://doi.org/10.1002/anie.202010723.

[12]. Duo, Y., Xie, Z., Wang, L., Mahmood Abbasi, N., Yang, T., Li, Z., … & Zhang, H. (2021). Borophene-based biomedical applications: Status and future challenges.

Coordination Chemistry Reviews, *427*, 213549. https://doi.org/10.1016/j.ccr.2020.213549.

[13]. Kaneti, Y. V., Benu, D. P., Xu, X., Yuliarto, B., Yamauchi, Y., & Golberg, D. (2021). Borophene: Two-dimensional boron monolayer: Synthesis, properties, and potential applications. *Chemical Reviews*, *122*(1), 1000-1051. https://doi.org/10.1021/acs.chemrev.1c00233.

[14]. Wang, Z. Q., Lü, T.-Y., Wang, H. Q., Feng, Y. P., & Zheng, J. C. (2019). Review of borophene and its potential applications. *Frontiers of Physics*, *14*, 33403. https://doi.org/10.1007/s11467-019-0884-5.

[15]. Rahman, A., Rahman, M. T., Chowdhury, M. A., Bin Ekram, S., Uddin, M. M. K., Islam, Md. R., & Dong, L. (2023). Emerging 2D borophene: Synthesis, characterization, and sensing applications. *Sensors and Actuators A: Physical*, *359*, 114468. https://doi.org/10.1016/j.sna.2023.114468.

[16]. Boustani, I. (1997). New quasi-planar surfaces of bare boron. *Surface Science*, *370*(2-3), 355-363. https://doi.org/10.1016/s0039-6028(96)00969-7.

[17]. Boustani, I., Quandt, A., Hernández, E., & Rubio, A. (1999). New boron based nanostructured materials. *The Journal of Chemical Physics*, *110*(6), 3176-3185. https://doi.org/10.1063/1.477976.

[18]. Lau, K. C., & Pandey, R. (2007). Stability and electronic properties of atomistically engineered 2d boron sheets. *The Journal of Physical Chemistry C*, *111*(7), 2906-2912. https://doi.org/10.1021/jp066719w.

[19]. Yakobson, B. I., Gonzalez Szwacki, N., & Sadrzadeh, A. (2007). The boron buckyball. *ECS Meeting Abstracts*, *MA2007-01*(28), 1093-1093. https://doi.org/10.1149/ma2007-01/28/1093.

[20]. Chand, H., Kumar, A., & Krishnan, V. (2021). Borophene and boron-based nanosheets: Recent advances in synthesis strategies and applications in the field of environment and energy. *Advanced Materials Interfaces*, *8*(15), 2100045. https://doi.org/10.1002/admi.202100045.

[21]. Li, C., Tareen, A. K., Long, J., Iqbal, M., Ahmad, W., Khan, M. F., … & Khan, K. (2023). Two dimensional borophene nanomaterials: Recent developments for novel renewable energy storage applications. *Progress in Solid State Chemistry*, *71*, 100416. https://doi.org/10.1016/j.progsolidstchem.2023.100416.

[22]. Kiraly, B., Liu, X., Wang, L., Zhang, Z., Mannix, A. J., Fisher, B. L., … & Guisinger, N. P. (2019). Borophene synthesis on au(111). *ACS Nano*, *13*(4), 3816-3822. https://doi.org/10.1021/acsnano.8b09339.

[23]. Baraiya, B. A., Som, N. N., Mankad, V., Wu, G., Wang, J., & Jha, P. K. (2020). Nitrogen decorated borophene: An empowering contestant for hydrogen storage. *Applied Surface Science*, *527*, 146852. https://doi.org/10.1016/j.apsusc.2020.146852.

[24]. Ranjan, P., Lee, J. M., Kumar, P., & Vinu, A. (2020). Borophene: New sensation in flatland. *Advanced Materials*, *32*(34), 2000531. https://doi.org/10.1002/adma.202000531.

[25]. Duan, J.-X., Tian, Y.-P., Wang, C.-B., & Zhang, L.-L. (2023). First-principles study of χ3-Borophene as a candidate for gas sensing and the removal of harmful gases. *Nanomaterials*, *13*(14), 2117. https://doi.org/10.3390/nano13142117.

[26]. Wang, Xiaoyuan, Wu, R., Tian, P., Yan, Y., Gao, Y., & Xuan, F. (2021). Borophene nanoribbons via strain engineering for the hydrogen evolution reaction: A First-principles study. *The Journal of Physical Chemistry C*, *125*(31), 16955-16962. https://doi.org/10.1021/acs.jpcc.1c02770.

[27]. Wang, R., & Zheng, J.-C. (2023). Promising transition metal decorated borophene catalyst for water splitting. *RSC Advances*, *13*(14), 9678-9685. https://doi.org/10.1039/d3ra00299c.

[28]. Zhou, Y-P., & Jiang, J-W. (2017) Molecular dynamics simulations for mechanical properties of borophene: parameterization of valence force field model and Stillinger-Weber potential. *Scientific Reports 7*, 45516. https://doi.org/10.1038/srep45516.

[29]. Penev, E. S., Kutana, A., & Yakobson, B. I. (2016). Can two-dimensional boron superconduct?. *Nano Letters*, *16*(4), 2522-2526. https://doi.org/10.1021/acs.nanolett.6b00070.

[30]. Hou, C., Tai, G., Hao, J., Sheng, L., Liu, B., & Wu, Z. (2020). Ultrastable crystalline semiconducting hydrogenated borophene. *Angewandte Chemie*, *132*(27), 10911-10917. https://doi.org/10.1002/anie.202001045.

[31]. Zhang, Z., Penev, E. S., & Yakobson, B. I. (2017). Two-dimensional boron: Structures, properties and applications. *Chemical Society Reviews*, *46*(22), 6746-6763. https://doi.org/10.1039/C7CS00261K.

[32]. Mannix, A. J., Zhang, Z., Guisinger, N. P., Yakobson, B. I., & Hersam, M. C. (2018). Borophene as a prototype for synthetic 2D materials development. N*ature Nanotechnology, 13*(6), 444-450. https://doi.org/10.1038/s41565-018-0157-4.

[33]. Qin, G., Yan, Q.-B., Qin, Z., Yue, S.-Y., Hu, M., & Su, G. (2015). Anisotropic intrinsic lattice thermal conductivity of phosphorene from first principles. *Physical Chemistry Chemical Physics, 17*(7), 4854-4858. https://doi.org/10.1039/C4CP04858J.

[34]. Liu, X., Wang, L., Yakobson, B. I., & Hersam, M. C. (2021). Nanoscale probing of image potential states and electron transfer doping in borophene polymorphs. *Nano Letters*, *21*(2), 1169-1174. https://doi.org/10.1021/acs.nanolett.0c04869.

[35]. Mannix, A. J., Zhou, X.-F., Kiraly, B., Wood, J. D., Alducin, D., Myers, B. D., … & Guisinger, N. P. (2015). Synthesis of borophenes: Anisotropic, two-dimensional boron polymorphs. *Science*, *350*(6267), 1513-1516. https://doi.org/10.1126/science.aad1080.

[36]. Myronov, M. (2018). Molecular beam epitaxy of high mobility silicon, silicon germanium and germanium quantum well heterostructures. *Molecular Beam Epitaxy*, 37-54. https://doi.org/10.1016/B978-0-12-812136-8.00003-7.

[37]. Feng, B., Zhang, J., Zhong, Q., Li, W., Li, S., Li, H., … & Wu, K. (2016). Experimental realization of

two-dimensional boron sheets. Nature Chemistry, 8(6), 563-568. https://doi.org/10.1038/nchem.2491.

[38]. hu, L., Zhao, B., Zhang, T., Chen, G., & Yang, S. A. (2019). How is honeycomb borophene stabilized on Al(111)?. *The Journal of Physical Chemistry C*, *123*(23), 14858-14864. https://doi.org/10.1021/acs.jpcc.9b03447.

[39]. Li, W., Kong, L., Chen, C., Gou, J., Sheng, S., Zhang, W., … Wu, K. (2018). Experimental realization of honeycomb borophene. *Science Bulletin*, *63*(5), 282-286. https://doi.org/10.1016/j.scib.2018.02.006.

[40]. Liu, X., Li, Q., Ruan, Q., Rahn, M. S., Yakobson, B. I., & Hersam, M. C. (2021). Borophene synthesis beyond the single-atomic-layer limit. *Nature Materials*, *21*(1), 35-https://doi.org/10.1038/s41563-021-01084-2.

[41]. Wu, Z., Tai, G., Liu, R., Hou, C., Shao, W., Liang, X., & Wu, Z. (2021). Van der waals epitaxial growth of borophene on a mica substrate toward a high-performance photodetector. *ACS Applied Materials & Interfaces*, *13*(27), 31808-31815. https://doi.org/10.1021/acsami.1c03146.

[42]. Mazaheri, A., Javadi, M., & Abdi, Y. (2021). Chemical vapor deposition of two dimensional boron sheets by thermal decomposition of Diborane. *ACS Applied Materials & Interfaces*, *13*(7), 8844-8850. https://doi.org/10.1021/acsami.0c22580.

[43]. Tai, G., Hu, T., Zhou, Y., Wang, X., Kong, J., Zeng, T., … Wang, Q. (2015). Synthesis of atomically thin boron films on copper foils. *Angewandte Chemie International Edition*, *54*(51), 15473-15477. https://doi.org/10.1002/anie.201509285.

[44]. Karikalan, N., Elavarasan, M., & Yang, T. C. K. (2019). Effect of cavitation erosion in the sonochemical exfoliation of activated graphite for electrocatalysis of acebutolol. *Ultrasonics Sonochemistry*, *56*, 297-304. https://doi.org/10.1016/j.ultsonch.2019.04.025.

[45]. Chowdhury, M. A., Uddin, M. M. K., Shuvho, Md. B., Rana, M., & Hossain, N. (2022). A novel temperature dependent method for borophene synthesis. *Applied Surface Science Advances*, *11*, 100308. https://doi.org/10.1016/j.apsadv.2022.100308.

[46]. Li, H., Jing, L., Liu, W., Lin, J., Tay, R. Y., Tsang, S. H., & Teo, E. H. (2018). Scalable production of few-layer boron sheets by liquid-phase exfoliation and their superior supercapacitive performance. *ACS Nano*, *12*(2), 1262-1272. https://doi.org/10.1021/acsnano.7b07444.

[47]. Ranjan, P., Sahu, T. K., Bhushan, R., Yamijala, S. S., Late, D. J., Kumar, P., & Vinu, A. (2019). Freestanding borophene and its hybrids. *Advanced Materials*, *31*(27), e1900353. https://doi.org/10.1002/adma.201900353.

[48]. Zhang, F., She, L., Jia, C., He, X., Li, Q., Sun, J., … & Liu, Z.-H. (2020). Few-layer and largeflake size borophene: Preparation with solvothermal-assisted liquid phase exfoliation. *RSC Advances*, *10*(46), 27532-27537. https://doi.org/10.1039/D0RA03492D.

[49]. Wu, Z., Yin, Y., Hou, C., & Tai, G. (2023). Borophene reinforcing copper matrix composites: Preparation and mechanical properties. *Journal of Alloys and Compounds*, *930*, 167370. https://doi.org/10.1016/j.jallcom.2022.167578.

[50]. Zielinkiewicz, K., Baranowska, D., & Mijowska, E. (2023). Ball milling induced borophene flakes fabrication. *RSC Advances*, *13*(25), 16907-16914. https://doi.org/10.1039/d3ra02400h.

[51]. Liu, T., Chen, Y., Wang, H., Zhang, M., Yuan, L., & Zhang, C. (2017). Li-decorated B12 borophene as potential candidates for hydrogen storage: A first-principle study. *Materials*, *10*(12), 1399. https://doi.org/10.3390/ma10121399.

[52]. Ledwaba, K., Karimzadeh, S., & Jen, T.-C. (2022). Enhancement in the hydrogen storage capability of borophene through yttrium doping: A theoretical study. *Journal of Energy Storage*, *55*, 105500. https://doi.org/10.1016/j.est.2022.105500.

[53]. Sosa, A. N., de Santiago, F., Miranda, Á., Trejo, A., Salazar, F., Pérez, L. A., & Cruz Irisson, M. (2021). Alkali and transition metal atom-functionalized germanene for hydrogen storage: A DFT investigation. *International Journal of Hydrogen Energy, 46*(38), 20245-20256. https://doi.org/10.1016/j.ijhydene.2020.04.129.

[54]. Cabria I, Lebon A, Torres MB, Gallego LJ, Vega A. (2021) Hydrogen storage capacity of Li decorated borophene and pristine graphene slit pores: A combined ab initio and quantumthermodynamic study. *Applied Surface Science, 562*, 150019. https://doi.org/10.1016/j.apsusc.2021.150019.

[55]. Wang, L.-C., Zhang, Z.-C., Ma, L.-C., Ma, L., & Zhang, J.-M. (2022). First-principles study of hydrogen storage on Li, na and K-decorated defective boron nitride nanosheets. *The European Physical Journal B*, *95*(3). https://doi.org/10.1140/epjb/s10051-022-00312-1.

[56]. Ma, C., Yin, P., Khan, K., Tareen, A. K., Huang, R., Du, J., … & Gao, L. (2021). Broadband nonlinear photonics in few-layer borophene. *Small, 17*(7). https://doi.org/10.1002/smll.202006891.

[57]. Shen, H., Li, Y., & Sun, Q. (2018). CU atomic chains supported on β-borophene sheets for effective co2 electroreduction. *Nanoscale*, *10*(23), 11064-11071. https://doi.org/10.1039/c8nr01855c.

[58]. Mortazavi, B., Rahaman, O., Ahzi, S., & Rabczuk, T. (2017). Flat borophene films as anode materials for Mg, Na or li-ion batteries with ultra high capacities: A first-principles study. *Applied Materials Today*, *8*, 60-67. https://doi.org/10.1016/j.apmt.2017.04.010.

[59]. Xia, Z., Chen, X., Zhang, W., Li, J., Xiao, B., & Du, H. (2018). Enhancement of lithium ion hopping on halogen-doped χ3 borophene. *Physical Chemistry Chemical Physics*, *20*(37), 24427-24433. https://doi.org/10.1039/C8CP03803A.

[60]. Göktuna, S., & Taşaltın, N. (2021). Preparation and characterization of Pani: α borophene electrode for supercapacitors. *Physica E: Low-Dimensional Systems and Nanostructures*, *134*, 114833. https://doi.org/10.1016/j.physe.2021.114833.

[61]. Li, H., Jing, L., Liu, W., Lin, J., Tay, R. Y., Tsang, S. H., & Teo, E. H. (2018). Scalable production of few-layer boron sheets by liquid-phase exfoliation and their superior supercapacitive performance. *ACS*

Nano, *12*(2), 1262-1272. https://doi.org/10.1021/acsnano.7b07444.

[62]. Mohanta, M. K., & Qureshi, M. (2023). Surface charge-directed borophene-phosphorous nitride nanodot heterojunction supports for enhanced photoelectrochemical performance. *Chemical Communications*, *59*(14), 1955-1958. https://doi.org/10.1039/d2cc05900b.

[63]. Zhang, X. S., Mao, S., Wang, J., Onggowarsito, C., Feng, A., Han, R., … & Huang, Z. (2024). Boron nanosheets boosting solar thermal water evaporation. *Nanoscale*, *16*(9), 4628-4636. https://doi.org/10.1039/d3nr06146a.

YAZAR KILAVUZU

GENEL BİLGİLER

• Makale başvurusu için Makale Metni Dosyası, Telif Hakkı Devir Dosyası ve Benzerlik Oran Dosyası olmak üzere üç ayrı formun doldurulması ve sisteme yüklenmesi gerekmektedir.
• Başvurularda iletişimde bulunulacak yazar ve diğer yazarların iletişim bilgileri bulunmalıdır.
• Makale metni içerisindeki makale kontrol listesi ve kapak sayfası eksiksiz olarak doldurulmalıdır.
• Makale metni dosyası içerisinde bulunan makale kontrol listesi ve kapak sayfası eksiksiz doldurulmalıdır.
• Derleme makalelerde başka yayınlara ait şekil ve tablolar kullanılacaksa, kaynak gösterilecek makalenin yayıncısından izin alınmalıdır. Yayıncıdan izin alındığı ve şekillerin uyarlanıp uyarlanmadığı veya doğrudan kullanılıp kullanılmadığı bilgisi şekil başlığında belirtilmelidir. İlgili izin yazısının journalofboron@tenmak.gov.tr adresine gönderilmesi gerekmektedir.
• Her makale, konusu ile ilgili en az iki hakeme gönderilerek şekil, içerik, özgün değer, uluslararası literatüre katkısı bakımından incelettirilir. Hakem görüşlerinde belirtilen eksikler tamamlandıktan sonra, son baskı formatına getirilir ve yazarlardan makalenin son halinin onayı alınır. Dergide basıldığı haliyle makale içinde bulunabilecek hataların sorumluluğu yazarlara aittir.

MAKALE METNİ DOSYASI

• Makale metninin yazımında yazım kurallarına uyulması gerekmektedir.
• Makale metninde kapsayıcı ve bilimsel bir dil kullanılmalıdır.
• Makale metni referanslar dahil araştırma makaleleri için 14.000 kelimeyi tarama makaleleri için ise 22.000 kelimeyi geçmemelidir.
• Makalenin metni, Times New Roman 12 punto ile Makale Metni Dosyası'nın sayfa düzeni değiştirilmeden yazılmalıdır.
• Makale metninin Microsoft Office Word 2010 ve üzeri bir kelime işlemci ile hazırlanması ve yazım hatalarının kontrol edilmesi ve düzeltilmesi gerekmektedir.
• Eğer makale Türkçe ise, Türkçe başlıklarla bire bir uyumlu olacak şekilde oluşturulmuş İngilizce başlıklar parantez içerisinde yazılmalıdır.
• Makale içerisinde kullanılan kısaltma ve sembollerin anlamları ilk kullanıldıklarında açıklanmalıdır.
• Makale metni içerisindeki alt başlıklar numaralandırılmalıdır. Numaralandırma işlemleri ana bölümler için 1.'den başlamalı ve tüm ana başlıklar (Özet, Teşekkür ve Kaynaklar ve Ekler bölümleri hariç) için devam etmelidir. İkincil başlıklar ana bölüm numaralandırmasına uygun olarak 1.1., 1.2., 1.3., ... şeklinde devam etmelidir. Üçüncü başlıklar ikinci başlıklara uygun olarak 1.1.1., 1.1.2., 1.1.3., ... şeklinde devam etmelidir.

TELİF HAKKI DEVİR DOSYASI

• İmzalı Telif Hakkı Devir Dosyası taranarak sisteme yüklenmelidir.
• İmzalı Telif Hakkı Devir Dosyası'nı göndermeyen yazarların başvuruları değerlendirmeye alınmaz.

BENZERLİK ORAN DOSYASI

• Makalenin referanslar bölümü hariç metni "iThenticate" veya "Turnitin" programları ile taranmalıdır.
• Benzerlik oranı raporunun PDF formatında sisteme yüklenmelidir.
• Benzerlik oranı %15'in üzerinde olmamalıdır.

GİZLİLİK POLİTİKASI

Journal of Boron gizliliğe saygı duymaktadır. Kişisel bilgiler, sadece derginin belirtilen amaçları doğrultusunda kullanılacak ve üçüncü kişilerle paylaşılmayacaktır.

YAZIM KURALLARI

MAKALE BAŞLIĞI
• Makale başlığı standart kısaltmalarla birlikte en çok 15 kelimeden oluşmalıdır.
• Eğer makale Türkçe ise, İngilizce başlıkla bire bir uyumlu olacak şekilde Türkçe makale başlığı da oluşturulmalıdır.

ÖZET
• Özet, 250 kelimeyi geçmemelidir.
• Standart olmayan kısaltmalar ilk kullanıldığında tam açıklamalarından sonra parantez içerisinde yazılmalıdır.
• Eğer makale Türkçe ise, İngilizce özetle bire bir uyumlu olacak şekilde Türkçe özet de oluşturulmalıdır.

ANAHTAR KELİMELER
• En fazla 5 anahtar kelime, alfabetik sıraya göre yazılmalıdır.
• Kısaltmalar anahtar kelime olarak kullanılmamalıdır.
• Eğer makale Türkçe ise, İngilizce anahtar kelimelerle bire bir uyumlu olacak şekilde Türkçe anahtar kelimelere de oluşturulmalıdır.

GİRİŞ
• İlgili literatürün özeti, çalışmanın amacı ve özgün değeri ve kurulmuş olan hipotezi içermelidir.
• Kaynaklar, toplu olarak ve aralıklı verilmemeli (örnek [1-5] veya [1, 2, 3, 5, 8]), her kaynağın çalışmaya katkısı irdelenmeli ve metin içerisinde belirtilmelidir.

MALZEMELER VE YÖNTEMLER
• Yürütülmüş olan çalışma deneysel bir çalışma ise deney prosedürü/metodu anlaşılır bir şekilde açıklanmalıdır.
• Teorik bir çalışma yürütülmüşse teorik metodu detaylı bir şekilde verilmelidir.
• Yapılan çalışmada kullanılan metot daha önce yayınlanmış bir metot ise diğer çalışmaya atıf yapılarak bu çalışmanın diğer çalışmadan farklı belirtilmelidir.

SONUÇLAR VE TARTIŞMA
• Elde edilen sonuçlar açık ve öz bir şekilde verilmelidir.
• Elde edilen tüm sonuçlar atıf yapılarak literatür ile karşılaştırılmalıdır.
• Tablolar numaralandırılmalıdır ve düzenlenebilir formatta olmalıdır. Eğer makale Türkçe ise, tablo üst yazılarının bire bir İngilizce çevirileri parantez içerisinde verilmelidir.
• Makale içerisindeki şekiller numaralandırılmalıdır ve en az 300 dpi çözünürlükte olmalıdır. Şekillerin üzerindeki yazılar okunabilir büyüklükte ve yazı tipinde olmalıdır. Kabul edilen şekil formatları TIFF, JPG ve JPEG'dir. Eğer makale Türkçe ise, şekil alt yazılarının bire bir İngilizce çevirileri parantez içerisinde verilmelidir.

SONUÇLAR
• Çalışmadan elde edilen ana sonuçlar ve çıkarımlar kısa ve öz bir şekilde verilmelidir.
• Çalışmaya ait gelecek perspektifleri bu bölümde verilir.

TEŞEKKÜRLER
• Çalışmanın gerçekleşmesi için sağlanan maddi kaynaklar ve kullanılan altyapı bu bölümde belirtilir.
Yazar Katkıları
• Her yazarın katkıları belirtilmelidir.
• Katkı rolleri şu şekildedir: kavramsallaştırma, veri analizi, veri iyileştirme, finansman sağlama, metodoloji, proje yönetimi, kaynak sağlama, yazılım analizi, denetim, doğrulama, görselleştirme, orijinal taslak yazma, inceleme yazma ve düzenleme.

KAYNAKLAR
• Basılmış kaynakların DOI ve ISBN numarası belirtilmelidir.
• İnternet sitesi adresleri (URL) kaynak olarak verilmemelidir. Ancak metin içerisinde istatistiksel bir verinin geçtiği yerde veriden sonra belirtilebilir.
• Kaynaklar listesi metin içerisinden kullanılma sırasına uygun olarak numaralandırılmalıdır.
• Kaynaklar, "APA Publication Manual, Seventh Edition" kurallarına uygun olarak hazırlanmalıdır.
• Kaynaklar İngilizce olarak hazırlanmalıdır. Türkçe kaynakların İngilizce karşılıkları köşeli parantez içerisinde belirtilmelidir.
• APA formatı ve örneklere aşağıdaki bağlantıdan ulaşılabilir.
https://apastyle.apa.org/style-grammar-guidelines/references/examples

EKLER
• Makaledeki ekler EK A (Appendix A), EK B (Appendix B) ve EK C (Appendix C) vb. olarak adlandırılmalıdır.
• Ekler içerisindeki denklemler A1, A2, A3 vb. olarak adlandırılmalıdır, tablo ve şekiller Tablo A1, Tablo A2, Şekil A1, Şekil A2 vb. olarak adlandırılmalıdır.

AUTHOR'S GUIDE

GENERAL INFORMATION

• For article application, 3 individual files which are Manuscript File, Copyright Transfer File and Similarity Ratio File, must be filled in and uploaded to the system.
• Applications should include the contact information of the author and other authors to be contacted.
• The article checklist and cover page in the Manuscript File should be filled in completely.
• Each article is sent to at least two referees related to its subject and examined in terms of format, content, novelty, contribution to literature.
• If figures and tables from other publications are to be used in review articles, permission must be obtained from the publisher of the article to be cited. The information that permission has been granted from the publisher and whether the figures have been adapted or used directly should be mentioned in the figure caption. The relevant permission letter should be sent to journalofboron@tenmak.gov.tr.
• After the deficiencies stated in the referee's comments are completed, it is brought to the final print format and the approval of the final version of the article is obtained from the authors. The responsibility of errors that may be found in the article as it is published in the journal belongs to the authors.

MANUSCRIPT

• Writing rules must be followed, during writing of the manuscript.
• Inclusive and scientific language must be used in the manuscript.
• Manuscript should not exceed 14,000 words for research articles and 22,000 words for review articles, including references.
• The manuscript should be written in Times New Roman 12 points without changing the page layout of the Manuscript File.
• The manuscript should be prepared with a word processor of Microsoft Office Word 2010 and above, and spelling errors should be checked and corrected.
• Abbreviations and symbols used in the manuscript must be explained when used fort he first time.
• Subheadings in the article should be numbered. Numbering should start at 1 for the main section and continue for all main headings (except the Summary, Acknowledgments and References and Appendices sections). Secondary titles continue as 1.1., 1.2., 1.3., ... in accordance with the main chapter numbering. The third headings continue as 1.1.1., 1.1.2., 1.1.3., ... in accordance with the second headings.

COPYRIGHT TRANSFER FILE

• Signed Copyright Transfer File should be scanned and uploaded to the system.
• Applications of the authors who do not send the signed Copyright Transfer File will not be evaluated.

SIMILARITY RATIO FILE

• The manuscript should be scanned with "iThenticate" or "Turnitin" programs, except for the references section.
• The similarity ratio report should be uploaded to the system in PDF format.
• The similarity ratio should not exceed 15%.

PRIVACY POLICY

Journal of Boron respects privacy. Any personal information will only be used in line with the stated purposes of the journal and will not be shared with third parties.

WRITING RULES

TITLE
• The title of the manuscript should consist of a maximum of 15 words with standard abbreviations.

ABSTRACT
• The abstract should not exceed 250 words.
• Non-standard abbreviations should be written in parentheses after their full explanation, when they are used for the first time.

KEYWORDS
• A maximum of 5 keywords should be written in alphabetical order.
• Abbreviations should not be used as keywords.

INTRODUCTION
• The summary of the relevant literature, aim and novelty of the study, and the established hypothesis should be included.
• References should not be given in bulk and in intervals (example [1-5] or [1, 2, 3, 5, 8]), the contribution of each source to the study should be examined and stated in the text.

MATERIALS AND METHODS
• If the study carried out is an experimental study, the test procedure/method should be clearly explained.
• If a theoretical study has been carried out, the theoretical method should be given in detail.
• If the method used in the study is a previously published method, the other study should be mentioned by citing.

RESULTS AND DISCUSSION
• Obtained results should be given in a clear and concise manner.
• All of the results should be compared with the literature by citing.
• Tables should be numbered and in editable format.
• Figures in the manuscript should be numbered and have at least 300 dpi resolution. The texts on the figures should be in legible size and font. Accepted figure formats are TIFF, JPG, and JPEG.

CONCLUSIONS
• Main conclusions and inferences obtained from the study should be given concisely.
• Future perspectives of the study are given in this section.

ACKNOWLEDGEMENTS
• The financial resources provided and the infrastructure used during the study are specified in this section.

AUTHOR CONTRIBUTIONS
• Contributions of each author must be stated.
• Contribution roles are as follows: conceptualization, data analysis, data curation, funding acquisition, methodology, project administration, sourcing, software analysis, supervision, validation, visualization, writing original draft, writing review and editing.

REFERENCES
• DOI and ISBN numbers of printed sources should be specified.
• Website addresses (URLs) should not be given as a source. However, it can be specified after the data where a statistical data is mentioned in the text.
• The list of references should be numbered according to the order in which they are used in the text.
• References should be prepared in accordance with the rules of “APA Publication Manual, Seventh Edition”.
• References should be prepared in English. English equivalents of sources should be indicated in square brackets.
• APA format and examples can be found at the link below.
https://apastyle.apa.org/style-grammar-guidelines/references/examples

APPENDICES
• Appendices in the manuscript must be named as Appendix A (Appendix A), Appendix B (Appendix B) and Appendix C (Appendix C) etc.
• Equations in the appendices must be named as A1, A2, A3, etc., and table and figures numberings must be named as Table A1, Table A2, Figure A1, Figure A2 etc.

BOR DERGİSİ
JOURNAL OF BORON
https://dergipark.org.tr/boron

İÇİNDEKİLER/CONTENTS

TENMAK Bor Araştırma Enstitüsü

Dumlupınar Bulvarı (Eskişehir Yolu 7. km), No:166, D Blok, 06530, Ankara
Tel: (0312) 201 36 00
Faks: (0312) 219 80 55
e-mail: boren.journal@tenmak.gov.tr
web:https://dergipark.org.tr/boron